ASM Handbook, Volume 11, *Failure Analysis and Prevention*
B. Miller, R. Shipley, R. Parrington, D. Dennies, editors
DOI 10.31399/asm.hb.v11.a0006778

Monotonic Overload and Embrittlement

Brett A. Miller, IMR Test Labs

OVERLOAD FAILURES, from the perspective of materials failure analysts, refer to the ductile or brittle fracture of a material when stresses exceed the load-bearing capacity of the material from either excessive applied stress or degradation of the load-bearing capacity of the material from damage, embrittlement, or other factors. However, the definition of overload failure is not uniformly agreed upon. Many engineers limit the definition of overload failures to those in which the applied stresses were higher than anticipated in design. This alternate viewpoint incorrectly presumes underdesign as the cause of all overload failure, because it does not include failures in which embrittlement or other causes result in fracture under normal loading.

The purpose of engineering failure analysis is to identify the root cause of component or system failure and to prevent similar occurrences. Underdesign is just one potential cause of an overload failure, and the time-consuming and potentially expensive process of redesign may indeed be necessary for prevention of further failures in some cases. However, from the standpoint of practical failure analysis, a wide variety of manufacturing and material characteristics can act singly or combine synergistically to reduce the strength, ductility, and toughness of metallic materials. These factors must also be considered in the evaluation and prevention of overload failures. Therefore, throughout this article, the term *overload failure* implies fracture due to stresses exceeding the capacity of the material in its current condition, whether or not the stress was higher than that anticipated by design.

The purpose of this article is to identify and illustrate the types of overload failures, which (for the purpose of discussion) are categorized as:

- Failures due to insufficient material strength and underdesign
- Failures due to stress concentration and material defects
- Failures due to material alteration

These categories are neither mutually exclusive nor collectively exhaustive, but they are a useful means for pinpointing those areas of the design and materials selection that may require corrective scrutiny. Factors associated with overload failures are discussed in this article, and, where appropriate, preventive steps for reducing the likelihood of overload fractures are included. In particular, overload failure due to material alteration is very complex. No engineering component is immune from changes in material properties from mechanical strain, gross damage, and change in material microstructure or embrittlement. Complex engineering failures also can result from simultaneous multiple alterations.

Fracture Modes and Mechanisms

When dealing with a fracture (not all failures are fractures), the failure analyst must identify the origin of the fracture and the mechanism(s) of crack propagation. In general, the three general modes or types of metal fracture include failures from overload, fatigue, and creep. These three modes of fracture are briefly summarized in Table 1, which includes concise summaries of contributing factors and the visual and microscopic aspects of each. In general, the growth or propagation of cracks during an overload fracture is more rapid than for the more progressive forms of cracking due to fatigue or creep. Hence, overload is described as instantaneous in Table 1 to distinguish it from the more progressive form of cracking due to fatigue or creep. These basic modes of fracture can also occur in combination, as when a fatigue or creep crack grows over time and ultimately leads to a rapid fracture through overload failure by ductile and/or brittle cracking.

The modes of fracture (overload, fatigue, and creep) cannot be considered independently of the underlying mechanisms of crack initiation and crack propagation. The occurrence and appearance of different fracture modes depend on the mechanism(s) of crack initiation and propagation. For brittle and ductile cracking, distinguishing characteristics at different scales of observation (1 to >10,000×) are briefly summarized in Table 2. The following sections also briefly review some mechanistic aspects of ductile and brittle crack propagation, including discussion of mixed-mode cracking, which can also occur when an overload failure is caused by a combination of ductile and brittle cracking mechanisms. This article only describes the general aspects of fracture mechanisms, because more details are described in other articles in this Volume.

Ductile Overload Failures

Ductile overload failures are simply those that exhibit significant visible macroscopic plastic deformation. Applied stress and energy from an external source are required to propagate the fracture, rather than residual stresses alone. Ductile cracks blunt and stop when the stresses are dynamically reduced and remaining energy is insufficient to create further distortion. The ability to deform and absorb energy at the tip of a crack permits ductile materials to fatigue crack or crack in a stable (i.e., noncritical) overload manner over a longer period of time. Well-formed and easily identified striations are often present in fatigue fractures of ductile materials.

Due to necking and other visible signs of deformation evidenced by ductile materials prior to failure, ductile overload can often be less surprising and catastrophic than brittle failures. Ductile overload thus can be a more forgiving fracture mode than brittle fracture. Materials that exhibit yielding prior to fracture also can redistribute their loading to the adjacent support structure, avoiding system failure.

Due to their very nature, monotonic ductile overload failures often occur during manufacture or relatively early in service (for example, collapse of a roof due to snow loading). Sometimes this suggests underdesign (for example, by miscalculation of the service stresses; misuse or abuse in service; improper materials selection, specification, or processing; poor manufacturing; or other reasons). Unfortunately, in some situations, ductile overload failures are routinely assumed to be design mistakes, a practice that ignores all of the other contributing factors to the failure and may result in unnecessary or ill-advised corrective actions. Perfunctory failure analysis or incomplete root-cause investigation can be very misleading or even dangerous.

Table 1 Fracture mode identification chart

Method	Instantaneous failure mode[a]		Progressive fracture mode	
	Ductile overload	Brittle overload	Fatigue	Creep
Visual, 1 to 50× (fracture surface)	• Necking or distortion in direction consistent with applied loads • Dull, fibrous fracture • Shear lips	• Little or no distortion • Flat fracture • Bright or coarse texture, crystalline, grainy • Rays or chevrons point to origin	• Flat progressive zone with beach marks • Overload zone consistent with applied loading direction • Ratchet marks where origins join	• Multiple brittle-appearing fissures • External surface and internal fissures contain reaction scale coatings • Fracture after limited dimensional change
Scanning electron microscopy, 20–10,000× (fracture surface)	• Microvoids (dimples) elongated in direction of loading • Single crack with no branching • Surface slip band emergence	• Cleavage or intergranular fracture • Origin area may contain an imperfection or stress concentrator	• Progressive zone: worn appearance, flat, may show striations at magnifications above 500× • Overload zone: may be either ductile or brittle	• Multiple intergranular fissures covered with reaction scale • Grain faces may show porosity
Metallographic inspection, 50–1000× (cross section)	• Grain distortion and flow near fracture • Irregular, transgranular fracture	• Little distortion evident • Intergranular or transgranular • May relate to notches at surface or brittle phases internally	• Progressive zone: usually transgranular with little apparent distortion • Overload zone: may be either ductile or brittle	• Microstructural change typical of overheating • Multiple intergranular cracks • Voids formed on grain boundaries or wedge-shaped cracks at grain triple points • Reaction scales or internal precipitation • Some cold flow in last stages of failure
Contributing factors	• Load exceeded the strength of the part • Check for proper alloy and processing by hardness check or destructive testing, chemical analysis • Loading direction may show failure was secondary • Short-term, high-temperature, high-stress rupture has ductile appearance (see creep)	• Load exceeded the dynamic strength of the part • Check for proper alloy and processing as well as proper toughness, grain size • Loading direction may show failure was secondary or impact induced • Low temperatures	• Cyclic stress exceeded the endurance limit of the material • Check for proper strength, surface finish, assembly, and operation • Prior damage by mechanical or corrosion modes may have initiated cracking • Alignment, vibration, balance • High cycle low stress: large fatigue zone; low cycle high stress: small fatigue zone	• Mild overheating and/or mild overstressing at elevated temperature • Unstable microstructures and small grain size increase creep rates • Ruptures occur after long exposure times • Verify proper alloy

(a) Failure at the time of load application without prior weakening

Table 2 Distinguishing characteristics of brittle versus ductile behavior depending on the scale of observation

Scale of observation	Brittle behavior	Ductile behavior
Structural engineer	Applied stress at failure is less than the yield stress	Applied stress at failure is greater than the yield stress
By eye (1×)	No necking, shiny facets, crystalline, granular	Necked, fibrous, woody
Macroscale (<50×)	"Low" reduction of area or ductility	Medium-to-high reduction of area
Microscale, scanning electron microscopy (100–10,000×)	Brittle microprocess, cleavage or intergranular	Ductile microprocess, microvoid coalescence
Transmission electron microscopy (>10,000×)	May have a large level of local plasticity	High amount of plasticity globally

Ductile fracture occurs from the nucleation, growth, and coalescence of microvoids during deformation. Second-phase particles and inclusions typically provide the nucleation sites for initiation of the microvoids, which then grow and coalesce as deformation progresses further. Ductile fracture by void growth and coalescence can occur by two modes during tensile loading. Mode I is plane-strain fracture, where void growth and fibrous tearing occur along a crack plane that is essentially normal to the axis of the tensile load. The fracture appearance typically has a dull and fibrous appearance, as in the classic cup-and-cone feature of ductile fracture, along with material necking in the simple cross section of a tensile testing specimen (for example, see Fig. 166 in "Medium-Carbon Steels: Atlas of Fractographs," *Fractography*, Volume 12 of the *ASM Handbook*, 1987).

The other fracture mode is plane-stress fracture (mode II fracture), which manifests itself as the shear lips in the cup-and-cone fracture specimens from tensile tests. During tensile loading, the fracture originates near the specimen center, where hydrostatic stresses develop during the onset of necking and where microvoids develop and grow. Multiple cracks join and spread outward along the plane normal to the loading axis, as representative of mode I (plane-strain) crack propagation. When cracks reach a region near the outer surface, the mode of fracture changes to mode II (plane-stress) condition, where shear strain becomes the operative mode of deformation (as maximum stresses occur along the shear plane in the basic principles of continuum mechanics). Thus, even though the overall applied stress is still a tensile load, deformation makes a transition to the shear plane in the outer regions of the specimen. In the mode II region, voids grow in sheets at an oblique angle (~45° to the plane of the major fracture or loading axis) to the crack plane under the influence of shear strains. This type of shear-band tearing results in the classic shear lips of a ductile cup-and-cone tensile fracture specimen. Shear-band formation also commonly occurs in deformation processing, where friction and/or geometric conditions produce inhomogeneous deformation, leading to local shear bands. Localization of deformation in these shear bands also results in localized temperature increases, which produce local softening.

Ductile fractures often progress as single cracks, without many separated pieces or substantial crack branching at the fracture location. They are characteristically flat and perpendicular to the maximum tensile stress for mode I (plane-strain) conditions, or at approximately a 45° angle to the maximum stress (although this angle may vary depending on material condition and loading condition). The crack profiles adjacent to the fracture are consistent with tearing. Ductile overload failures of engineering components typically exhibit the characteristics of dimple rupture, as discussed further.

The second mode of ductile fracture, shear-band formation, is a phenomenon associated more with deformation processes during metalworking, where localized and inhomogeneous deformation can potentially lead to crack formation. The concern of inhomogeneous deformation and shear-band formation in metalworking is not discussed in this article. However, shear-band formation can occur in dimple-rupture failures under certain circumstances. In some ductile materials, shear-band fractures can also show evidence of microvoid coalescence (MVC), typically associated with

dimple rupture. In pure metals and alloys refined to remove all impurities (where there is no ready supply of sites for microvoids to nucleate), the material can fail by adiabatic shear-band formation, resulting in a somewhat flat fracture surface devoid of dimples.

Transgranular dimple rupture due to MVC is the most prevalent fracture mechanism of ductile overload failures. During deformation, cavities (or microvoids) nucleate at small particles (such as inclusions and second-phase particles) when the matrix material separates from the particle by interfacial decohesion and when the inclusion or second phase fractures. The level of extensional growth of the microvoids is dependent on the level of plastic strain the material can undergo prior to fracture.

Microscale fractographic features consist of ruptured dimples, and both diffuse and local necking may be macroscopically visible depending on the component geometry. Mechanical conditions and metallurgical features can influence the appearance of MVC. Examples are shown for a ferritic steel (Fig. 1a), ductile iron (Fig. 1b), and cast titanium alloy (Fig. 1c). The dimple features are evident in equiaxed form for tensile loading (Fig. 1a, b). Parabolic or elongated shear dimples occur from torsional loading (Fig. 1c) or from mode II (in-plane) shear. However, metallic materials can behave in a ductile manner but not exhibit the classical dimple-rupture morphology, as shown in Fig. 1(d) for a cast aluminum alloy. The cast aluminum alloy fracture surface should show dimples in the aluminum matrix (original dendrites), but they can be difficult to see because fracture-surface morphology is impacted by cleavage in second-phase (silicon) particles and other second phases.

Very pure materials, particularly unalloyed metals with few inclusions, can exhibit extremely high reduction in area, or necking, at the fracture site. Impurities and second-phase particles are always present in most engineering materials. An increased volume fraction of these constituents reduces the true fracture strain and the reduction in area (Ref 1). The type, distribution, and size of these constituents are also mechanistically important and are discussed in greater depth later in this article.

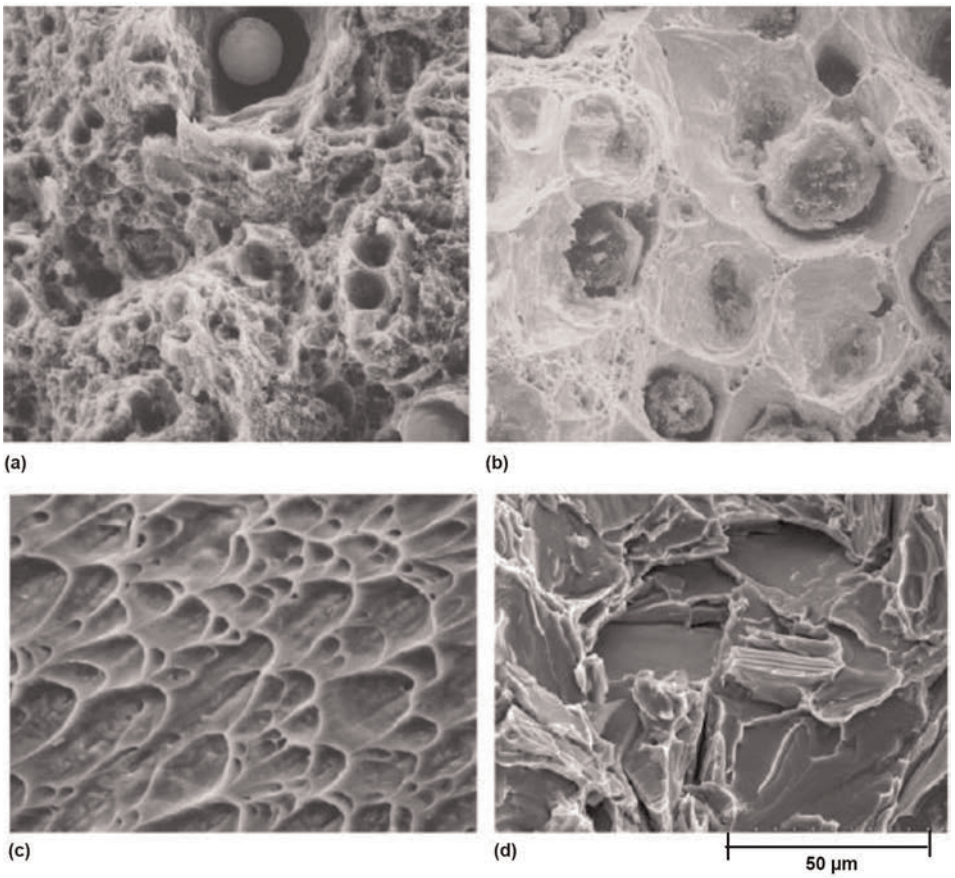

Fig. 1 Scanning electron microscopy images of dimple-rupture fractures. (a) Fracture of low-alloy medium-carbon steel bolt (SAE grade 5). Original magnification: 1750×. (b) Equiaxed tensile dimples originating around the graphite nodules of ASTM 60-45-10 ductile iron. Original magnification: 350×. (c) Parabolic shear dimples in cast Ti-6Al-4V from torsional loading. Original magnification: 1400×. (d) Dimple rupture in cast aluminum alloys. Original magnification: 593×. (a), (b), and (c) Courtesy of M. Chaudhari, Columbus Metallurgical Services, Inc.

Examples of Simple Ductile Overload Failures

Simple overload fractures are not uncommon in bulk deformation manufacturing processes. Even when not resulting in fracture, severe room-temperature forming processes result in unavoidable MVC concentrated in regions of highest plastic deformation. Forming-induced microvoids can serve as subsequent fracture-initiation sites, which may be of particular importance with regard to fatigue crack propagation. Fatigue cracking also requires a level of ductile behavior; otherwise, after a crack is initiated, it would result in instant unstable crack growth, fracturing in a macroscopic brittle manner. However, unlike ductile overload, fatigue most often initiates and propagates at overall stresses below the yield stress. Examples 1 and 2 illustrate uncomplicated types of ductile overload failures.

Example 1: Fracture of High-Strength Screws during Installation.

One lot of size M5 × 0.8 mm, class 8.8 metric screws with a proprietary head design were failing during application. The screws were reportedly failing at the normal installation torque.

Investigation

Typical failed fasteners are shown in Fig. 2(a). All fractures showed substantial necking. Fractographic features were consistent with dimple rupture, and macroscopic necking is shown metallographically in Fig. 2(b). The chemical composition of the fasteners was not verified, but proof load and tension testing of exemplar screws from the same lot revealed satisfactory results. The level of necking on the tension-tested screws was analogous to those that failed during installation.

Metallographic examination revealed a relatively uniform martensitic microstructure. Minor laps were apparent at the thread crests, but they were acceptable according to the applicable specifications. No gross defects or evidence of brittle behavior were identified.

Conclusions

The analytical results indicated that the fasteners failed via ductile overload in the absence of gross defects or embrittlement. It was subsequently determined that a nonapproved lubricant was added to the questioned fastener lot during installation.

In fastener design where tension preload is controlled by torque measurement, the general relationship $T = KDP$ is often used, where T is torque, K is a torque coefficient including a friction factor, D is the fastener diameter, and P is the tensile load. Assuming a predetermined torque for bare steel screws, the tension preload can be more than twice as high on lubricated fasteners. In this case, the reduced friction level resulted in a tension preload sufficient to fracture the screws in ductile overload.

Example 2: Forming Cracks on Stainless Steel Wire.

Cold-drawn 6.4 mm (0.25 in.) diameter type 303 stainless steel wire sections failed during a

forming operation. All wires failed at a gradual 90° bend.

Investigation

High-magnification visual examination disclosed many fine ruptures accompanying a typical fracture (Fig. 3a) occurring at the outside of the bend. The rupture interior surfaces (Fig. 3b) were entirely ductile in nature. No defects from manufacture of the wire were evident. The fracture and crack surfaces exhibited dimples (Fig. 3c), which appeared to initiate at nonmetallic inclusions inherent in this free-machining steel. Microstructural examination indicated there was no alteration in the fracture and crack regions. Substantial distortion of the grains was apparent at the ruptures.

Conclusions and Recommendations

It was concluded that the wires were cracking via ductile overload. The forming stresses were sufficient to initiate surface ruptures, suggestive of having exceeded the forming limit.

The results suggested that the forming process should be examined; in particular, lubrication and workpiece fixturing would be of interest, together with examination of successfully formed wire stock.

Brittle Overload Failures

Brittle overload failures, in contrast to ductile overload failures, are characterized by little or no macroscopic plastic deformation. Fracture features and mechanisms on a microscopic scale can have components of ductile or brittle crack propagation, but the macroscopic process of fracture is characterized by little or no work being expended in the form of permanent (i.e., plastic) deformation. The macroscopic behavior is essentially elastic up to the point of failure. The energy of the failure is principally absorbed by the creation of new surfaces, that is, cracks. For this reason, brittle failures often contain multiple cracks and separated pieces, which are less common in ductile overload failures. Brittle overload failures are sometimes identified as catastrophic, because there may not be any warning signs such as warpage or distortion prior to the final fracture, and the failures may cause substantial collateral damage. Energy released during brittle fracture in these failures can be very loud and, in some cases, explosive.

Brittle fractures are characterized by relatively rapid crack growth to final fracture. The cracking process is sometimes referred to as being unstable or critical, because crack propagation leads quickly to final fracture. Brittle fracture initiates and propagates more readily than ductile fracture (or for so-called subcritical crack propagation processes such as fatigue and stress-corrosion cracking). Representative crack extension rates for brittle and ductile fracture have been measured at 1000 and 6 m/s (3300 and 20 ft/s), respectively. In addition, supplemental or continuously applied energy may not be necessary to continue the brittle crack propagation once it is initiated; elastic strain energy may be sufficient.

Brittleness does not necessarily imply material flaws or processing mistakes, although this is very often the case. In some circumstances, brittle fracture is the expected overload failure mode. This is true for inherently brittle materials, such as extremely high-strength materials where ductility is sacrificed for maximum deformation or wear resistance. Additionally, embrittling conditions and metallurgical phenomena can impose brittle fracture characteristics on materials that would generally evince the more desirable ductile overload behavior. Brittle overload failures are typically differentiated by a primary crack that occurs from either transgranular or intergranular crack propagation, which indicates whether the cracks propagate through the grains or around them, respectively. The use of the infrequently encountered term *intragranular* to describe transgranular features is discouraged due to its similarity in pronunciation to *intergranular*.

All brittle fracture mechanisms can exhibit chevron or herringbone patterns, which indicate the fracture origin and direction of rapid fracture progression. Ductile cracking by MVC cannot have a herringbone pattern, although a macroscale radial pattern and chevrons can occur from MVC. River lines on a macroscopic scale may be revealed in glassy polymers but not on a macroscopic scale in a metallic material. With regard to fatigue, materials with poor ductility can still experience crack initiation and growth, because some slight plasticity may by present. Relatively brittle metals such as hardened steel and gray cast iron do not always form microscopically identifiable striations and macroscopic beach marks in cyclic failures.

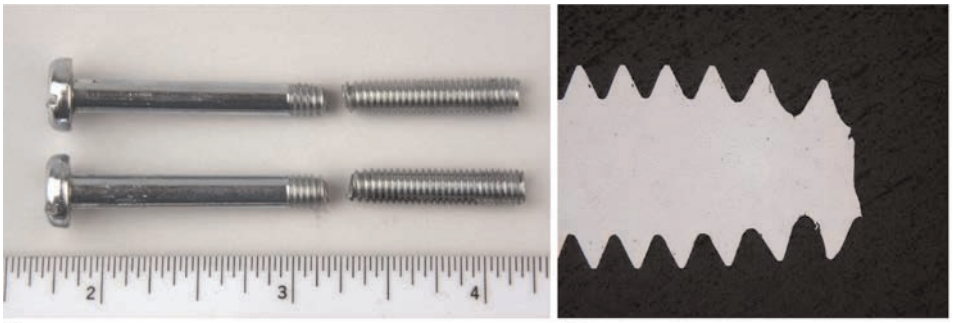

Fig. 2 Fracturing of high-strength screws (Example 1). (a) Two grade 8 high-strength steel fasteners that failed on installation. (b) Necking and stretching between adjacent thread crests are evident on a cross section. Unetched. Original magnification: 8.9×

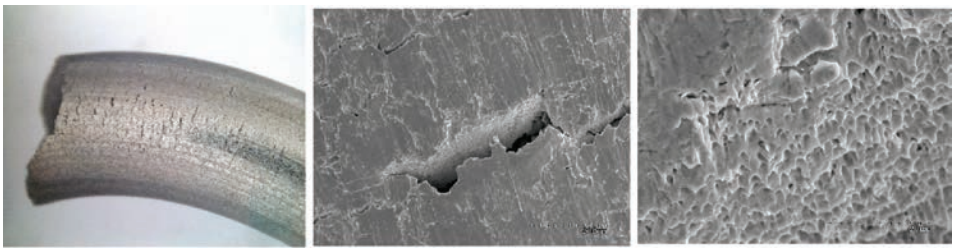

Fig. 3 Forming cracks on stainless steel wire (Example 2). (a) The fracture, which occurred during bending, shows many parallel fissures. Original magnification: 5.3×. (b) A typical fissure on the wire surface. Scanning electron micrograph. Original magnification: 71×. (c) The interior of the fissures and the fracture surface exhibit dimple-rupture morphology. Scanning electron micrograph. Original magnification: 1187×

Transgranular Cleavage

Transgranular cleavage is cracking through the discrete grains. *Intracrystalline* is an equally descriptive term, but it is not preferred terminology. Crystallographic cleavage occurs preferentially in individual grains in directions that do not readily deform, by slip processes, under strain. Therefore, specifically oriented grains tend to crack, leaving a shiny, faceted appearance easily differentiated from dull and fibrous dimple-rupture features. Cleavage in a steel sample is shown in Fig. 4. Face-centered-cubic (fcc) metals (for example, copper, aluminum, nickel, and austenitic steels) exhibit the greatest ductility during rapid fracture and, in benign environments, do not normally fracture via cleavage. However, brittle cracking of fcc metals can occur under conditions of environmentally assisted cracking (for example, transgranular stress-corrosion cracking of austenitic stainless steels). High-nitrogen austenitic stainless may also be less ductile during rapid crack growth.

Cleavage initiates via microcrack nucleation at the leading edge of piled-up dislocations. The crack propagates through the grain in which it initiated. The crack then continues across the grain boundaries very rapidly as the critical crack size is exceeded. The fracture surface continues across the grain boundary, but during the cracking process it is very

unlikely that the crossing is strictly continuous across the grain boundary. Cleavage cracks cannot cross a grain boundary if the body has a twist component. The crack must reinitiate, and therefore, the classic fine-scale convergence of multiple river lines develops as the crack progresses. Cleaved grains often exhibit river patterns, further confirming transgranular cleavage as the mechanism of crack propagation. River-mark features on individual facets can also be used to determine local crack propagation direction. Cleavage occurs in materials with a high strain-hardening rate and relatively low cleavage strength, or when a geometric constraint (i.e., large hydrostatic stresses) functions as an initiator of cleavage fracture. It also occurs in materials that are embrittled within the grains rather than at the grain boundaries. All materials are sensitive to hydrostatic stresses, which can also induce brittle fracture. Fractographically, it is very unlikely that cleavage facet size can exceed the grain size, and thus, the size of the fracture facets can be a measure of the grain size if there is only one cleavage facet per grain. There is also a possibility of subgrain boundaries and therefore multiple growth directions in a single grain for those cleavage cracks that cannot propagate across a boundary that has a twist component. In lath martensitic and bainitic microstructures, cleavage facet size correlates with packet size, not prior-austenite grain size.

The term *quasi-cleavage* is historically applied when significant dimple rupture and/or tear ridges accompany the cleavage morphology. Grains oriented favorably with respect to the axis of loading can slip and exhibit ductile behavior, whereas those oriented unfavorably cannot slip and exhibit transgranular brittle behavior. The term *quasi-cleavage* was somewhat confusing, so the phrase "cleavage with ductile tear ridges" is preferred. A failure analysis example illustrating brittle transgranular fracture follows.

Example 3: Cracking of a Dump Truck Transmission Housing.

Both halves of a gray cast iron transmission housing from a 50 ton dump truck contained numerous cracks. No service duration or material specifications were provided.

Investigation

Visual examination revealed that all the cracks occurred adjacent to stiffening ribs and at changes in section thickness. One of the cracks is shown in Fig. 5(a). A crack that was opened to permit examination is shown in Fig. 5(b). All cracks appeared to have the high light reflectivity of cleavage facets with no postfracture indication of ductility or mechanical damage. None of the casting cracks contained stains, casting defects, or features suggestive of fatigue cracking. The housing halves did not contain any internal damage.

Tensile specimens from both halves exhibited ultimate tensile strengths exceeding 205 MPa (30 ksi). Although testing of samples removed from a cast component may not necessarily bear relation to grade/condition determination based on separately poured test bars, results suggested the G3000 grade designation for automotive gray cast iron. The typical fracture morphology within the matrix was transgranular cleavage. The microstructure consisted of size 5 type A graphite flakes in a matrix of approximately 73% pearlite/27% ferrite. No free carbides were present. The brittle crack followed the profile of the graphite flakes, as shown in Fig. 5(c).

Conclusions

The transmission housing castings exhibited brittle overload cracks at highly stressed locations. Failure was due to applied loading sufficient to fracture the castings, probably unexpected bending forces. The cleavage cracking occurred preferentially along the graphite flakes, which is typical for this material. No cold shuts, porosity, or other casting flaws were evident within the cracks. The source of the unexpected bending was not determined. Fracture could be transgranular (and most likely is), but the fracture path is heavily influenced by cleavage cracking in the graphite flakes.

Decohesive Rupture

Decohesive rupture is a fracture mechanism where separation occurs at prior boundaries between grains or second-phase particles. The decohesion is macroscopically brittle in all cases but may be microscopically ductile or brittle. In either case, visual and low-magnification stereomicroscopic examination typically reveal the facets of the individual grains along which cracking or separation occurred. The distinction is the presence of MVC in the case of dimpled intergranular fracture and its absence in intergranular brittle fracture. In failure analysis, the investigator must distinguish which type of intergranular fracture has occurred, because the causes and corrective actions can be substantially different.

Intergranular fracture is the most prevalent form of decohesive rupture, and this is the classic "rock candy" appearance in brittle materials. Materials that are identified as embrittled are usually prone to intergranular brittle fracture, although some embrittlement mechanisms are manifested as transgranular cleavage, dimpled intergranular fracture, and dimple rupture. The term *rock candy* is most often applied to coarse-grained materials, where this appearance is visually evident.

Dimpled intergranular fracture could be easily mistaken for pure brittle intergranular fracture if high-magnification fractography is not performed to examine for microscopic void formation in the grain boundaries. This mechanism of MVC in the grain boundaries can also result in a greater level of secondary cracking than evidenced by ductile overload failures.

In some circumstances, dimple rupture occurs along the interface between the matrix and a relatively weak intergranular phase (for example, at high temperatures). Weakening of the grain boundary can occur at elevated temperatures and result in creep-stress rupture. It can also occur adjacent to the grain boundary due to elemental segregation causing a denuded zone. As materials with this inherent or imposed tendency are stressed, normal MVC initiates at inclusions, second phases, and other crystallographic imperfections (for example, the grain boundaries). Due to the preexisting crack path provided by the grain boundaries, dimpled intergranular fracture requires less energy to effect separation than that for typical transgranular ductile rupture. The following example is a case history where this behavior was noted.

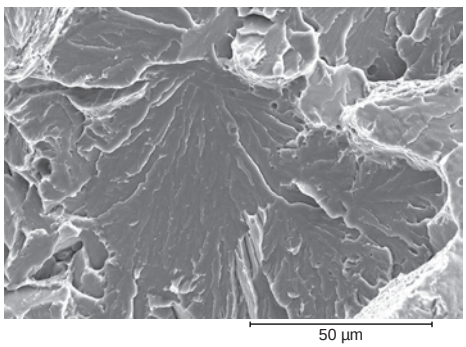

Fig. 4 Cleavage fracture in a carbon steel component. Scanning electron micrograph. Original magnification: 593×

Fig. 5 Cracking in a truck transmission housing (Example 3). (a) Typical crack at a stiffening rib. (b) An opened crack at a stiffening rib exhibited brittle features. (c) Longitudinal metallographic cross section showing secondary brittle cracking along the graphite flakes. 2% nital etch. Original magnification: 59×

Example 4: Overload Failure of a Bronze Worm Gear.

A very large-diameter worm gear that had been in service in a dam for more than 60 years exhibited cracks and was removed. It was reported that the cast bronze gear was only rarely stressed during service, associated with infrequent opening and closing of gates. Due to the age of the gear and the time frame of its manufacture, no original material specifications or strength requirements could be located. Likewise, no maintenance records of possible repairs to the gear were available.

Investigation

As part of the investigation, a number of representative sections excised from the gear were submitted for metallurgical analysis. The cracks were primarily located on the gear faces and were not associated with traditional regions of high service stresses, such as the tooth roots. Some portions of the gear face exhibited light discoloration, which suggested weld repairs. The cracks were evident within the base metal at the repair weld fusion lines and within the weld metal. Figure 6(a) shows the opened crack features in an area where a weld and remaining casting imperfection were apparent. The macroscopic fracture features differed substantially between the base metal and the welds. Some of the cracking did not occur at casting imperfections or repair welds.

Scanning electron microscopy revealed the typical weld and base metal fracture features shown in Fig. 6(b) and (c), respectively. The weld exhibited fine features that consisted of both dimple-rupture and grain-boundary dimple-rupture evidence. The base metal exhibited rather large-grained intergranular brittle cracking features with many types of inclusions.

Chemical analysis revealed a standard high-strength, manganese bronze composition, and the weld filler metal was considered compatible. Tensile testing of specimens removed from gear segments remote to repairs revealed tensile strengths near 690 MPa (100 ksi), yield strengths near 517 MPa (75 ksi), and 5% elongation at fracture. Weld and base metal hardnesses were similar.

The microstructure at the transition between the base metal and weld metal is shown in Fig. 6(d). The continuous grain-boundary phase in the weld metal responsible for the decohesive rupture features is evident.

Conclusions

It was concluded from the investigation that the bronze gear cracked via mixed-mode overload, rather than by a progressive mechanism such as fatigue or stress-corrosion cracking. The cracking was not associated with regions that would be highly stressed and did not appear to be consistently correlated to casting imperfections, repair welds, or the associated heat-affected zones. The cast gear was a high-strength, low-ductility bronze. Cracking across the gear face suggested bending forces from misalignment were likely responsible for the cracking, and further review of this potential root cause could be recommended.

Intergranular brittle fracture can be due to many conditions, including a brittle grain-boundary phase, high strain rates, and embrittlement. Visually, the macroscopic plane of the intergranular brittle fracture appears relatively flat, perpendicular to the axis of the applied stress responsible for the overloading. This mechanism is usually due to an improper condition of the materials or the alteration of the material during service. Intergranular brittle fracture is very prevalent in ceramic materials and is often present in poorly sintered powder metallurgy constructs. It is necessary for the practicing failure analyst to understand that intergranular brittle fracture is not always due to defects and improper processing. This mechanism can result from well-controlled processes that provide benefit that can outweigh the expectation of brittle failure. One example is in the process of carburization, as discussed in the case history that follows.

In some cases, intergranular brittle fracture can occur at previous grain boundaries, such as in the case of martensitic steels where fracture can occur at prior-austenite grain boundaries, which can also coincide with some of the boundaries in the martensite. Intergranular cracking has been documented in nearly all engineering metals and alloys and is caused by a wide variety of mechanical and environmental factors, such as grain-boundary embrittlement and decohesive separation along the grain boundaries at elevated (creep-regime) temperatures. For service temperatures below the creep regime (i.e., approximately 0.4 to 0.5 times the melting temperature of the alloy) and with appropriate materials selection and design, intergranular brittle fracture is often (but not always) indicative of improper materials processing. Transgranular cleavage is usually the brittle mode anticipated in normal conditions for brittle materials. Intergranular brittle fracture is atypical, because the grain boundaries are usually stronger than the grains at temperatures below the creep regime. For additional mechanistic information on intergranular fracture, see the article "Intergranular Fracture" in this Volume.

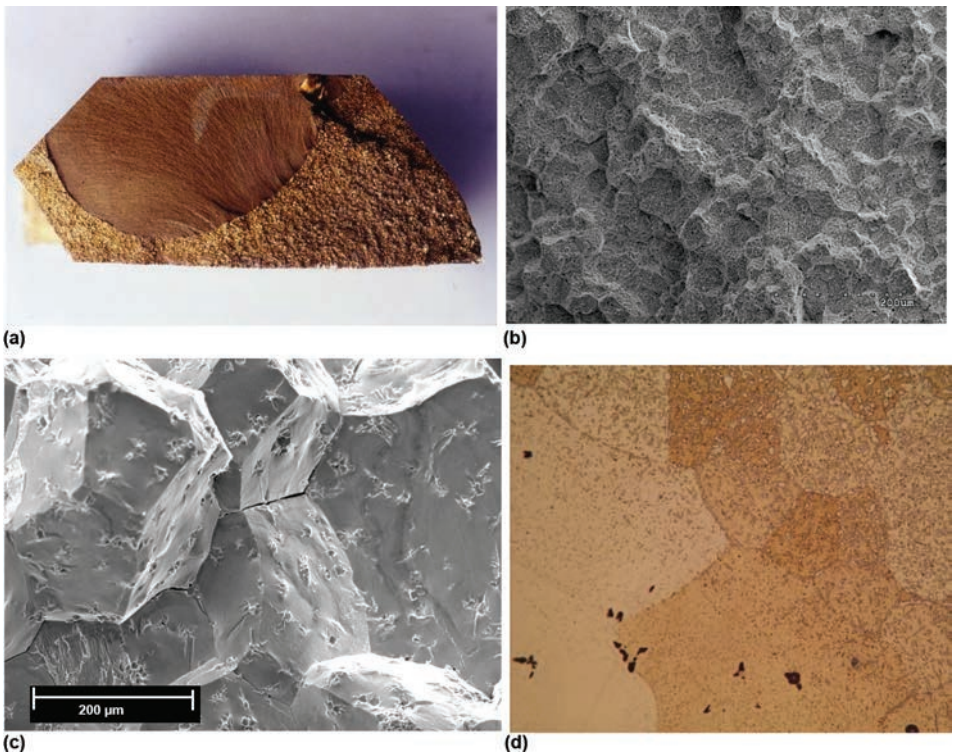

Fig. 6 Overload failure of a bronze worm gear (Example 4). (a) An opened crack is shown with a repair weld, a remaining casting flaw, and cracking in the base metal. (b) Electron image of decohesive rupture in the fine-grained weld metal. Scanning electron micrograph. Original magnification: 119×. (c) Morphology in the large-grained base material at the same magnification as (b), showing intergranular brittle fracture features. Scanning electron micrograph. Original magnification: 119×. (d) Metallographic image showing the weak grain-boundary phase in the weld. Potassium dichromate etch. Original magnification: 297×

Example 5: Valve Seat Fractures.

Valve seats fractured during testing and during service. The seats were machined from grade 11L17 resulfurized and rephosphorized low-carbon steel and were surface hardened by carburization.

Investigation

Fracture occurred through the relatively thin wall of the seat, between circular holes in the cylindrical barrel. Secondary cracks were evident adjacent to the fractures in every failed ligament region. The fracture surfaces visually had the faceted or crystalline appearance of intergranular fracture near the exterior surfaces, as shown in Fig. 7(a). No fracture origins were apparent, although corners at circular crossholes were considered the probable origins. The core fracture morphology consisted of elliptical dimples.

The seat surface hardness was 55 HRC, which is typical for case-hardened steel. A metallographic cross section through the fracture surface is shown in Fig. 7(b). A secondary crack has opened substantially and blunted in the ductile core. Plastic distortion of the core grain structure at the crack tip was evident. The seat wall was not through-carburized. The near-surface case microstructure was tempered martensite and retained austenite, along with the large nonmetallic inclusions inherent in this material. No case-hardening microcracking was evident, and no grain-boundary carbides were apparent.

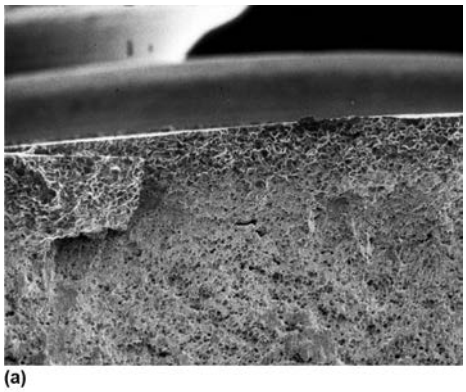

(a)

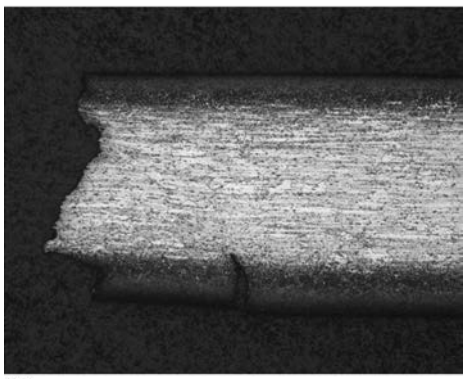

(b)

Fig. 7 Valve seat fractures (Example 5). (a) View of the seat fracture surface with intergranular near-surface features from the carburizing heat treatment. Scanning electron micrograph. Original magnification: 59×. (b) Cross section showing the case depth and the blunting of a secondary bending crack by the ductile core microstructure. 2% nital etch. Original magnification: 15×

Conclusions

The fracture occurred via brittle overload, which was predominantly intergranular. The amount of bending evidence and the directionality of the core overload fracture features suggested that the applied stresses were not purely axial, as would be anticipated in this application. Resulfurized steels are typically case hardened for wear resistance, but the hardened structure has relatively poor ductility. Stress concentration occurs at the ligaments of hardened microstructure between the soft inclusions. These materials characteristically have low transverse mechanical properties, even when they are not case hardened. The level of retained austenite in the hardened case layer likely contributed to the failure.

Mixed-Mode Cracking

As shown in several of the previous examples, it is not unusual to observe fractographic evidence of multiple mechanisms on a single fracture surface. The failure analyst must rely on experience to interpret mixed-mechanism and mixed-mode features. The morphology at the fracture origin is of primary importance. Atypical features among uniform fracture features may not be of significance other than pinpointing microstructural inhomogeneities and discontinuities (see, for example, the section "Material Factors" in this article).

A blunted crack in a ductile iron impeller that failed via mixed brittle and ductile mechanism overload fracture is shown in Fig. 8. The crack stopped in this area where deformation and necking of the ductile bull's-eye ferrite is evident. Much of the remaining cracking through the lamellar pearlite was very brittle. Although the ferrite phase was not predominant in the matrix, it imparted substantial ductile behavior.

In many cases, a combination of fracture mechanisms suggests a minor phase has acted detrimentally. Figures 9(a) and (b) show fracture through globular carbides in a thin tool steel component, resulting in matrix fracture. The tempered martensitic matrix was somewhat ductile, yet fracture occurred when brittle massive carbides near the surface shattered.

Overload fracture by ductile or brittle crack growth is often the final result of fracture following other subcritical cracking phenomena, such as fatigue and corrosion. In these cases, it is necessary to identify the proximate cause that was followed by the subsequent overload behavior. The final fracture occurs at a critical point when the remaining intact ligament of material can no longer support the applied stress. Figure 10 shows the fatigue to final ductile overload transition in a relatively soft austenitic stainless steel. Some dimples due to MVC are evident in the last few striations that formed before the crack size became critical.

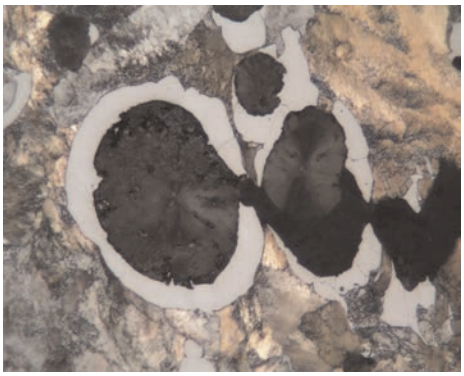

Fig. 8 Crack in a high-strength ductile iron (grade 100-70-03) impeller showing deformation in the ferrite, resulting in blunting of this secondary crack. 2% nital etch. Original magnification: 492×

Material Factors

Determining the root cause of a failure requires a comprehensive understanding of the material, loading, and environmental factors that can contribute to failure. Monotonic

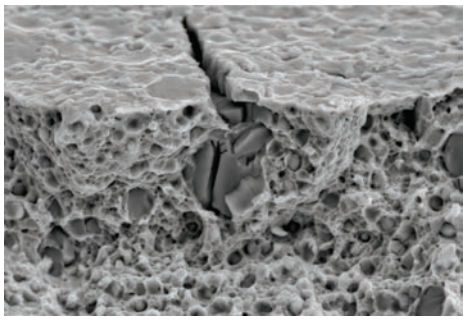

(a)

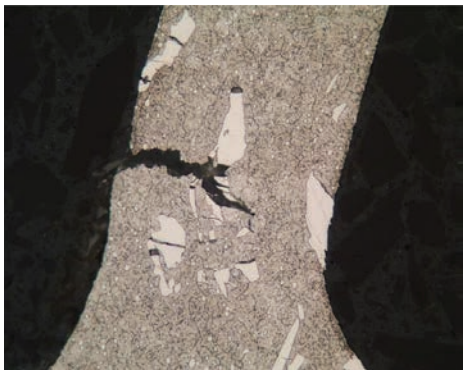

(b)

Fig. 9 Fracture in a thin medical device manufactured from type D2 tool steel. (a) View showing a fractured massive carbide and associated matrix crack. Scanning electron micrograph. Original magnification: 1187×. (b) Cross section through a cracked region in a similar part showing brittle fracture in the carbides and plastic deformation of the surrounding matrix. Vilella's reagent. Original magnification: 297×

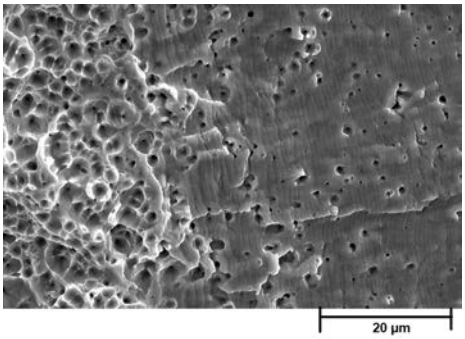

Fig. 10 Stainless steel component that was flexed in service. The transition between fatigue and dimple rupture is shown. Scanning electron micrograph. Original magnification: 1187×

overload fracture characteristics are dictated by a large variety of material characteristics. These important characteristics and interrelationships are summarized here for the discussion of monotonic overload, but they are explained in depth in the article "Fracture Appearance and Mechanisms of Deformation and Fracture" in this Volume. The mechanisms of fracture are influenced by complex, interrelated factors, which can provide competing or synergistic conditions leading to fracture. This illustrates some of the complexities and difficulties inherent in engineering failure analysis.

This section briefly reviews some of the material factors that can be considered in the evaluation of unstable, rapid fracture. Ductile and brittle overload failures and the resultant fracture morphology are influenced by various material factors from the atomic level to the bulk material level. Although it has been stated in many ways, one of the guiding principles of materials science is that properties are a function of structure and structure is a function of processing.

At the atomic structure level, individual atoms exhibit differences in the number of electrons in the various electron shells, resulting in different types of bonding and bond strength. Bonding can be covalent (strong), ionic (strong), metallic (intermediate), or van der Waals (weak). Metallic materials are metallically bonded and ceramic materials are predominantly ionically bonded. Carbon atoms in the backbone of a polymer chain are covalently bonded, and the pendant side groups are covalently bonded to the backbone. However, bonding between chains can be covalent (cross linked) or van der Waals.

Bonds between atoms can occur in various spatial orientations. The spatial arrangement of atoms can be random (amorphous) or periodic in either two or three directions, resulting in sheet structures (two-dimensional, such as graphite) or crystalline (three-dimensional). Over still greater distances, atom arrangements can be completely amorphous, oriented (as parallel alignment of carbon backbone chains in polymers), mixtures of crystalline and noncrystalline regions, or totally crystalline but in which crystalline regions are rotated with respect to each other (polycrystalline). In most metals, metallic bonds between atoms typically result in a crystalline structure, which in most engineering metals are face-centered cubic (fcc), body-centered cubic (bcc), or hexagonal close-packed (hcp) structures.

The formation of crystal lattices occurs as a result of bonding between atoms. Strong bonding forces between atoms cause atoms to pack efficiently (high packing densities). These arrangements exhibit planes of high atomic density, which contain close-packed directions. This results in the three lattices (fcc, bcc, and hcp) being especially common for metallic materials. The higher symmetry of the cubic lattices relative to noncubic lattices has implications regarding their inherent ductility, as discussed later. In general, the extent of ductility is influenced by the strength of electronic bonding, the crystal structure, and the degree of order. Three basic atomic-level influences on ductile behavior in order of increasing influence on ductile behavior, with highest ductility at the top and increasing influence toward brittle behavior at the bottom, are:

Influence of electronic bonding (most to least ductile)

- Metallic bonds
- Resonating covalent bonds
- Ionic bonds
- Covalent, van der Waals bonds
- Covalent bonds

Influence of crystal structure (most to least ductile)

- Close-packed face-centered cubic
- Body-centered cubic
- Hexagonal close-packed. Note: The relative ranking of ductility between hcp and bcc materials can vary depending on temperature and available slip systems.
- Rhombohedral
- Less symmetrical through triclinic

Influence of degree of order (most to least ductile)

- Random solid solution
- Ordered or intermetallic compound
- Ionic compound
- Covalent compound

Crystal structures of ceramic materials are often more complex than those of metallic materials. High-packing-density cubic structures do exist in some ceramic materials (rock salt and cesium chloride structures), but the presence of more than one type of atom together with ionic bonding causes differences in critical stresses for ductile (slip) and brittle (cleavage) behavior compared with metallic materials. Qualitatively, the critical stresses for slip are so high relative to those required to propagate cleavage that these materials are considered inherently brittle.

The ability of polymeric materials to form crystalline solids depends in part on the complexity of the pendant side groups of atoms attached to the covalently bonded carbon atom backbone. Crystallinity is also decreased if the polymer is branched. Seldom is crystallinity complete in a polymeric material. Crystal structures that do form are less symmetrical than those of metallic materials, caused in part by the inability to tightly pack the pendant side groups. Triclinic and monoclinic lattices are common. Like ceramic materials, crystalline polymers and oriented polymers tend to not be very ductile.

The stress-strain behavior depends strongly on the long-range spatial arrangement, together with the type of bonding. For example, ionically bonded ceramic materials are crystalline and typically show little plastic deformation prior to fracture. Randomly oriented polymers show considerable ductility prior to alignment of the molecular chains but then quickly fracture. Polymeric materials containing mixtures of crystalline and noncrystalline regions show decreased ductility and increased strength and stiffness as the degree of crystallinity increases. Polymeric materials also show decreased ductility as the extent of cross linking between chains increases. Finally, polymeric materials show a considerable stiffening, increase in strength, and loss in ductility if they are loaded at temperatures below the glass transition temperature.

Effect of Grain Size

Grains are the discrete crystalline regions present in metals. A grain can exhibit a lattice orientation different from surrounding grains based on nucleation and postsolidification processing effects. Grain size is a very important factor, because a finer grain structure provides higher strength and ductility. This situation is rather unique, because most other strengthening mechanisms result in decreased toughness. Strengthening by finer grain size is achieved, in part, by the increase in the amount of grain-boundary regions as the grain size is reduced. Grain boundaries are stronger than individual grains (when temperatures are below the so-called equicohesive temperature), and thus, a finer grain size imparts more grain-boundary regions for improved strength. Moreover, because a greater number of arbitrarily aligned grains are achieved when grain size is reduced, the stressed material has more opportunity to allow slip, thus improving ductility. In contrast, coarser-grain material tends to exhibit generally poorer mechanical properties (lower yield strength, higher ductile-brittle transition temperature, poorer long-life fatigue properties). Thus, grain size refinement provides a means for the materials engineer to increase both strength and ductility (toughness).

Effect of Strain Rate on Ductility

As previously noted, deformation and fracture behavior can be influenced by complex material, mechanical, and environmental conditions. In addition to the material condition, ductility is also greatly affected by the rate of deformation (i.e., strain rate). Slow strain rates enable rearrangement of complicated three-dimensional dislocations and thus permit more plasticity. In contrast, the rapid application of loads and high strain rates do not permit as much lattice reorganization, resulting in a tendency toward more brittle behavior during fracture. The effect of a higher strain rate on ductility is analogous to a decrease in temperature, as shown schematically in Fig. 11. At a higher strain rate, the transition to brittle fracture of a bcc metal occurs at a higher temperature (T2 in Fig. 11). Similarly, higher strain rates lower fracture toughness, as shown in Fig. 12. This illustrates the complexity of deformation and fracture behavior, because it is affected by material factors, strain rate, and temperature.

Effect of Texture

Texture, where the crystalline grains in a metal have a preferred orientation, can result in anisotropic elastic, plastic, and fracture mechanical properties as well as physical properties (electrical conductivity, magnetic behavior, etc.). The level of anisotropy from texture is dependent on the crystal structure and elemental composition and the specific preferred orientation that is present. Polycrystalline metals consist of many individual crystalline grains, which often are largely randomly oriented throughout the material. In such a case, isotropic mechanical properties on a macroscopic scale are expected with random grain orientations. However, if grains in a polycrystalline body are not randomly oriented (i.e., they have a preferred orientation or texture), the macroscopic properties can be anisotropic. The degree of anisotropy depends on the anisotropy of the single crystal and the amount of nonrandom grain orientation. In practical situations, anisotropy is created by three different mechanisms: texture, banding, and fibering. Texture is created by deformation systems in grains; banding is created by nonhomogeneous distribution of alloying elements and/or constituents. Fibering is created by the volume fraction, deformability, and distribution of inclusions in the material.

Anisotropy of mechanical and physical properties due to texture depends on whether strong textures can develop from mechanical and thermal processing. Textures tend to not develop strongly in polyphase alloys containing a large volume fraction of second phases or constituents. Thus, texture can develop more strongly in single-phase alloys used primarily for fabrication by plastic working (drawing and stretching, bending) and less strongly in hot working of a medium-carbon steel, which contains a large volume fraction of pearlite. Anisotropy of the yield strength due to texture is low for materials having a cubic lattice. Anisotropy of ductility is great enough that specific heat treating procedures are used to enhance the formability of materials used for stretching and deep drawing.

Texture can be developed (intentionally or unintentionally) to varying extents for different alloys by working and heat treatment. This grain texture can impart directionality of properties, especially ductility, toughness, and fatigue crack propagation rate. Also of considerable importance in commercial-quality materials, and especially those having a large volume fraction of second phases and/or inclusions, is the banding of compositional segregations and grain fibering in wrought forms. Banding gradients and grain fibering in wrought metals results in nonuniform distribution of inclusions and chemical segregations. In some alloys, chemical segregation can result in banding of microconstituents and greater anisotropy. Examples include bands of pearlite in annealed or hot rolled steels and ferrite stringers in austenitic stainless steels.

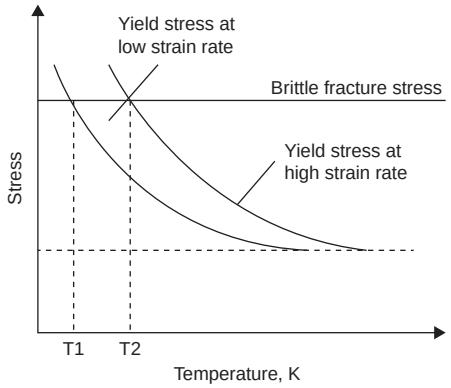

Fig. 11 Effect of strain rate on ductile-to-brittle transition temperature in body-centered cubic metals

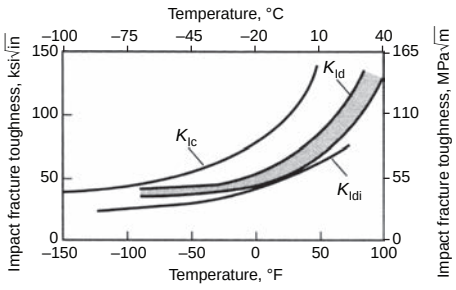

Fig. 12 Comparison of static (K_{Ic}), dynamic (K_{Id}), and dynamic-instrumented (K_{Idi}) impact fracture toughness of precracked specimens of ASTM A533 grade B steel as a function of test temperature. The stress-intensity rate was approximately 1.098×10^4 MPa$\sqrt{m} \cdot s^{-1}$ (10^4ksi$\sqrt{in.} \cdot s^{-1}$) for the dynamic tests and approximately 1.098×10^6MPa$\sqrt{m} \cdot s^{-1}$ (10^6ksi$\sqrt{in.} \cdot s^{-1}$) for the dynamic-instrumented tests.

Effect of Interstitial and Substitutional Alloying Elements

In addition, undesirable tramp (impurity) element atoms and intentional alloying element atoms are typically present in engineering materials. These atoms can occupy interstitial and substitutional positions in the crystal lattices, both of which result in lattice distortion and almost always provide strengthening, among many other effects. The short-range net effects of these atoms are typically to increase strength by resistance to slip. Intentional alloying to achieve these effects is referred to as solid-solution strengthening. Nonmetal atoms typically encourage brittleness more than metal atoms.

Microstructure

Long-range order in metals forms the matrix microstructure. The microstructure is dependent on the composition and processing, and many metals and alloys can exhibit a number of different structures at the same nominal composition, which is known as polymorphism. For example, some steels can contain a matrix microstructure of ferrite and pearlite, martensite, bainite, or a combination of these, based on thermal history. The strength and toughness of a material during fracture can be drastically different based on the microstructure. In the case of heat treated microstructures, tempering can reduce hardness and strength as well as either increase or decrease the toughness.

Although there are some exceptions, most metals of engineering significance are alloys rather than pure (unalloyed) metals. Solid-solution strengthening occurs with the homogeneous dispersion of solute atoms. However, uniform composition control is not usually possible with traditional cast and ingot-based processing of wrought metals, although more uniform composition control is the motivation for some powder metallurgy processing and additive manufacturing. Dendritically solidified metals exhibit microscopic and/or macroscopic gradients in composition concentrations, which may not be completely removed by deformation processing and thermal treatment. In rolled materials, this is known as banding, which occurs in the primary direction of hot work. An overload failure where banding was of primary importance is shown in Example 6.

Example 6: Failure of Brittle Lawn Mower Blades.

Mower blades made of grade 1566 high-manganese carbon steel failed a standard 90° bend test. The blades had been austempered and reportedly fractured in a brittle manner during testing. The austempering treatment is intended to result in a bainitic microstructure.

Investigation

The cross section of a representative blade that was heat treated but not bend tested is shown in Fig. 13(a). Substantial microstructural banding was apparent. The near-surface zone of the blade exhibited a thin layer of total decarburization and oxide formation. The typical core microstructure contained alternating bands of martensite and bainite, as shown in Fig. 13(b).

Conclusions and Recommendations

The nonuniform microstructure was likely responsible for the atypical brittle behavior of the blades. Much of the microstructure consisted of martensite, which is more brittle at the same hardness level than is lower bainite. The observed structure suggests that the austempering heat treatment was performed too close to the nominal martensite start temperature (M_s). Alternate bands of slightly different alloy composition, which resulted from rolling practice and are not unusual for this alloy, resulted in actual M_s temperatures above and below the nominal M_s temperature. Because it has been shown that the M_s is generally an inverse function of alloy content, the martensitic regions were lower alloy zones.

It was recommended that the austempering salt bath temperature be raised 55 °C (100 °F) in the future to account for the expected localized compositional variation.

Intentional Inclusions and Included Phases

When sufficient solute is present, various phases can form that exhibit a different crystalline structure from the matrix. A supersaturated solution can develop, and the excess solute forms a discrete, pure inclusion or second-phase particle. Processing and aging can also create precipitates of compositions that are favored by diffusion kinetics. Precipitates, whether within the grains or at the grain boundaries, tend to add strength by impeding dislocation motion. This is known as pinning. Grain-boundary regions are also a source of pinning, so precipitates in the grain boundaries may not add very much more pinning over that of the grain-boundary structure itself. Nonetheless, the basic intent of precipitation strengthening is to impede dislocation movement. Dispersion-strengthening processes, where very fine nonmetallic particles are mechanically added to a metal, are also done for this purpose.

Rounded precipitates and second-phase particles are often preferable from a ductility perspective. For example, graphite shape control is an essential factor in the ductility of cast irons, as shown in Example 7. Rounded carbides in spheroidized steels and rounded eutectic silicon in solution-annealed aluminum-silicon alloys are other examples of preferred shapes. A channel or trough-shaped ductile morphology is often produced in metals with elongated inclusions and is described as a "woody" fracture.

In some instances, clusters of inclusions can be segregated into lamellae, which can lower strength in the short-transverse direction, depending on the orientation of the lamellae. Additionally, separation during nonuniform heating, such as welding, can cause cracking identified as lamellar tearing. This is most often seen in thick rolled plates, where the beneficial mechanical disruption or breakup of midthickness nonmetallic inclusions does not occur to the same extent as outer regions during metalworking.

Example 7: Failure of a Ductile Iron Cone-Crusher Frame.

The upper frame from a large cone crusher failed in severe service after an unspecified service duration. The ductile iron casting was identified as grade 80-55-06, signifying minimum properties of 552 MPa (80 ksi) tensile strength, 379 MPa (55 ksi) yield strength, and 6% elongation.

Investigation

The upper frame supports the crusher bowl section and can be unevenly loaded during crushing. The fracture surface of the frame section received for analysis was obliterated by postfracture corrosion. Repeated attempts at cleaning using progressively stronger chemicals revealed that no telltale fracture morphology remained. The fracture occurred at a poorly radiused thickness transition, and the fracture surface was relatively rough. No gross casting imperfections were visually apparent.

The chemical composition satisfied the typical specifications for this cast iron grade. Although samples removed from a cast component may bear little relation to grade/condition determination based on separately poured test bars, mechanical properties were obtained for a specimen removed adjacent to the fracture. Test results from the specimen were 470 MPa (68 ksi) tensile strength, 370 MPa (54 ksi) yield strength, 1.5% elongation, and 1% reduction in area. The near-surface tensile strength and elongation were far below requirements, but the measured core hardness was within the center of the acceptance range.

Microstructural evaluation indicated that the casting surface at the fracture contained corrosion damage, inclusions, and incomplete nodulization of the graphite (Fig. 14a). The etched matrix is shown in Fig. 14(b). The core microstructure consisted of pearlite and bull's-eye ferrite, typical for this material, whereas the near-surface microstructure exhibited mixed graphite morphology. Many transgranular, secondary cracks were apparent next to the fracture surface. No carbides were observed.

Conclusions and Recommendations

The crusher frame failed via brittle overload fracture, likely due to excessive service stresses and substandard mechanical properties. Predominantly pearlitic ductile irons are very sensitive to a reduced degree of nodularity, which is exhibited as a significant reduction in strength and ductility.

Degenerate graphite forms are not unusual at the surfaces of very large castings. Additional quality-control measures were suggested to provide better spheroidal graphite morphology at the frame surface.

Volume and Nature of Inclusions

The volume percent or number of foreign particles as well as their shape and deformability index in a material alters the mechanical properties, because the load-bearing cross-sectional area is affected. Large numbers of desirable inclusions can provide benefits other than strength. Normal manganese sulfide inclusions provide excellent machinability because the stringers serve as chip-breakers. Naturally, these also decrease toughness and affect the level of anisotropy due to their elongated pancake shape and parallel orientation.

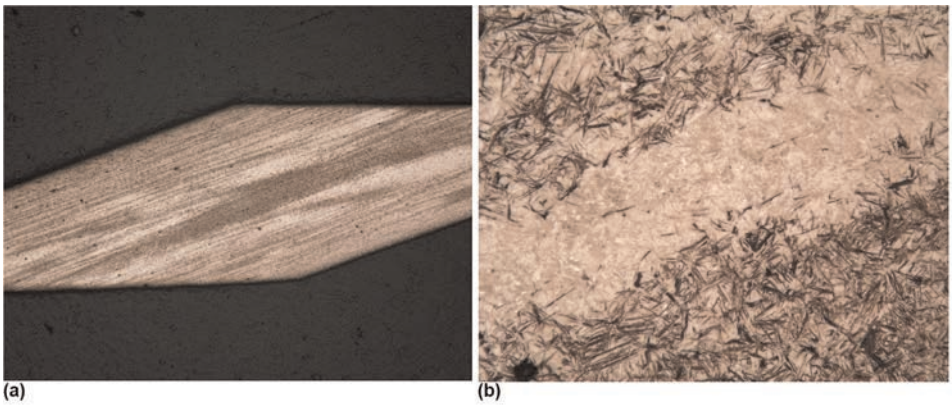

Fig. 13 Fracture of a brittle lawn mower blade (Example 6). (a) Low-magnification view of the formed blade showing substantial banding. 2% nital etch. Original magnification: 8.9×. (b) High-magnification view of the banding showing alternating tempered martensite (light) and bainite (dark). 2% nital etch. Original magnification: 196×

Inclusions and included phases share boundaries with the matrix that may or may not be approximate continuations of the surrounding matrix lattice. These interfacial boundaries are called coherent and incoherent boundaries, respectively. The level of coherency can dictate the relative ease at which microvoids or cracks can initiate at inclusion interfaces. High levels of coherency increase the likelihood that fractures in brittle inclusions or second phases will continue as cracks in the adjacent matrix.

Impurity Inclusions

Undesirable impurity inclusions can also be inherently ductile or brittle in character and can facilitate matrix cracking, as shown in Examples 8 and 9. In these cases, the properties of impurity inclusions compromised the toughness of the more ductile matrix. Continuous intergranular phases, such as brittle carbides, or ductile phases can promote brittle overload behavior via intergranular fracture and dimpled intergranular fracture, respectively. The net effect of many brittle phases is directly proportional to their relative level of continuity. It is the individual and combined effects of atomic structure, microstructure, shape and orientation, and phases present that determine the relative ductility or brittleness of a metallic material. All these variables are controlled by processing. However, service alteration is also possible in many circumstances, as discussed later in this article.

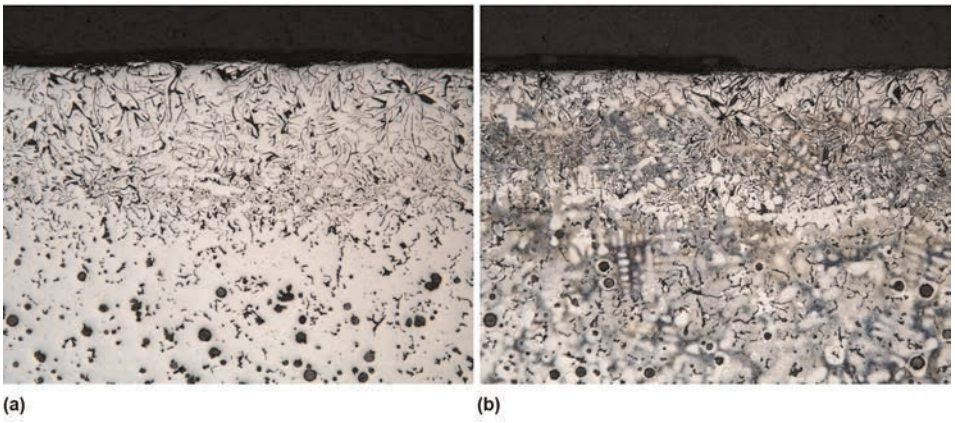

Fig. 14 Failure of a ductile iron cone-crusher frame (Example 7). (a) Near-surface microstructure of the frame showing degenerate graphite morphology rather than the intended nodular structure evident in the core. Unetched. Original magnification: 30×. (b) The typical frame microstructure also exhibits high levels of ferrite in the undercooled surface graphite. 2% nital etch. Original magnification: 30×

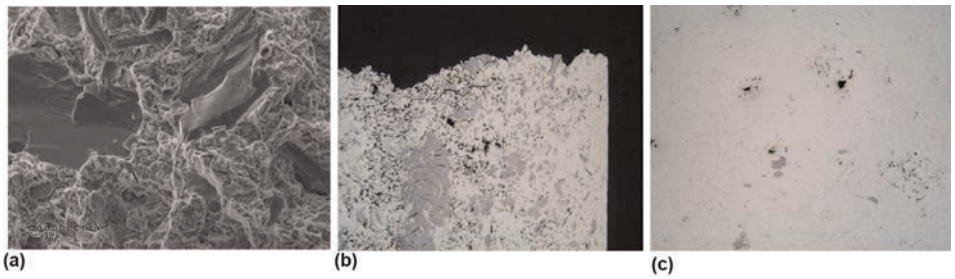

Fig. 15 Brittle overload of a die-cast zinc snow-thrower adapter (Example 8). (a) Fracture surface of failed zinc casting contained many large, brittle constituents. Energy-dispersive spectroscopy analysis revealed these were high-iron-content inclusions. Scanning electron micrograph. Original magnification: 178×. (b) Microstructure of the failed casting showing massive, cracked inclusions and shrinkage. Unetched. Original magnification: 30×. (c) Microstructure of an exemplar zinc casting showing fewer, finer inclusions and less shrinkage porosity. Unetched. Original magnification: 30×

Example 8: Brittle Overload Failure of Die-Cast Zinc Snow-Thrower Adapters.

A die-cast zinc adapter used in a snow-thrower application failed catastrophically in a brittle overload manner. The mechanical properties and alloy designation were not specified. An exemplar casting from a lot known to be acceptable was provided for comparison purposes.

Investigation

The macroscopic fracture features, even in lab fracture regions, appeared brittle. Substantial shrinkage porosity was also apparent within the casting wall on the fracture surface. Scanning electron microscope examination of the fracture surface revealed transgranular brittle features and secondary cracking through platelike inclusions (Fig. 15a). Energy-dispersive x-ray spectroscopy analysis revealed that the platelike inclusions were high in iron content. A small, relative proportion of the overload fracture features appeared to be dimple rupture, and the porosity exhibited a dendritically solidified appearance.

Chemical analysis revealed a chemical composition similar to that for a standard zinc alloy ZA-27 (UNS Z35840), but the iron content was much higher than specified, and the copper content was slightly lower than specified. The measured hardness of the failed casting in a region without porosity was 109 HB, whereas the exemplar casting was 89 HB.

Metallographic cross sections through a representative region of the fractured casting and an analogous region of the exemplar casting are shown in Fig. 15(b) and (c), respectively. Gross and fine porosity were evident in some regions of the failed casting. Scanning electron microscope examination showed the microstructure contained an abundance of blocky iron-zinc platelets, many of which near the fracture exhibited cracking, indicating that this phase was hard and brittle. The exemplar casting did not contain a significant amount of the brittle phase, suggesting a lower iron content. Less porosity was also apparent in the exemplar die casting.

Conclusions

It was concluded that the casting failed as a result of brittle overload fracture due to excessive levels of an iron-zinc phase and gross porosity. These conditions acted synergistically to reduce the strength of the material. The composition was nonstandard, and the inherent brittleness suggests that it is unlikely that this material was an intentional proprietary alloy.

Example 9: Fracture of a Cast Steel Bracket.

A cast steel bracket manufactured in accordance with ASTM A148 grade 135/125 failed in railroad maintenance service. Ancillary property requirements included a 285 to 331 HB hardness range and minimum impact energy of 27 J (20 ft · lbf) at −40 °C (−40 °F). The conditions at the time of failure were characterized as relatively cold.

Investigation

The bracket fractured catastrophically and exhibited no plastic deformation within the region containing several exterior fracture origins. The shiny macroscopic features were suggestive of microshrinkage and brittle overload fracture. Scanning electron microscope examination revealed primarily cleavage fracture features between dendritic shrinkage porosity and brittle fracture through inclusion troughs. Fracture had apparently occurred

below the ductile-to-brittle transition temperature for this material.

The molybdenum, cobalt, and vanadium contents all exceeded the specification limits, and the sulfur content was near the maximum allowable. The aluminum content was relatively low, and the tensile strength appeared to be substantially lower than specified. The casting was very brittle, and shrinkage was apparent on the tensile specimen fracture surfaces. The impact strength was very low at the specified test temperature.

The typical microstructure is shown in Fig. 16(a) and (b). The casting exhibited a tempered martensite microstructure with massive, eutectic type II manganese sulfide (MnS) stringer inclusions at the prior-austenite grain boundaries. These are characteristically more embrittling than the globular type I manganese sulfides. It was considered probable that grain-boundary formation of aluminum nitride contributed to the failure, but the presence of this nonmetallic compound is often difficult to verify.

Conclusions and Recommendations

The bracket failed through brittle overload fracture due to a number of synergistic characteristics. The quenched-and-tempered microstructure contained solidification shrinkage, inherently poor ductility, and type II MnS inclusions that are known to reduce ductility. Macro- and microscale fracture features confirmed that the casting was likely in low-temperature service at the time of failure, potentially below the ductile-to-brittle transition temperature of the material. The composition and mechanical properties of the casting did not satisfy the design requirements.

It was recommended that better composition control be exerted, primarily with regard to melting, deoxidation, and nitrogen control. Better deoxidation practice would be recommended to generate the more desirable MnS inclusion morphology. Reevaluation of the casting design to minimize shrinkage would also be beneficial.

Temperature Effects

Temperature is one of the most important extrinsic variables that influence the mechanical behavior of materials. As previously noted, the temperature dependence of the mechanical properties of fcc materials is quite distinct from those of bcc materials. This dissimilar behavior is related in part to the nature of dislocation motion within the individual crystal lattices, and fcc metals exhibit plastic deformation and ductile fracture mechanisms even as temperatures are lowered. This general difference in the temperature-dependent mechanical behavior for fcc and bcc metals is shown in the deformation behavior maps of Fig. 17(a) and (b).

Figure 17 is for annealed unalloyed metals, and it illustrates general differences. The ultimate tensile strengths of fcc metals have stronger temperature dependence than those of bcc metals. However, the variation of yield strength with temperature of fcc metals is not as pronounced as for bcc metals. Characteristics can be altered with alloying, but the general trends remain relatively consistent. For example, solid-solution strengthening typically increases the yield strength and ultimate tensile strength while also increasing the temperature dependence of yield strength of fcc alloys. However, the temperature dependence of ultimate tensile strength is still greater than that of yield strength, thus allowing ductile behavior in fcc alloys.

The ductility of fcc metals is also evident in terms of toughness at low temperature, as shown in Fig. 18. This is why fcc metals such as austenitic stainless steels and aluminum alloys are used extensively in cryogenic applications. However, it is important to note that some metallurgical transformations at low temperature can alter the structure. For example, some austenitic steels are susceptible to martensitic transformation at cryogenic temperatures (Ref 2), which can lead to low-temperature embrittlement and brittle fracture.

Low Temperature

In general, lowering the temperature of a solid increases its flow strength and fracture strength. At low temperatures, the thermal activation of dislocations is reduced; therefore, more applied stress is required for deformation. This inverse proportionality is generally true and is also applicable to nonmetallic materials such as polymers and ceramics. The primary exceptions to the inverse proportionality are the result of a wide variety of microstructural alterations and other alloy-specific changes. These changes are dictated by the desirable minimization of free energy in whatever manner it can be achieved. Spontaneous isothermal phase changes can affect ductility as operating temperature is decreased. There are relatively few engineering alloys that

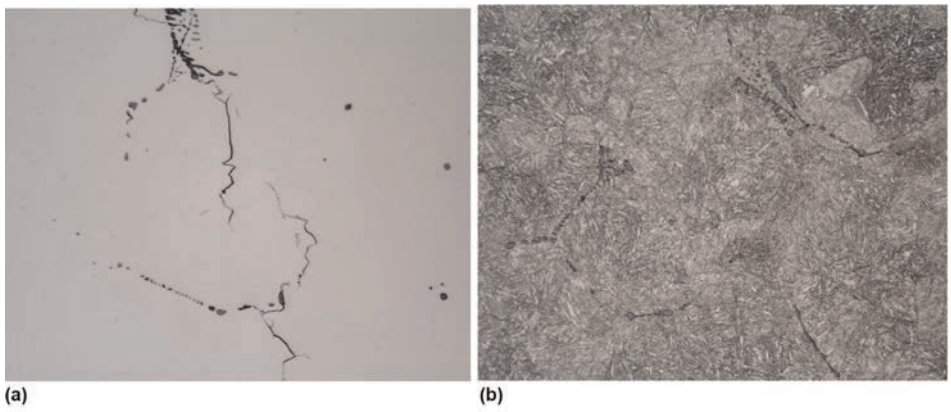

Fig. 16 Fracture of a cast steel bracket (Example 9). (a) Bracket microstructure exhibiting gross type II manganese sulfide stringer inclusions. Unetched. Original magnification: 119×. (b) The microstructure consisted of tempered martensite, with the inclusions likely present at the prior-austenite grain boundaries. 2% nital etch. Original magnification: 119×

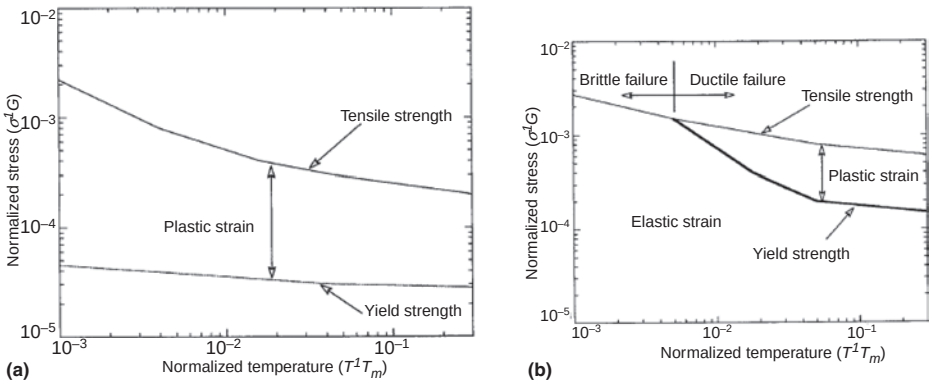

Fig. 17 Simplified deformation behavior (Ashby) maps of unalloyed annealed metals with (a) face-centered cubic crystal structure and (b) body-centered cubic crystal structure. Engineering alloys may behave somewhat differently than unalloyed metals, but these general trends are relatively consistent (see text). Source: Ref 2

undergo phase changes at cryogenic temperatures or at room temperature, although as noted, some austenitic steels are susceptible to martensitic transformation and embrittlement at low temperature. Some effects such as aging, or precipitation hardening, can occur at room temperature or lower. Low temperatures can also retard other processes. For example, the so-called "icebox" rivets often used in aerospace applications are solution-annealed aluminum rivets (typically alloys 2017 and 2024) that must be stored at low temperature prior to installation. After they are driven, the rivets naturally age to the desired moderate-strength T4 temper condition.

Ductile-to-Brittle Transition

This is the well-known drop in ductility and toughness of some metals with decreasing temperature. The ductile-to-brittle transition temperature (DBTT) refers to the region in which the toughness drops and the fracture mechanisms and features change from ductile to brittle (Fig. 17b and Fig. 18). This transition is between dimple rupture and transgranular or intergranular brittle features. This transition is primarily evident in bcc and hcp metals, but it is somewhat analogous to the glass-transition temperature evinced by polymeric materials. Metals that have a high-yield-strength sensitivity to temperature fluctuation exhibit a DBTT. Many factors affect the transition temperature, including the grain size and strain rate. An increase in grain diameter raises the DBTT (Fig. 19), as does an increase in loading rate (Fig. 11). Some elements, such as nickel and manganese, can reduce the DBTT.

Changes in toughness as a function of temperature are quantified by a number of different measures, which are used in materials evaluation, design, and failure analysis. In particular, dynamic fracture toughness of engineering alloys as a function of temperature is evaluated by various methods of impact testing and instrumented drop-weight testing (see the article "Impact Toughness Testing" in *Mechanical Testing and Evaluation*, Volume 8 of the *ASM Handbook*, 2000). Measurement of dynamic fracture toughness is important, because many structural components are subjected to high loading rates during service or must survive high loading rates during potential accident conditions. Furthermore, because dynamic fracture toughness is generally lower than static toughness, impact toughness testing can be a more conservative measure of toughness under dynamic conditions. However, measurement of dynamic fracture toughness is more complex than quasi-static (e.g., K_{Ic}) toughness. Impact toughness tests, such as the Charpy test, are only a qualitative measure for materials evaluation. Results from impact toughness on laboratory specimens cannot be used for quantitative design of components, because results depend on specimen size. In contrast, results from fracture-mechanics testing (e.g., K_{Ic} or K_{Id} under dynamic conditions) do scale.

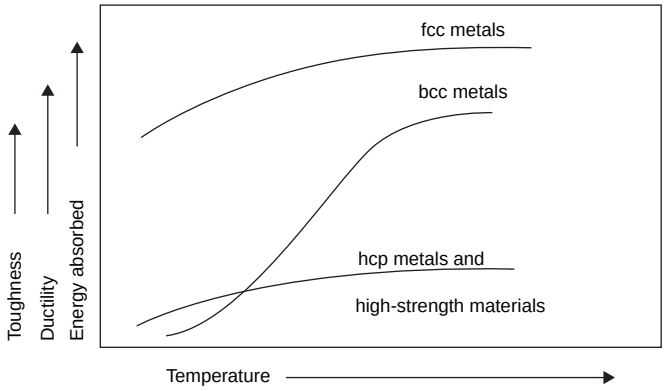

Fig. 18 Effect of temperature on toughness and ductility of face-centered cubic (fcc), body-centered cubic (bcc), and hexagonal close-packed (hcp) metals

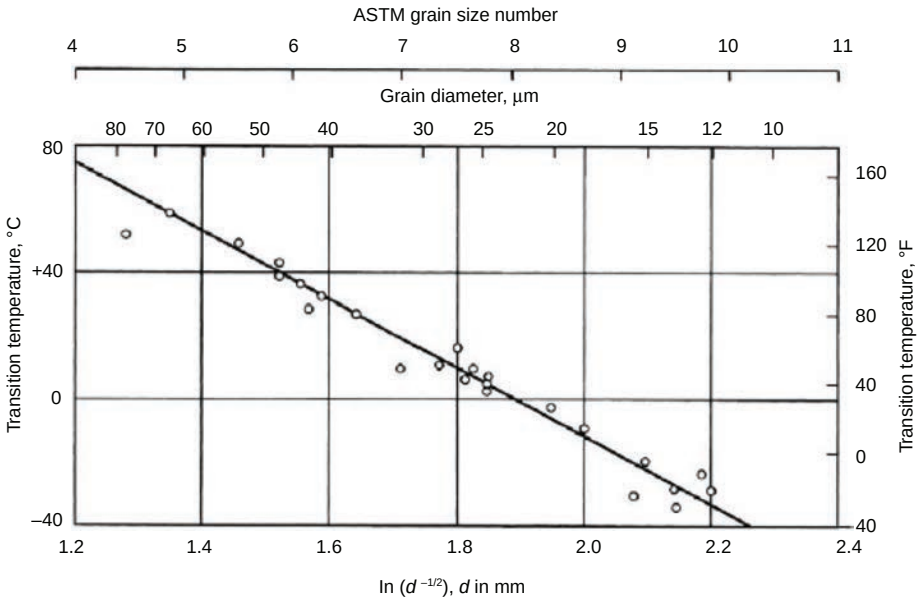

Fig. 19 Effect of grain size on the ductile-to-brittle transition temperature of 0.11% C mild steel. Source: Ref 3

Nonetheless, impact toughness testing such as the Charpy test does provide a useful way to screen and evaluate materials. Several types of criteria are used to evaluate the effect of temperature on toughness from impact testing. For example, impact testing over a spectrum of test temperatures is commonly done to determine the effects of temperature and the DBTT region of bcc metals. Other evaluation criteria include:

- *Nil ductility transition temperature:* usually measured by drop-weight test and based on a crack/no crack criterion
- *Fracture appearance transition temperature:* a measure of the percentage of shear morphology measured on impact specimens

The upper- and lower-shelf regions and the transition zone can be identified by impact testing at a variety of temperatures and comparing the impact energy, the shear percentage, the lateral expansion, or all three. Regardless of the test procedure or the method used to define the DBTT transition, results depend on the metal and loading conditions and strain rate. Many design criteria use a standard but arbitrarily selected impact energy value, for example, 20 J (15 ft · lbf), in some cases to empirically specify the gradual change in toughness with temperature of a material when determining suitability for service.

Many catastrophic brittle failures are associated with the reduction of toughness at low temperatures. The Liberty ships of World War II are well-known examples. Of the 4694 ships considered in the final investigation, 24 sustained complete fracture of the strength deck, and 12 ships were either lost or broke in two. In this case, the need for tougher structural steel was even more critical,

because welded construction was used in shipbuilding instead of riveted plate. In riveted-plate construction, a running crack must reinitiate every time it runs out of a plate. Similar long brittle cracks are less likely or rare in riveted ships, which were predominant prior to welded construction (although even some riveted ships have provided historical examples of long brittle fracture due, in part, to low toughness).

Low notch toughness is a more critical factor for long brittle cracks in welded ships, because the fabricated structure provides a continuous path for brittle cracking. For example, the fracture origins in the Liberty ships were at weld discontinuities, and unstable crack propagation resulted in brittle fracture of entire welded ship structures. The existence of coarse pearlitic structure (from furnace-cooled plate) was the basis for the brittle structural failures experienced by the ships, which split decks even while at dockside (for example, see Fig. 1 in the article "Failures Related to Welding" in *Failure Analysis and Prevention*, Volume 11 of the *ASM Handbook*, 2002). The cracking was minimized by specifying normalized plate, which had fine-grain pearlite microstructure, which is much more tolerant of weld discontinuities than coarse pearlite formed by furnace cooling. Low temperatures at or below the transition temperature of the steel was also a factor in these failures.

Elevated Temperature

Generally, increasing the processing or operating temperature will initially result in a decrease in mechanical strength and an increase in ductility. Hot working takes advantage of this extreme plastic behavior. The simultaneous relaxation of deformation stresses also results in the suppression of nucleated microvoids, permitting more reduction without fracture than possible during cold deformation. It should also be noted that the alloy-dependent drop in the elastic modulus with temperature limits the materials suitable for high-temperature service.

All metals exhibit an elevated-temperature transition from normal overload morphology to brittle intergranular fracture (with an accompanying loss in toughness and ductility). At this temperature, the strength of the grains and the grain boundaries is equal; therefore, this is often identified as the equicohesive temperature (ECT). Similar to the DBTT, the ECT is affected by material characteristics and loading conditions. The ECT is equivalent to the recrystallization temperature. There are so many variables that affect the ECT that quantification of an actual temperature is possible for only a specific set of conditions and may not be useful.

Heat treatment is performed to achieve desired mechanical properties by precipitation, recovery, formation of desirable matrix microstructure and included phases, grain refinement, and homogenization. Excessive time at temperature, primarily in high-temperature service, can cause undesirable diffusion of alloying elements, formation of deleterious phases, grain growth, and many other changes. All changes affect overload behavior. At even higher temperatures, the mechanical properties of a metal are compromised as the melting point is approached.

On heating and cooling, the normal expansion and contraction stresses due to thermal gradients are complicated by the volumetric changes accompanying crystalline structure and phase changes. Metals can exhibit allotropic transformations, where different crystalline structures are evident in the material based on whether they are above or below a critical temperature. In steels, for example, normal bcc ferrite changes to fcc austenite on heating above the Ac_3 temperature. The stresses accompanying phase changes can result in brittle fracture such as hot cracking, cold cracking, and quench cracking, as detailed in the embrittlement section of this article.

Effects of Mechanical Loading

Overload failures, by definition, are incidents in which the stress state of the component at the time of fracture is of primary concern to the failure analyst. The type and magnitude of stresses placed on a part in service must be considered, together with the physical and analytical evidence, to identify the cause(s) of the failure. Loading information is usually available in the engineering design specifications, but much can be logically inferred by analysis alone. It is not unusual for the results of a failure investigation to suggest the actual service stresses were drastically different from those anticipated during original design.

Brittle and ductile overload failures can occur simply as a result of insufficient strength for the applied forces. This can be due to either underdesign or incorrect material use. Design faults can result from inaccurate determination of the forces that would be applied to a component in service. The type, magnitude, and application of the stress can be miscalculated, such as anticipating purely static tensile forces when cyclic impact actually occurs. The materials selection process is then based on flawed assumptions, and an inappropriate material or material condition is selected. Overload failure can also be due to extreme loading, which could not have been logically foreseen during design, such as intentional misuse or abuse.

In some cases, the wrong material or material condition is inadvertently used. Deviation from the correct material specification can be subtle or profound. Subtle deviation can result in reduced service life or distortion, whereas profound deviation from the specified material can result in cracking or fracture. Underdesign, poor-quality materials, improper heat treatment, and incorrect processing are often encountered in metallurgical failure analyses. Due to the differences in corrective actions typically employed, embrittlement-related failures are not typically considered underdesigned.

Overload failures due to underdesign are uncommon. This is primarily due to the current state of engineering design expertise, which has grown through analysis of past failures and applied mechanical testing. The use of design safety factors also reduces the frequency of underdesign failures. Design review is another method of preventing failure. Design reviews can also be part of the failure analysis process (for example, see the article "Design Review for Failure Analysis and Prevention" in *Failure Analysis and Prevention*, Volume 11 of the *ASM Handbook*, 2002). In some cases, materials failure analysis is also done first to identify potential materials- or manufacturing-related causes. If nothing is evident from this stage of the investigation, then the evaluation of causes could require a design review, which can include stress analysis by traditional techniques, finite-element analysis, and/or fracture mechanics. These techniques are discussed at length elsewhere in this Volume.

Stress Conditions

Stress Type

The type of stress applied to a component is of interest to the failure analyst, because it will help to explain the fracture features, fracture location, and many other attendant characteristics. Stresses are usually identified as tension, compression, or shear (i.e., the state of stress at a point is defined in terms of three normal orthogonal components and six shear components). The loading, which produces the stresses in particular regions of a component, can be pure tension, pure compression, pure bending, pure torsion, or some combination of these. External loading conditions, component geometry, and the presence of cracklike imperfections control the internal state of stress. Complex stress states can occur when components are not loaded uniformly and/or when geometric factors cause regions of stress concentration. An overload failure that occurred under a complicated stress state is presented in Example 10.

The stress states in a component often contain a hydrostatic component, that is, the mean of the three normal stresses at any point. A compressive hydrostatic stress is often less of a concern in metals than a tensile hydrostatic stress. A tension hydrostatic stress promotes brittle fracture because the maximum shear stress, which is a function of the difference in the principal stresses, is decreased by hydrostatic tension. One observes shear lips at the surface of a cross section because plane stress exists there; that is, one of the principal stresses is zero at the surface. Triaxial tension is promoted by notches and so forth, due to the constraint exercised by the surrounding

material away from the stress concentrator. Thus, plane-strain deformation (in which a hydrostatic stress is present) results in fracture that is macroscale brittle. The microscale appearance can be either ductile (i.e., MVC) or brittle (cleavage, mixed mode). This state can prevent yielding by dislocation slip in the preferred directions, thereby encouraging brittle fracture during overloading. However, the effect of a hydrostatic stress component on the total stress state is usually discussed in terms of macroscopic appearances; on a microscopic scale in a polycrystalline body, the local stresses can still cause some dislocation motion.

When a discontinuity or cracklike imperfection is present in a material, the magnitude of the hydrostatic stress increases as the section thickness increases, and fracture is more brittle with a mode of plane-strain fracture. Thick materials can exhibit low toughness and generally flat fracture features (although the microscopic features and mechanisms can be either MVC or cleavage). Additionally, heavy sections typically have a nonconstant microstructure through the thickness, with poorer properties at midthickness. Thin materials, or situations when cracks approach free surfaces to approximate thin materials, deform (neck) and are thus in a plane-stress state. This permits ductile fracture manifested by a shear lip at the edges of fractures and at the final fracture location under plane-stress conditions. Materials can exhibit a geometrical transition from plane-strain to plane-stress behavior analogous to a temperature transition. The various transitions evidenced by metals are not mutually exclusive occurrences.

Stress Magnitude

The magnitude of the applied and residual stresses is also an important part of an overload failure. When an overload fracture has occurred, as indicated by the physical evidence, the actual magnitude of the stresses must have been sufficient to initiate fracture; that is, the stresses applied to the material that fractured exceeded the capacity of that specific material. Mechanical testing is often an integral portion of a failure analysis investigation to determine whether the stresses were excessive, whether the part or material was weak, or both. The magnitude of applied stress is usually compared to the material yield strength in distortion failures and to the material fracture strength in the cases of ductile and brittle overload fractures. The failure analyst also compares these values to what the designer anticipated for service stresses and material properties.

Stress Application

To develop a complete understanding of the forces on a failed component, the analyst must consider the application of stresses. Loading can be constant or cyclic, slow or rapid, concentrated or distributed, or any mixture of these, and thus, different internal stresses occur at different locations and/or at different points in time. Failure initiates where the *local* stress exceeds the *local* strength. Materials exhibit differing overload failure characteristics based on these stress application variables. Cyclic loading most often results in fatigue failures rather than overload failures. A delayed overload fracture in a cyclic application suggests an unusual loading event or that embrittlement of the material has occurred. Progressive fracture features in a statically loaded component may suggest a corrosion mechanism.

Example 10: Failure of a Jack Cylinder.

A jack cylinder split open during simulated service testing (Fig. 20a). The intended internal test pressurization was reportedly analogous to typical service. The material and mechanical properties of the cylinder pipe were unknown.

Investigation

The single-event crack was longitudinal and bulged noticeably in its center. The crack center, which was identified as the likely crack origin, is shown after excision in Fig. 20(b). The surfaces were relatively flat, but they exhibited angled shear lips at the inside- and outside-diameter surfaces. Visible chevron markings pointed back to the origin in the center of the bulged cylinder. Fractographic examination revealed cleavage and dimple-rupture features throughout the flat-fracture region and shear-lip region, respectively.

Chemical analysis indicated that the pipe satisfied the requirements for a grade 1045 medium-carbon, plain carbon steel. Tension testing of a specimen removed from the pipe section opposite the crack revealed 779 MPa (113 ksi) tensile strength, 634 MPa (92 ksi) yield strength, and 12% elongation.

Microstructural examination confirmed the crack surface profile with somewhat flat fracture in the core with shear lips. The near-surface grains were severely distorted. The inside-diameter shear lip is shown in Fig. 20(c). The microstructure away from the crack consisted of cold-worked ferrite and pearlite, suggestive of the normalized condition. Surface decarburization and oxide formation were evident on the pipe surfaces.

Conclusions and Recommendations

The cylinder pipe burst in a mixed brittle and ductile manner due to overpressurization. The bearing strength of the pipe was likely to be slightly compromised by a low-strength layer of decarburization. The pipe was a moderately cold-worked plain carbon steel.

The analysis results indicated that the testing procedure should be evaluated for the possibility of inadvertent overpressurization. If no accidental burst could occur with the test configuration, it may be necessary to analyze successfully tested cylinders to identify changes in material, and perhaps heat treatment, which may have contributed to this failure.

Residual Stresses

Residual tensile stresses can be present in components, resulting from welding, casting, heat treatment, and grinding as well as other manufacturing and assembly processes. In many cases, residual stresses can be additive to applied stresses and thereby contribute to overload failure. Hot working allows immediate stress relaxation, but cold working does not. Cold working is a strengthening mechanism for many materials, including those that may otherwise have been heat treated to achieve the necessary strength level. In wrought aluminum, for example, the "H" temper designations indicate cold-work strengthening, whereas the "T" tempers indicate heat treatment with or without cold-work strengthening. Some strain-hardened alloys (especially those of aluminum) can exhibit a spontaneous decrease in strength due to recrystallization, sometimes referred to as age softening.

Residual compressive stresses at the surface, induced by processes such as shot peening and some surface-hardening treatments such as carburization in steels, are generally considered beneficial, both in overload and fatigue resistance. However, the effects of the surface treatment can be overcome if stress concentrators, corrosion, and similar effects penetrate the compressive stress layer. Even after surface treatments, there is still a subsurface

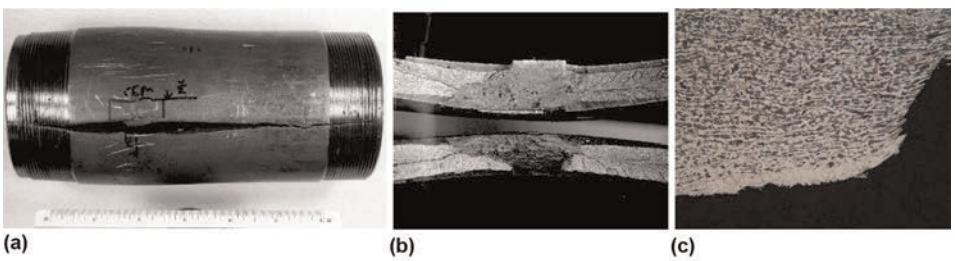

Fig. 20 Failure of a jack cylinder (Example 10). (a) Cylinder that split during testing. Substantial bulging is apparent at the failure location. (b) Opened crack surfaces from the cylinder in (a). Both the inside- and outside-diameter surfaces exhibited a shear-lip appearance. (c) Metallographic cross section near the inside-diameter surface showing decarburization and a shear lip. 2% nital etch. Original magnification: 119×

tensile stress under the compressive stress layer. Thus, the residual compressive surface stress is especially beneficial in delaying fatigue crack initiation at the surface, but it has little or no influence during the stage of critical (unstable) crack propagation.

Stress Concentration and Defects

Good engineering designs, even when encompassing quality standards, cannot totally prevent the presence of inadvertent discontinuities. These deleterious discontinuities can be present as casting and forging imperfections, thermomechanical processing cracks, welding anomalies of all types, and others. These features can serve as stress raisers and can impart brittle character. A failure resulting from an undetected crack is presented in Example 11.

Even in enlightened engineering design, where a proper fracture-mechanics approach considers the imperfections that are most assuredly present, unexpected stress concentrators can cause failure. It is not always feasible to create components without the possibility of inadvertent scratches, nicks, and gouges. All manufacturing processes contain variability that must be understood and monitored, if not controlled. For these reasons, the level of inspection and nondestructive examination applied to a component is usually a measure of its criticality and the consequences of its failure. *However, the designer should anticipate the types of imperfections likely to be present, and the manufacturing process should include controls and inspections to ensure that the design allowables are not exceeded.*

Example 11: Failure of Tension Springs during Installation.

Two large tension springs fractured during installation. The springs were manufactured from a grade 9254 chromium-silicon alloy steel spring wire. The associated material specification allows wire in the cold-drawn or oil-tempered (quenched-and-tempered) condition. The specified wire tensile strength range was 1689 to 1793 MPa (245 to 260 ksi). The finished springs were to be shot peened for greater fatigue resistance.

Investigation

The springs fractured within the coils rather than at the end hooks, where fatigue fracture often occurs. The springs were painted black. Examination of the fracture locations revealed that the features were similar and both springs contained a discolored precracked region. A representative fracture surface is shown in Fig. 21(a). No additional cracks were observed.

The chemical composition of the tested spring satisfied the specification requirements. Energy-dispersive x-ray analysis of the discolored precracked region detected a very high level of phosphorus, suggestive of a phosphate coating applied prior to painting. This tenacious contamination could not be removed by chemical means, which were limited to minimize the potential for damage to the remaining fracture features. Scanning electron microscope examination did not reveal discernible fracture features in the precrack zone, but the remainder of the fracture consisted of dimple-rupture evidence.

A longitudinal metallographic cross section through the wire in Fig. 21(a) is shown in Fig. 21(b). The precrack region is toward the left of this micrograph. Some transgranular, secondary cracking was apparent near the surface. The near-surface microstructure consisted of tempered martensite, but some partial decarburization and corrosion pits were evident at the wire surface. The surface did not appear to have been shot peened.

The Knoop microindentation hardness of the wire averaged 591 HK (500 gram force). This equates to an approximate ultimate tensile strength slightly higher than the specified range.

Conclusions and Recommendations

The springs failed during installation due to the presence of preexisting defects. The crack surfaces were corroded and phosphate coated, confirming that cracking occurred during manufacture. Installation, which presumably entailed some axial extension, resulted in ductile overload failure at the crack sites.

The manufacturing steps should be evaluated to identify the process(es) wherein the cracking is likely occurring. The spring-coiling process was of particular interest due to the appearance of the cracks. It was further recommended that a suitable nondestructive method such as magnetic-particle inspection be implemented.

Service Damage or Alteration

Overload failures can result from service damage such as mechanical alteration of the material by dynamic loading or distortion or progressive forms of damage by corrosion, wear, and subcritical crack growth. Damage can result in a net-section instability from a reduction in section size, or it can result in a critical crack size that leads to overload. In addition, parts that are dynamically loaded or deflected can experience strain hardening to an extent based on the material and loading characteristics. Some materials are also sensitive to the rate of load application and can be altered by strain-rate hardening. Mechanical twinning occurs in some alloy systems. These effects can change the ductility substantially, but fatigue cracking results more often than overload failure, because these hardening effects are often gradual.

More severe mechanical alteration can result in buckling and distortion effects. Plastic deformation and elastic instability, such as buckling, can create a site for stress concentration. Localized tensile or compressive yielding creates microvoids that can reduce the mechanical strength and the fatigue resistance. Loading history can also significantly alter the load-bearing characteristics of a component. For example, compressive yielding can result in a reduced elastic modulus upon subsequent tension testing. This phenomenon is called the Bauschinger effect, and the softening effect is shown in Fig. 22.

Progressive forms of damage can also lead to overload failure by unstable cracking from a discontinuity or, in the absence of a critical crack size, processes that reduce the effective cross section. In static-loading applications, overload failure is the likely consequence, while cyclic loading with corrosion or wear damage is more complex. In damage situations, it is imperative that the relative importance of the damage to the component be determined during the metallurgical failure analysis investigation. For instance, ductile overload failure with relatively little preexistent corrosion damage can suggest a severe loading event occurred and that the corrosion was of little consequence. When the damage is the proximate cause of a failure, such as abrasive wear or pitting corrosion, it is disingenuous to identify it as an overload failure, although overloading certainly occurred at the time of final separation. Somewhat severe

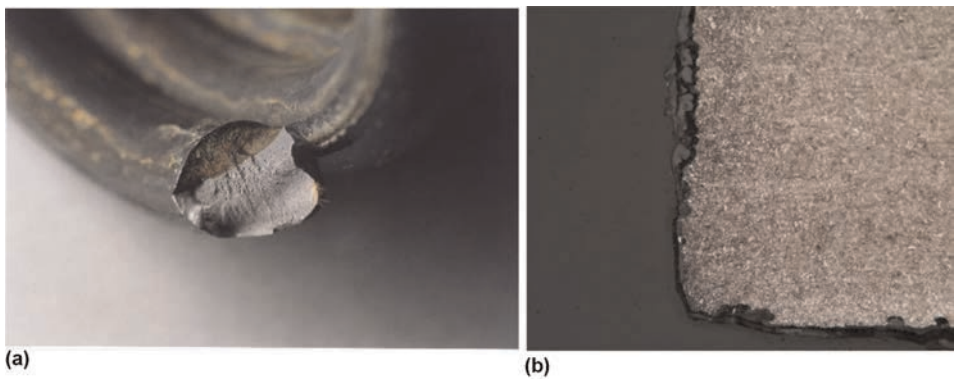

Fig. 21 Failure of tension springs (Example 11). (a) Spring fracture surface showing the presence of a discolored precrack region. Original magnification: 3×. (b) Cross section through the precracked region of the spring revealing a thick scale (vertical surface) on the fracture surface. 2% nital etch. Original magnification: 148×

mechanical alteration that occurred by an abused piece of coal mining equipment is shown in Fig. 23. Continued abrasion distortion of the near-surface material occurred after cracking. In the most severe cases of mechanical alteration during service, cracks are formed and can possibly lead to failure.

Embrittlement of Metallic Materials

Many engineering alloys are susceptible to embrittlement from specific mechanisms manifested during heat treatment, processing, storage, and service. The specific causes of embrittlement vary, depending on the metallurgical stability of the specific type or family of alloy under various manufacturing or service conditions. However, in general, embrittlement of metals is typically activated by thermal or environmental conditions, as described further in this section. Many types of embrittlement have been identified for ferrous and nonferrous metals. A greater number of embrittling phenomena are presented in this article for steels, because their varying service conditions have revealed numerous conditions for embrittlement. Table 3 provides a brief summary of many types of metallic embrittlement. Embrittlement phenomena of steels also are discussed in greater depth in the article "Embrittlement of Steels" in *Properties and Selection: Irons, Steels, and High-Performance Alloys*, Volume 1 of the *ASM Handbook*, 1990 (Ref 4). Similar content is also provided in the article "Visual Examination and Light Microscopy" in *Fractography*, Volume 12 of the *ASM Handbook*, 1987 (Ref 5).

This article focuses primarily on the contribution of embrittlement to overload failure. The following sections describe a number of thermally and environmentally induced embrittlement effects that can alter the overload fracture behavior of metals. Most of these are embrittling phenomena, where normally ductile materials evince brittle characteristics. These phenomena are described and differentiated by their causes, effects, and remedial methods, so that failure characteristics can be directly compared during practical failure investigation. For the purposes of failure prevention, possible steps for failure avoidance or component remediation augment the diagnostic information. When embrittlement includes crack formation, this usually renders a component unusable, especially in cyclic service. Cracks can become quiescent, under null or very low loading, but their presence remains and can be a future source of crack propagation.

Thermally Induced Embrittlement

Strain-Age Embrittlement

If low-carbon steel is deformed, its hardness and strength will increase upon aging at room or slightly elevated temperature. Strain-age embrittlement or strain-age cracking occurs when uncombined interstitial solute atoms, usually carbon and nitrogen, diffuse to dislocations and lattice discontinuities. The ordering of carbon and nitrogen atoms at the dislocations assists in the pinning of dislocations and

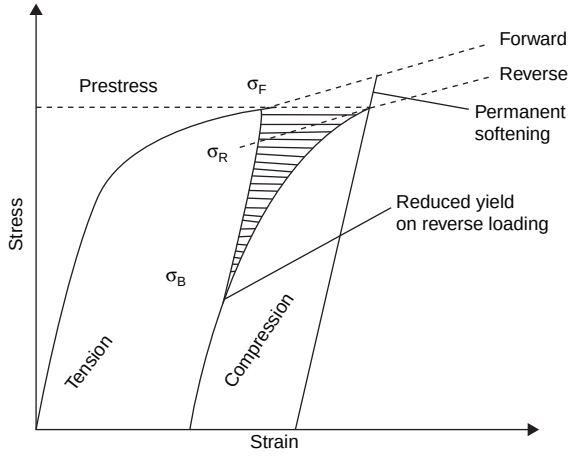

Fig. 22 Bauschinger effect. The softening effect is exaggerated for clarity. σ_F, forward stress; σ_R, reverse stress; σ_B, backward stress

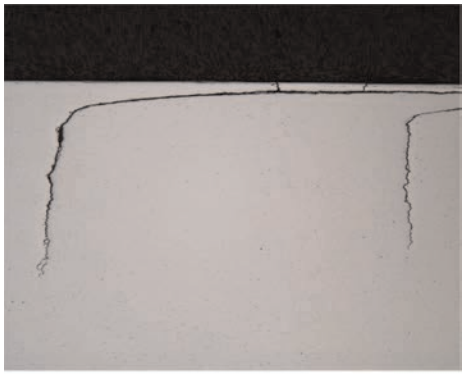

Fig. 23 Near-surface cracking present on a heavily abraded mining component. Continued abrasion after intergranular crack formation has deflected the perpendicular cracks. Unetched. Original magnification: 30×

Table 3 Types of embrittlement experienced by ferrous alloys

Embrittlement type	Susceptible steels	Causes	Result
Strain-age embrittlement	Low-carbon steel	Precipitation after deformation processing	Strength increase, ductility decrease
Quench-age embrittlement	Low-carbon steel	Quenching followed by precipitation	Strength increase, ductility decrease
Blue brittleness	Carbon and alloy steels	230–370 °C (450–700 °F) exposure	Strength increase, toughness and ductility decrease
Stress-relief embrittlement	Alloy and stainless steel	Postweld heat treatment	Toughness decrease
Temper embrittlement	Carbon and low-alloy steel	375–575 °C (710–1070 °F) exposure	Increase in ductile-to-brittle transition temperature
Tempered martensite embrittlement	Heat treated alloy steel	200–370 °C (390–700 °F) exposure	Toughness decrease
400–500 °C embrittlement	Stainless steel (>15% Cr)	400–500 °C (750–930 °F) exposure	Strength increase, ductility decrease
Sigma-phase embrittlement	Ferritic and austenitic stainless steel	560–980 °C (1040–1800 °F) exposure	Toughness decrease
Graphitization	Carbon and alloy steel	Exposure >425 °C (800 °F)	Toughness decrease
Intermetallic compound embrittlement	All steel	Exposure to metal that forms an intermetallic	Brittleness
Neutron embrittlement	All steel	Neutron irradiation	Increase in ductile-to-brittle transition temperature
Hydrogen embrittlement	Cold-worked or heat treated hardened steel	Processing, service, corrosion, etc.	Ductility decrease, cracking
Liquid-metal-induced embrittlement	All steel	Molten low-melting-temperature metal exposure	Ductility decrease
Solid-metal-induced embrittlement	All steel	Near-molten low-melting-temperature metal exposure	Ductility decrease

thus causes an increase in strength and a decrease in ductility.

The effect of strain-age embrittlement is manifested as a time- and temperature-dependent increase in strength and decrease in ductility (Ref 6). The amount of cold work is also important; approximately 15% reduction provides the maximum effect. Room-temperature aging is very slow. Room-temperature aging can require from a few hours to a year; generally, several months are required for maximum embrittlement. As the aging temperature increases, the time for maximum embrittlement decreases. This process may take only a few minutes at 200 °C (390 °F).

Strain-age embrittlement is of most concern in sheet materials for drawing or other cold forming processes (although it should be noted that some components are intentionally allowed to strain age, either naturally or artificially, in circumstances when forming is completed and when the additional strength is desirable). Embrittled material can exhibit poor formability, including creation of aesthetically undesirable Lüders bands (stretcher strains) from discontinuous yielding, or rupture at normal processing stresses. The return of the yield point or the presence of Lüders strain in the stress-strain curve is evidence that strain-age embrittlement has occurred. These steels are often temper rolled to suppress the yield point, but a pronounced yield point can return due to strain-age embrittlement. In nonaluminum-killed sheet steels, a small amount (~1%) of deformation suppresses the yield-point phenomenon for several months. If the material is not formed within this safe period, the discontinuous yielding problem will eventually return and impair formability.

Rimmed or capped sheet steels are particularly susceptible to strain-age embrittlement, although strain aging has also been encountered in plate steels and weld heat-affected zones. Certain coating treatments, such as hot dip galvanizing, can produce a high degree of embrittlement in areas that were cold worked the critical amount, leading to brittle fractures. This can be prevented if the material is annealed before coating. An example of strain-age embrittlement from a galvanizing treatment is provided in Example 12.

Avoidance/Remediation

Rimmed or capped steel sheet is especially prone to strain-age embrittlement. These steel types, as well as other materials with high inclusion and interstitial element contents, should be avoided when maximum formability, such as deep drawing, is required. Many drawing-quality materials are aluminum-killed, so the aluminum will combine with the nitrogen, and have very low carbon contents. Interstitial-free steels and those alloyed with sufficient titanium do not strain age. Some manufacturers have prevented this aging problem by prompt forming after temper rolling, or by ordering stock immediately prior to use.

Example 12: Fracture of Galvanized Reinforcement Bar.

Concrete-reinforcement bar, or rebar, had fractured in bend regions after fabrication but prior to service. The bars were identified as ASTM A706 size 4, grade 60 steel rebar. It was stated that 90° angle bends in the bars had been made prior to hot dip galvanizing treatment. These bends could reportedly be broken off by hand.

Investigation

The fracture profile of a typical rebar sample is shown in Fig. 24(a). The fractures were relatively flat with no obvious stretching or evidence of mechanical impact damage. The fracture surfaces had corroded but appeared relatively brittle, as shown in Fig. 24(b). In some areas, the zinc coating surrounding the fracture had flaked off. The actual radius of curvature in the bend regions could not be accurately measured due to the fractures, but tighter radii are more prone to fracture.

Chemical analysis confirmed the steel was not discrepant. Bend testing in accordance with the material specification caused cracks in the zinc coating (Fig. 24c), but no base metal cracking occurred. Tension testing was performed on a straight section of one bar sample, and the properties satisfied the specification requirements for tensile strength, yield strength, and elongation. The fractured tensile specimen (Fig. 24d) exhibited substantial necking or stretching deformation, which is consistent with a ductile overload fracture mechanism and dissimilar from the bend fracture features. Measured hardness values on a polished cross-sectional specimen revealed an increased hardness level at the fractured bend region.

Tenacious deposits on the fracture surfaces prevented thorough scanning electron microscope fractography, other than to verify that the typical features were predominantly transgranular cleavage fracture. The only region that exhibited ductile morphology was at the outside diameter of the bends, which is consistent with this being the final region of separation. No intergranular cracking or forming flaws were present, and no deposited zinc was apparent on the fracture surfaces. The microstructures of the rebar samples consisted of fine lamellar pearlite within a matrix of blocky and Widmanstätten ferrite. There were no significant differences in the region where bending had been performed.

Conclusions and Recommendations

Metallurgical failure analysis of the reinforcement steel bar samples indicated that the fractures were likely the result of strain-age cracking or strain-age embrittlement. The plain carbon steel bars were bent at a relatively tight angle and then hot dip galvanized prior to service. The coating was applied after bending, so the zinc layer would not be fractured and the

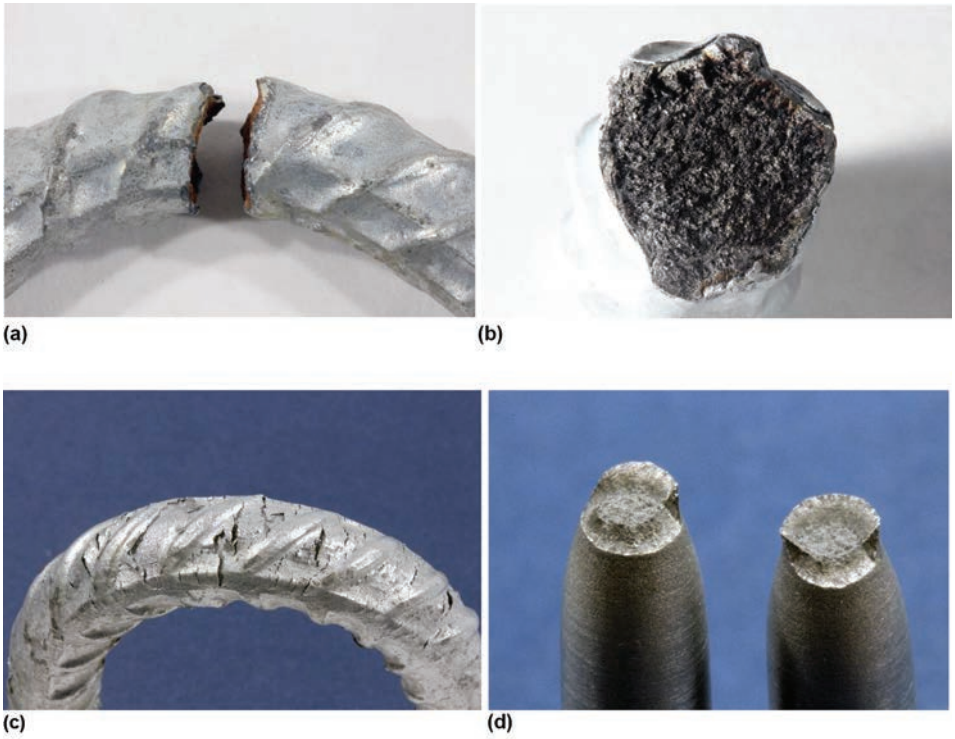

Fig. 24 Fracture of galvanized reinforcement bar (Example 12). (a) Brittle fracture at a bend in the galvanized rebar. (b) Oxidized fracture surface with no apparent shear lips. (c) Laboratory bend testing resulted in cracks in the zinc coating but no base metal cracks. (d) Ductile fracture of a tensile specimen from the rebar

corrosion resistance compromised. The heating of the cold-worked bar during galvanizing caused embrittlement and an increase in hardness, which did not occur in nonbent regions. Many carbon steels exhibit a strain-aging phenomenon, which occurs relatively slowly at low temperature but more rapidly at elevated temperature, such as the temperature necessary for hot dip galvanizing. The effects of strain-age embrittlement include an increase in mechanical strength and a decrease in ductility.

Alternate coatings have been developed for rebar that can withstand the bending process. Hot-dipped zinc can be replaced by electroplated zinc or mechanical zinc coatings in some applications, but this may not be suitable for rebar.

Quench-Age Embrittlement

If a low-carbon steel is heated to temperatures immediately below the lower critical temperature (Ac_1) and then quenched, it becomes harder, stronger, and less ductile upon aging at room or slightly elevated temperature. As with strain aging, quench-age embrittlement is a function of time at the aging temperature until the maximum degree of embrittlement is reached. Steel can require several weeks of room-temperature aging to reach the maximum embrittled state.

This embrittlement is somewhat similar to strain aging, except the impetus for carbon diffusion is a concentration gradient rather than cold working stresses. Quench aging involves actual precipitation of carbides (whereas strain aging involves interaction of carbon and other atoms with dislocations). The solubility of carbon in ferrite is higher at elevated temperature, resulting in carbon diffusion to relieve the stresses in the supersaturated lattice. Quench-age embrittlement results from precipitation of solute carbon at existing dislocations and from precipitation hardening due to differences in the solid solubility of carbon in ferrite at different temperatures. Nitride precipitation can also occur, but the amount of nitrogen present is generally too low for substantial hardening.

Steels with carbon contents of 0.04 to 0.12% appear most susceptible to quench-age embrittlement; increasing the carbon content above 0.12% reduces the effect. Quenching must be from below the Ac_1 temperature yet above 560 °C (1040 °F), which is reportedly an approximate lower boundary for this condition. Embrittlement effects increase at higher temperatures within this range.

Avoidance/Remediation

The quenching process necessary to initiate this embrittlement does not have much practical, metallurgical significance. Subcritical quenching is sometimes performed to reduce the cooling time between sequential high- and low-temperature processing operations. Avoiding the rapid quench enables the normal equalization of carbon content that occurs in slow cooling. Annealing and slow cooling of quench-age embrittled steel can restore ductility.

Blue Brittleness

When plain carbon steels and some alloy steels are heated to temperatures between 230 and 370 °C (445 and 700 °F), they experience an increase in strength and a marked decrease in ductility and impact strength. The term *blue brittleness* is derived from the characteristic blue coloration on steel that has been exposed to oxygen-containing atmospheres within this temperature range.

Blue brittleness is an accelerated form of strain-age embrittlement. The increase in strength and decrease in ductility are caused by carbide and/or nitride precipitation hardening within the critical-temperature range. Deformation while the steel is heated in the blue-heat range results in even higher hardness and tensile strength after cooling to room temperature. If the strain rate is increased, the blue-brittle temperature range increases.

Avoidance/Remediation

Use of susceptible steels that have been heated in the blue-brittleness range should be avoided, especially if the steels are subjected to impact loads, because the toughness of these materials will be considerably less than optimum. Tempering in the blue-heat range should be avoided for materials expected to be sensitive to blue brittleness. It can be avoided by specifying materials with low carbon and nitrogen levels or with alloying elements that are strong carbide and nitride formers.

Stress-Relief Embrittlement and Reheat Cracking

Stress-relief embrittlement results in the loss of toughness, typically within the heat-affected zone (HAZ) and/or the weld metal as a result of stress relieving of a welded structure. Stress-relief embrittlement of welds occurs during subsequent, usually subcritical, thermal treatment after welding. When severe, this can result in intergranular brittle cracking, typically referred to as postweld heat treat cracking or reheat cracking. Both phenomena have been observed only in those alloy systems that undergo precipitation hardening. These systems include low-alloy structural and pressure vessel steels, ferritic creep-resisting steels, austenitic stainless steels, and some nickel-base alloys. In addition, a tendency for creep embrittlement, notch weakening, and poor creep ductility during short-term elevated-temperature tests usually occurs in these materials.

During welding, the HAZ is exposed to high temperatures, ranging up to the melting point of the alloy. At these temperatures, existing precipitates in the base metal (carbides and nitrides in steels) are taken into solution, and grain coarsening occurs. During cooling, some precipitation occurs at grain boundaries or within the grains, but the majority of the precipitates remain in solution. Subsequent exposure at stress-relieving temperatures causes precipitate formation, primarily alloy carbides, within the grains and at the grain boundaries in the HAZ. This is responsible for strengthening and embrittlement. Embrittlement can be more pronounced in welds with substantial grain coarsening in the HAZ due to high heat input.

Cracking occurs when the nonuniform stresses, including both residual stresses from welding and thermal expansion stresses, exceed the local reduced creep ductility. This often occurs at the weld toe. Rapid or nonuniform heating increases cracking severity as less elastic recovery occurs, but precipitate formation is still diffusion related. In addition, the combined heating and stress effects can nucleate creep voids in the grain boundaries surrounding the strengthened grains. During stress relief, residual stresses are relieved through creep deformation. However, the strengthening of the precipitates of the grain interiors tends to concentrate creep strain at grain boundaries, leading to intergranular cracking.

Example 13 illustrates a welded component that failed from stress-relief embrittlement. Although this embrittlement is usually manifested in the HAZ or weld metal, other situations can occur. Reheat cracking is sometimes apparent upon startup of high-temperature boilers in areas not associated with welding. As noted, low-alloy structural steels, austenitic stainless steels, and some nickel alloys have been found to be susceptible to stress-relief embrittlement. Strong carbide-forming elements contribute to this embrittlement, vanadium, molybdenum, and boron in particular. Ferritic high-strength, low-alloy (HSLA) steels can be more susceptible than quenched-and-tempered grades. Some HSLA grades should never receive a postweld heat treatment.

Avoidance/Remediation

The possibility for stress-relief embrittlement and cracking can be reduced by specifying cleaner steels made with better deoxidation practice. In susceptible materials, service in the as-welded condition should be explored. Welding practice can also be altered somewhat to reduce residual stresses and HAZ grain coarsening by reducing heat input where possible. Steel that is embrittled, but not cracked, can be annealed to restore ductility.

Example 13: Stress-Relief Cracking of a Welded Alloy Steel Tube.

A thick-walled tube that was weld fabricated for use as a pressure vessel exhibited cracks, as depicted in Fig. 25. Similar cracking was apparent at the weld toes after postweld stress relief through quench-and-temper heat treatment. The cracks were not detectable by nondestructive examination after welding, immediately prior to heat treatment. Multipass arc welds secured the carbon steel flanges to the Ni-Cr-Mo-V alloy steel tubes.

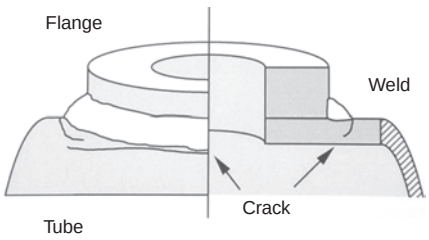

Fig. 25 Schematic of large welded tube that cracked upon postweld stress-relief heat treatment (Example 13)

Investigation

Visual examination revealed that the centers of the cracks were at the weld fusion line, but the ends of the cracks were in the adjacent tube HAZ. There was no cracking in the carbon steel flanges adjacent to the circular welds. The opened crack surfaces were heavily oxidized and discolored, because an air atmosphere had been used for the postweld heat treatment. The crack features were oxidized but appeared to be intergranular, whereas the room-temperature lab fracture features were consistent with ductile rupture. The crack was evident at the weld toe, but it did not follow the fusion line or HAZ, as is sometimes the case in hot cracks. Weld penetration was shallow and irregular. The base metal microstructure consisted of tempered martensite.

Conclusions

Evaluation of the fabrication history and the analysis data indicated that the tube failed as a result of stress-relief cracking. Very high residual stresses often result from welding thick sections of hardenable steels, even when preheating is used. Quenched-and-tempered steels containing vanadium, as well as HSLA steels with a vanadium addition, have been shown to be susceptible to this embrittlement. Manufacturers of susceptible steels recommend use of these materials in the as-welded condition.

Temper Embrittlement

Alloy steels containing certain impurities (phosphorus, antimony, tin, and arsenic) become embrittled during tempering in the range of 350 to 570 °C (660 to 1060 °F) or during slow cooling through this region. Embrittlement occurs because of the segregation of phosphorus, antimony, arsenic, and/or tin to the grain boundaries. Temper embrittlement is a diffusion-related process. The degree of embrittlement depends on the impurity content and the time within the critical tempering range. Embrittlement occurs fastest at approximately 455 to 480 °C (850 to 895 °F). Fortunately, temper embrittlement is reversible and can be removed by retempering above the critical tempering range, followed by rapid cooling. A case history example of temper embrittlement failure is provided in Example 14.

As noted, the impurity elements most associated with temper embrittlement are the metalloids phosphorus, arsenic, tin, and antimony. Silicon, germanium, selenium, tellurium, and bismuth are also identified as embrittling agents. The metallic element manganese is thought to both cause and facilitate temper embrittlement to an extent that the effects are difficult to differentiate. Plain carbon steels that contain less than 0.3% Mn are not considered susceptible. Alloy content also influences embrittlement. Nickel-chromium steels are particularly prone to temper embrittlement, but molybdenum additions reduce the susceptibility. Carbon, chromium, manganese, silicon, and nickel enhance embrittlement, both singly and in synergistic combination. Ferritic and pearlitic microstructures are less susceptible than the heat treated metastable martensitic and bainitic microstructures.

Prior to development of electron fractographic techniques, the degree of embrittlement was identified by macroscopic fracture examination, degradation of mechanical properties, and use of grain-boundary etchants. Temper embrittlement is manifested as a substantial increase in the DBTT, but strength and hardness are largely unaffected. It is most easily observed using toughness tests, but tensile properties will be affected by severe embrittlement. The magnitude of the DBTT shift can be dramatic, and transition temperature increases as high as 200 to 300 °C (360 to 540 °F) have been reported. Intentional doping with embrittling elements during research studies has resulted in even more severe shifts of the DBTT.

Electron fractography has added another tool for assessment of the degree of embrittlement by determination of the area fraction of intergranular facets on the fracture surface. Intergranular fracture usually results from temper embrittlement. The amount of grain-boundary fracture depends on the degree of impurity segregation to the grain boundaries but is also influenced by the matrix hardness, the prior-austenite grain size, and the temperature. In specimens from Charpy V-notch tests, the amount of intergranular fracture will also vary as a function of the distance from the root of the V-notch.

Avoidance/Remediation

Temper embrittlement is simply avoided by tempering outside of the critical range, although this may not always be possible depending on the inherent hardenability and tempering response of the selected steel. The use of alloys with only the minimum hardenability necessary for service can employ tempering temperatures below the embrittlement range. Ferritic and pearlitic structures are also less susceptible. Embrittlement of thick materials, which can occur by slow cooling through the critical range, can be avoided by rapid cooling or quenching, or by additional tempering at a temperature above the critical range, followed by rapid cooling.

Example 14: Catastrophic Chain Failure.

A chain sidebar failed unexpectedly shortly after installation. The link plate was identified as fabricated from hot rolled grade 4140 low-alloy steel bar stock that had been quenched and tempered to 300 to 400 HB.

Investigation

An image of the chain fracture site is provided in Fig. 26(a). The fracture was relatively flat and macroscopically brittle. The fracture was at an angle from the outside diameter to the inside diameter of the hole in the end of the chain link. Fracture features were somewhat shiny and crystalline, as revealed by oblique lighting in Fig. 26(b). Fan-shaped fracture features radiated from an origin site at the slightly worn outside-diameter surface. The remainder of the peripheral edges of the fracture surface consisted of dull, angled features that were identified as shear lips.

The primary fracture features at the origin site were intergranular, as shown in Fig. 26(c) and (d). Intergranular features were also observed within the core and around the entire periphery, except for the angled lips. Dimple rupture accompanied the intergranular brittle fracture in some regions, but the features were primarily brittle. The shear lips around the fracture were confirmed as dimple-rupture ductile tearing. Room-temperature impact testing of a specimen removed from the link revealed an impact energy of 9.5 J (7 ft · lbf).

Conclusions

Evaluation of the chain sidebar revealed that it failed catastrophically due to brittle overload fracture. The fracture was intergranular, which is not typical for low-alloy steels in the quenched-and-tempered condition. Temper embrittlement was the most likely cause. The probable tempering temperature to achieve the desired 300 to 400 HB hardness range is probably between 370 and 510 °C (700 and 950 °F), within the center of the temper embrittlement temperature range.

Equations and factors that can be used to identify the temper embrittlement susceptibility of base metals and filler metals were developed as a result of welding research. For example, thick-section 2Cr-1Mo steel plates used in pressure vessels for petroleum and chemical service at elevated temperatures are susceptible to temper embrittlement in service. The problem has been attributed to the presence of residual elements such as phosphorus and antimony. Bruscato (Ref 7) established an X factor to describe the effect of the residual elements:

$$X = \frac{10\text{P} + 5\text{Sb} + 4\text{Sn} + 1\text{As}}{100}$$

where X is in parts per million. Acceptable weld metal ductility can be obtained if the manganese and silicon contents and the X factor are low. Reduction of these elements can

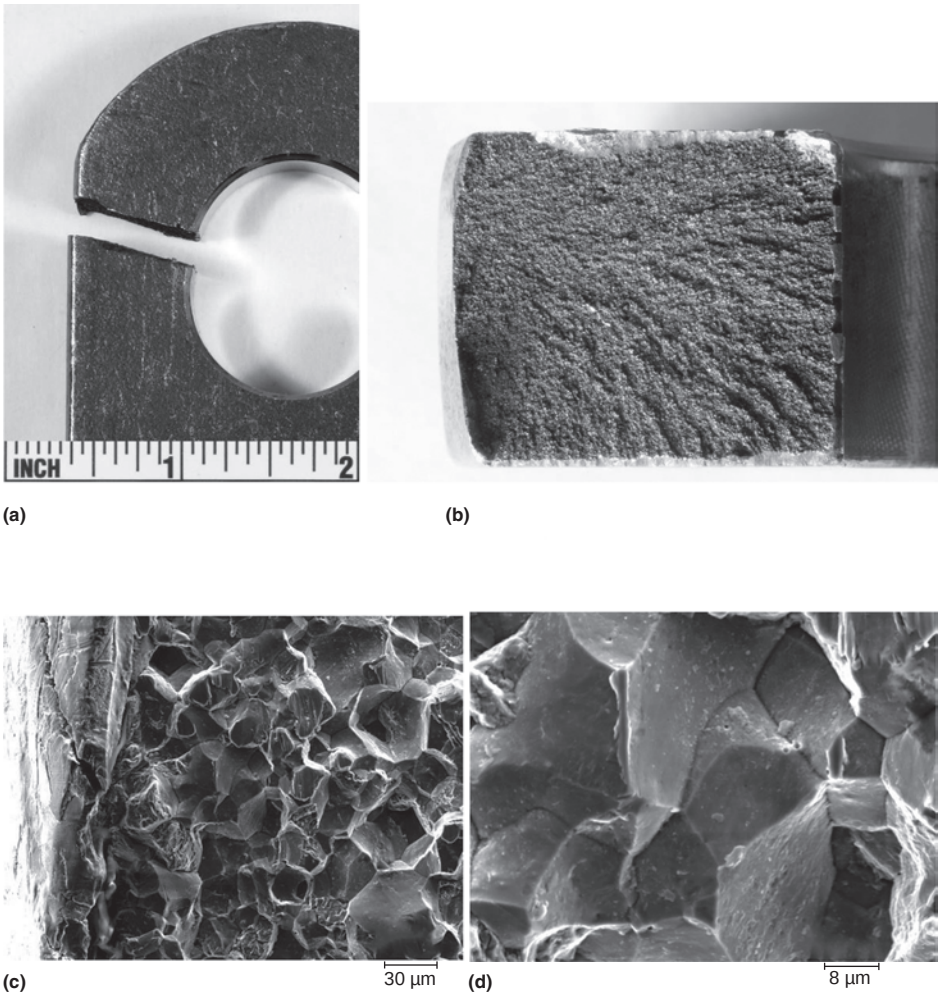

Fig. 26 Catastrophic chain failure (Example 14). (a) Flat fracture through the chain link. (b) Link fracture surface showing somewhat shiny, crystalline features in fan-shaped direction. (c) Near-surface brittle fracture features. Original magnification: 500×. (d) Intergranular brittle fracture morphology in the center of the link cross section. Original magnification: 2000×

be achieved by using basic fluxes. Another indicator, the Watanabe number, *J*, shows that welds and base metal are not susceptible to temper embrittlement if *J* is less than 200 (Ref 8):

$$J = (\text{Si} + \text{Mn})\ (\text{P} + \text{Sn}) \times 10^4$$

Tempered Martensite Embrittlement

Tempered martensite embrittlement (TME) of quenched-and-tempered low-alloy steels occurs over a temperature range of approximately 200 to 370 °C (390 to 700 °F) (Ref 9). Tempered martensite embrittlement is also referred to as 350 °C (660 °F) embrittlement, although the greatest alteration reportedly occurs at approximately 315 °C (600 °F). It differs from temper embrittlement in the strength of the material and the temperature exposure range. In temper embrittlement, the steel is usually tempered at a relatively high temperature, and embrittlement occurs upon slow cooling after tempering and during service at temperatures within the embrittlement range. In TME, the steel is tempered within the embrittlement range, and service exposure is usually at room temperature. Therefore, temper embrittlement is often called two-step temper embrittlement, while TME is often called one-step temper embrittlement.

Tempered martensite embrittlement occurs in the tempering range in which ε-carbide changes to cementite. It occurs mainly in steels with a microstructure of tempered martensite, but steels with microstructures of tempered lower bainite are also susceptible to TME. Other structures, such as upper bainite and pearlite-ferrite, are not embrittled by tempering in this region. The mechanisms of TME are not completely understood, but the main explanations for TME are based on the effects of impurities and cementite precipitation on the prior-austenite grain boundaries. Early studies concluded that TME was due to precipitation of thin platelets of cementite at the grain boundaries. However, TME has also been found to occur in very-low-carbon steels, and residual impurity elements have also been shown to be essential factors in TME.

Thus, it appears that TME results from a combination of effects due to cementite precipitation on prior-austenite grain boundaries or at interlath boundaries and/or the segregation of impurities, such as phosphorus and sulfur, at the prior-austenite grain boundaries. The predominant mechanism depends on many alloy and processing variables, but the effect of impurity segregation is more pronounced at the higher range of the embrittlement temperature region. Fracture by TME also can be either transgranular or intergranular. Transgranular TME fractures are observed from tempering between 200 and 300 °C (390 and 570 °F), with the formation of coarse carbides at martensite lath boundaries. Intergranular TME fractures usually, but not always, are observed from tempering at approximately 350 °C (660 °F), with the presence of coarse carbides at the impurity-weakened grain boundaries. These differences can be due to differences in carbon, alloy, and impurity content as well as in strength level, test temperature, nature of the test, and grain size. Impurities appear to influence coarse-grain steels to a greater degree than fine-grain steels.

Depending on the test temperature, TME produces a change in the fracture mode from either predominantly transgranular cleavage or MVC to intergranular fracture along the prior-austenite grain boundaries. In room-temperature tests, the fracture can change from MVC to a mixture of cleavage/ductile tear ridges and intergranular fracture. Tensile strength, yield strength, elongation, and reduction in area are not affected by this embrittlement, but it has an adverse effect on Charpy V-notch impact energy (Ref 10). Charpy V-notch absorbed energy plotted against the tempering temperature is the most common procedure to reveal the embrittlement. The DBTT can also increase some with tempering in this range, but the increase in DBTT is not as pronounced as in temper embrittlement.

Avoidance/Remediation

Avoiding the embrittling temperature range is necessary to prevent TME, although the range is somewhat variable. Use of steels with low impurity contents, particularly phosphorus, can prevent the impurity segregation contribution to total embrittlement. Embrittled steels can be annealed to restore maximum impact energy when necessary.

400 to 500 °C (750 to 930 °F) Embrittlement

Fine-grain high-chromium stainless steels normally possess good ductility. However, if they are held for long periods of time at temperatures of 400 to 500 °C (750 to 930 °F), they will become harder and embrittled. Time and temperature of exposure affect the level of embrittlement. This phenomenon is

sometimes called 475 °C (885 °F) embrittlement, because the embrittlement is most pronounced at this approximate temperature. Moderate temperature exposure enables diffusion of chromium to the grain boundaries for the formation of chromium-rich carbides. This segregation also results in reduced corrosion resistance in the denuded regions adjacent to the grain boundaries, analogous to sensitization in austenitic stainless steels. However, it should be noted that sensitization does not normally result in any embrittlement. At least 15% Cr is considered necessary for 400 to 500 °C embrittlement. Increasing chromium contents and higher levels of silicon, niobium, and titanium appear to promote embrittlement.

Embrittlement of high-chromium ferritic stainless steels in the 400 to 500 °C temperature range produces iron-rich α and chromium-rich α′ ferrites. Chromium nitrides also precipitate during aging and are observed at grain boundaries, dislocations, and inclusions. The formation of α′ can occur in two ways: by nucleation and growth and by spinodal decomposition. The latter mechanism appears to be operative in higher-chromium-content alloys and has been the commonly observed formation process. The reaction is reversible; heating above the embrittlement range dissolves α′. In duplex stainless steels, the embrittlement temperature range appears to be broader, with additional phases precipitating in the upper portion of the range. An example of 475 °C (885 °F) embrittlement of a duplex alloy similar in composition to type 329 stainless steel is shown in Fig. 101 in "Malleable Irons/White Irons: Atlas of Fractographs," *Fractography*, Volume 12 of *ASM Handbook*, 1987.

Avoidance/Remediation

The occurrence of 400 to 500 °C embrittlement can be prevented in various ways. A low-chromium grade (less than 15%) could be used if critical range exposure is unavoidable. Stress relief in this range could be avoided for nonhardenable ferritic grades. Martensitic grades could be preferentially selected for tempering response that would use a tempering temperature outside of the critical range. Embrittled stainless steels can be retempered at temperatures above the critical range, at least 540 °C (1000 °F), to remove this effect (Ref 11). Tempering should be as brief as possible if it is performed at a higher temperature, because sigma phase can form.

Sigma-Phase Embrittlement

Sigma (σ) is an iron-chromium phase that forms in stainless steels with chromium contents typically between 25 and 76 wt%, although σ formation can occur in ferritic stainless steels with chromium contents below 25 wt%. Sigma forms more readily from ferrite in stainless steels than from austenite, so austenitic stainless steels are typically less susceptible to σ formation than ferritic grades. However, many austenitic grades will form σ phase. In addition, σ-phase formation is enhanced in grades of austenitic stainless steels that intentionally have a small amount of δ ferrite (approximately 5%) to prevent hot cracking during welding. Sigma-phase formation in duplex stainless steels is also common.

Some superalloys also can be embrittled by σ-phase formation. However, the presence of σ in superalloys is not necessarily damaging to properties. Various morphologies may be encountered, some of which are quite detrimental to properties. Sigma in the form of platelets or as a grain-boundary film is detrimental, but globular intergranular precipitation can improve creep properties. Considerable effort has been devoted to determining how composition influences σ-phase formation in nickel-base superalloys, and this has substantially influenced alloy development.

In stainless steels, σ generally forms with long-time exposure in the range of 565 to 980 °C (1050 to 1800 °F), although this range varies somewhat with composition and processing. This can occur during slow cooling, tempering or stress relief, and welding. Sigma formation exhibits C-curve behavior, with the shortest time for formation (nose) generally occurring between approximately 700 and 810 °C (1290 and 1490 °F) for stainless steels. In austenitic stainless steels, σ precipitates at grain and twin boundaries at temperatures between approximately 595 and 900 °C (1100 and 1650 °F). Sigma precipitation occurs fastest at approximately 845 °C (1550 °F).

Coarse grain sizes from high solution-annealing temperatures retard σ formation, while cold working generally promotes σ formation. The influence of cold work on σ formation depends on the amount of cold work and its effect on recrystallization. If the amount of cold work is sufficient to produce recrystallization at the service temperature, σ formation is enhanced. If recrystallization does not occur, the rate of σ formation may not be affected. Small amounts of cold work that do not promote recrystallization may actually retard σ formation.

The σ phase is extremely hard and brittle and imparts a reduction in toughness with an increase in notch sensitivity. These effects are most notably observed at low temperatures following the embrittling heating event. Steels containing this phase also suffer a reduction in corrosion resistance. The creep resistance and thermal fatigue resistance are also compromised in high-temperature applications for embrittled steels. Embrittlement from σ phase is most detrimental after the steel has cooled to temperatures below 260 °C (500 °F). At higher temperatures, stainless steels containing σ phase can usually withstand normal design stresses. However, cooling to 260 °C or below results in essentially complete loss of toughness. A case history of high-temperature cracking caused by this embrittling mechanism is detailed in Example 15.

Additions of silicon, molybdenum, nickel, and manganese permit σ to form at lower chromium levels. Silicon, even in small amounts, markedly accelerates σ formation. In general, all elements that stabilize ferrite promote σ formation. Molybdenum has an effect similar to that of silicon; aluminum has a lesser influence. Small amounts of nickel and manganese also increase the rate of σ formation, although large amounts, which stabilize austenite, retard σ formation. Additions of tungsten, vanadium, titanium, and niobium also promote σ formation. Carbon additions retard σ formation by forming chromium carbides, thereby reducing the amount of chromium in solid solution.

Avoidance/Remediation

To a large extent, judicious alloy selection and heat treatment can prevent σ-phase embrittlement. Extraction replicas have been used to determine the amount of σ phase in the microstructure, and the amount of σ phase has been directly related to the creep rate (Ref 12). Components that are suspected of being embrittled can be reannealed at a suitable temperature to dissolve the σ phase, along with care not to dwell in the critical embrittlement temperature range.

Example 15: Coker Tube Damage.

Coker tubes were found to have cracked during refinery service. The interior of the tubes contained vacuum distillation residue, and the service temperature was typically between 595 and 760 °C (1100 and 1400 °F). The furnace had reportedly been in service for 13 years prior to tube removal. The 114 mm (4.5 in.) diameter tubes were fabricated from type 347H austenitic stainless steel.

Investigation

The coker tube samples contained longitudinal cracks, as shown in Fig. 27(a). Many of the cracks were through most of the wall thickness, resulting in fracture during normal flattening tests that were performed. Some thickness variations were also identified around the tube circumferences. The tube composition was confirmed, but the extent of cracking prevented evaluation of the tensile properties. Scanning electron microscope inspection of the oxidized crack surfaces revealed intergranular morphology.

Transverse metallographic cross-sectional specimens revealed intergranular cracking with some secondary branching. Images of the microstructure are provided in Fig. 27(b) and (c). The near-inside-diameter microstructures of the tubes were severely altered, with substantial carbide formation in the austenitic matrix. The carbides were both at grain boundaries and within the grains. Some alteration surrounding the grain boundaries was suggestive of sensitization. Potassium hydroxide etching revealed coloration, indicating σ-phase formation, as shown in Fig. 27(d). No creep

void formation had contributed to the embrittlement of the coker tubes.

Conclusions and Recommendations

Internal cracking in the coker tubes was a result of σ formation, likely with the contribution of carbide formation. The tubes had been removed from service prior to fracture, which may have been catastrophic in this application.

This application is very severe, from both process exposure and temperature exposure. Some nonferrous alloys are superior in this application but would be significantly more expensive. Periodic inspection for the level of deterioration and subsequent replacement would be recommended.

Graphitization

The process of graphitization of steel is the decomposition of pearlite into ferrite and randomly dispersed graphite, which can result in embrittlement when the graphite particles form along a continuous zone through a component. The degree of embrittlement depends on the distribution, size, and shape of the graphite. When the graphite is present in a sufficient amount and the inclusions are aligned or continuous, brittle fracture can occur along this relatively weak pure-iron/carbon-free interface. Continuous graphite formation is sometimes called chain graphitization. The severity of graphitization is frequently evaluated by bend testing.

Graphitization is a diffusion process, and the rate and severity are functions of service duration and temperature. It typically occurs in carbon and low-alloy steels subjected to moderately high temperatures (~450 to 600 °C, or 840 to 1110 °F) for extended periods of time. At higher temperatures, pearlite decomposition is dominated by the formation of spheroidal carbides. Graphitization and spheroidization are competing mechanisms with different activation energies and rates for the decomposition of pearlite (Fig. 28). Graphitization is the usual mode of pearlite decomposition at temperatures of approximately 550 °C (1025 °F), while the formation of spheroidal carbides predominates at higher temperatures. Although spheroidization reduces the strength, the material remains ductile rather than embrittled. The critical temperature is dependent on alloying and many other factors.

The deoxidation practice used in making the steel is the most important parameter influencing graphitization. High levels of aluminum deoxidation strongly promote graphitization for both carbon and carbon-molybdenum steels. The graphitization tendency of carbon and carbon-molybdenum steels is increased when the aluminum content exceeds approximately 0.025%. Steels deoxidized with silicon can also be susceptible to graphitization. Deoxidation with titanium usually produces good resistance to graphitization. While nitrogen appears to retard graphitization, high levels of aluminum remove nitrogen and thus promote graphitization (Ref 4). Molybdenum additions (0.5%) help stabilize cementite but do not fully offset the influence of high aluminum additions. Both manganese and silicon affect graphitization, but their influence is small at the levels used in low-alloy chromium-molybdenum steels.

Chromium appears to be the best alloy addition for stabilizing carbides. Graphitization can be resisted by steels containing more than 0.7% Cr; chromium-containing ferritic steels for high-temperature service typically contain at least 0.5% Mo as well, largely to impart elevated-temperature strength and resistance to temper embrittlement. Molybdenum is a carbide stabilizer and can limit available carbon for graphitization, and carbon-molybdenum steels exhibit greater resistance to graphitization than do carbon steels. However, use of carbon-molybdenum steel has been limited at

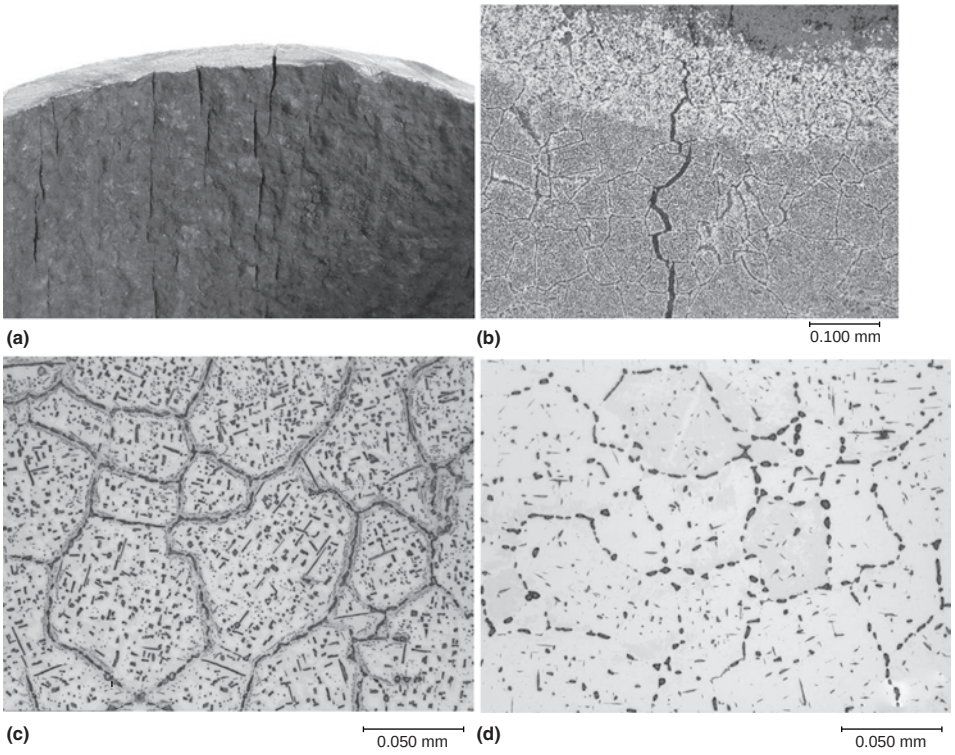

Fig. 27 Coker tube damage (Example 15). (a) Tube interior contains longitudinal cracks in the thick scale. (b) Near-surface microstructural alteration with substantial carbide formation in the austenitic matrix. (c) Near-surface microstructure including sigma phase. Original magnification: 500×. (d) Potassium hydroxide etching confirms the presence of sigma phase at grain boundaries in the core microstructure. Original magnification: 500×

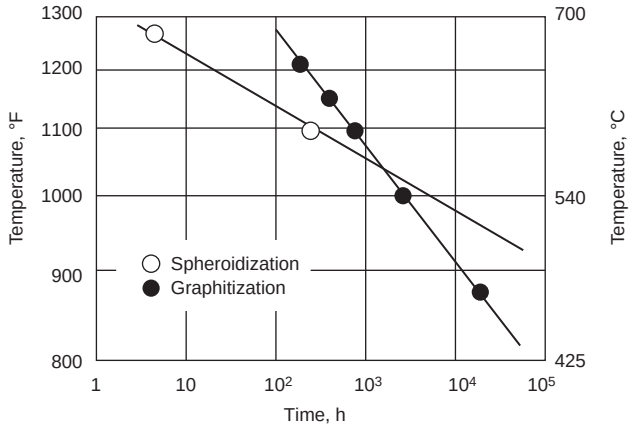

Fig. 28 Temperature-time plot of pearlite decomposition by spheroidization and graphitization. The curve for spheroidization is for conversion of one-half of the carbon in 0.15% C steel to spheroidal carbides. The curve for graphitization is for conversion of one-half of the carbon in aluminum-deoxidized 0.5% Mo cast steel to nodular graphite.

higher temperatures because of graphitization. Chromium steels are highly resistant to graphitization and therefore are preferred when service temperatures become greater than approximately 425 to 455 °C (800 to 850 °F). As an example of maximum-use temperatures based on oxidation or graphitization criterion, the following are maximum-use temperatures for superheater tube materials covered in ASME boiler codes:

Material	Maximum-use temperature at surface based on oxidation/graphitization criteria	
	°C	°F
SA-106 carbon steel	400–500	750–930
0.5Cr-0.5Mo	550	1020
1.2Cr-0.5Mo	565	1050
2.25Cr-1Mo	580	1075
9Cr-1Mo	650	1200
Type 304H	760	1400

Graphitization of carbon and carbon-molybdenum steel piping during service at temperatures above 425 °C (800 °F) has caused numerous failures in steam power plants and refineries. Graphite formation generally occurs in a narrow region in the HAZ of a weld where the metal has been briefly heated above the lower critical temperature. If graphitization is detected in its early stages, the material can often be rehabilitated by normalizing and tempering just below the lower critical temperature. Steel that has undergone more severe graphitization cannot be salvaged in this manner; the defective region must be cut out and rewelded, or the section must be replaced. Carbon and carbon-molybdenum steels can be rendered less susceptible to graphitization by tempering just below the lower critical temperature. An example of graphitization damage in a carbon steel is included in Example 16.

Because graphitization involves prolonged exposure to moderate temperatures, it seldom occurs in boiler-surface tubing. Economizer tubing, steam piping, and other components that are exposed to temperatures from approximately 425 to 550 °C (800 to 1020 °F) for several thousand hours are more likely than boiler-surface tubing to be embrittled by graphitization. The HAZs adjacent to welds are among the most likely locations for graphitization to occur.

Avoidance/Remediation

Materials selection for specific service temperatures is the best way to avoid graphitization embrittlement. Safe operating temperatures have been identified for susceptible materials, and many alloys that are not susceptible have been developed. In cases where graphitization is suspected, it is often possible to perform in situ metallographic examination to identify gross graphitization without component removal. Severe graphitization cannot be repaired. Slight graphitization can be removed by normalizing, followed by tempering slightly below the lower critical temperature.

Example 16: Failure of a Power Plant Steam Drain.

A section of steam drain line piping failed in service. This pipe was in the main steam drain to the condenser. The reported steam conditions were identified as 510 °C (950 °F) at a pressure of 8.6 MPa (1250 psi). The drain was subjected to infrequent service for short periods of time. The carbon steel pipe had been in service only five years prior to the failure.

Investigation

Figure 29(a) shows the region of the steam drain that fractured. A large fishmouth rupture occurred at the end of a length that was slightly bent. The exterior surface of the pipe had a scale layer, and the interior appeared to have a magnetite layer from the steam. The likely origin was a straight line along the pipe axis. Stereomicroscope inspection of the fracture surface revealed substantial material thinning. The remainder of the rupture was a helical fracture from both ends of the axial crack. The helical crack edges were substantially thicker but also exhibited an angled aspect, which was suggestive of overload fracture.

Chemical analysis showed that the failed pipe met the chemical requirements for ASME SA-106 grade B carbon steel piping. Scanning electron microscope examination revealed primarily dimple-rupture features. A strip-type tensile specimen was machined from the remote end of the pipe, and the tensile properties satisfied the requirements for ASME SA-106 grade B carbon steel. Metallographic cross-sectional images of the failed pipe are shown in Fig. 29(b) to (d). The grains at the origin site were substantially stretched, consistent with stress rupture. Additional cracking or fine fissures were created at some graphite particles due to the stretching that accompanied the rupture. There was no evidence of grain growth or creep damage. The entire pipe appeared to have been graphitized, but some spheroidized cementite remained. The graphite was largely globular rather than a continuous grain-boundary film. The graphite formed in linear alignment in some areas, a condition called chain graphitization.

Conclusions and Recommendations

The steam drain pipe failure was by stress rupture through the material, which had been compromised by thermal degradation in the form of graphitization. It is not known if a high-pressurization event could have also contributed.

In this type of service, the pipe should be replaced by a chromium-molybdenum alloy steel with superior high-temperature characteristics.

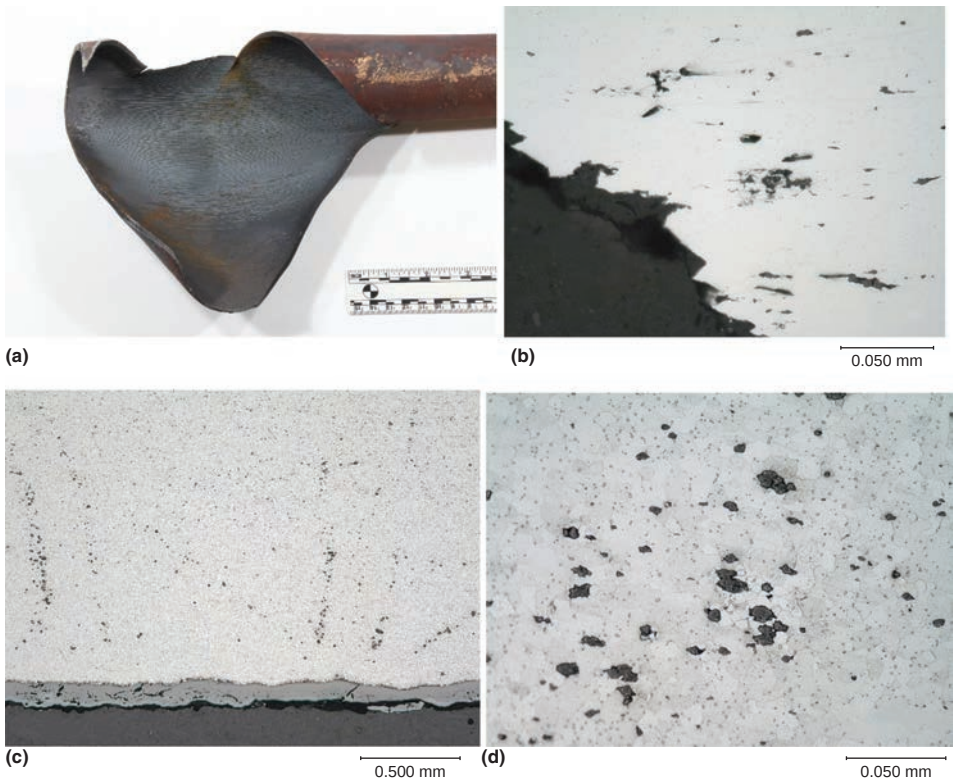

Fig. 29 Failure of a power plant steam drain (Example 16). (a) Failed steam drain section. (b) Fracture-surface profile showing tearing at graphite particles. Original magnification: 500×. (c) Alignment of graphite in the pipe remote from the failure. Original magnification: 50×. (d) Higher magnification of area in (c) shows graphite within a clustered region. Original magnification: 500×

Intermetallic Compound Embrittlement

Embrittlement of metals can be caused by the formation of brittle, intermetallic compounds during elevated-temperature processing or service. This phenomenon is considered irreversible, and embrittlement by intermetallic compounds can be avoided by not using susceptible material combinations at elevated temperatures.

This phenomenon has been documented in galvanized steels where a brittle, intergranular iron-zinc phase forms at the grain boundaries, resulting in embrittlement. At slightly elevated temperatures, the zinc and iron undergo spontaneous formation of intermetallic alloy particles. Iron and zinc can form a number of stable phases, all of which exhibit crystalline structures different from bcc iron. Grain-boundary formation occurs preferentially due to the relative ease of zinc atom diffusion. This is different from liquid-metal-induced embrittlement in that no melting occurs. Additionally, this is different from solid-metal-induced embrittlement by the intergranular diffusion of the foreign solute together with intermetallic compound formation. Intermetallic compound embrittlement can also occur during elevated-temperature brazing, as demonstrated in Example 17.

Example 17: Braze Joint Failure (Ref 13).

The failure of a hot water expansion joint in the heating system of a high-rise office building resulted in a catastrophic water leak. Fracture of the expansion joint was sudden, since it occurred only several hours or a few days after the system had been completed and put into service. Brittle cracking occurred at a dissimilar-metal braze joint between copper and stainless steel components.

Investigation

A diagram of the failed end of the expansion joint is provided in Fig. 30(a). The joint was a braze weld between a copper elbow and a welded austenitic stainless steel expansion joint. Fracture occurred through the brazement, which had the appearance of a copper alloy filler metal. The fracture appeared macroscopically brittle, without any permanent plastic deformation. A representative cross-sectional specimen that was prepared through the joint in a cracked region is shown in Fig. 30(b). The microstructures of the copper elbow and stainless steel components were considered typical, although grain growth in the copper suggested excessive torch brazing temperatures. It was noted that some of the stainless steel weld had been consumed into the braze joint, which is atypical for a brazing operation. All of the cross-sectional specimens contained an irregular phase that formed between the braze alloy and the stainless steel weld. This phase was continuous, from the outside to the inside diameter of the joint. The features suggested this was an intermetallic phase rather than trapped flux or slag. Cracking was isolated to this intermetallic phase and did not follow a particular structure. Higher-magnification images of the intermetallic phase are included in Fig. 30(c) and (d). The unusually thick intermetallic compound contained both lamellar and somewhat cubic-appearing structures.

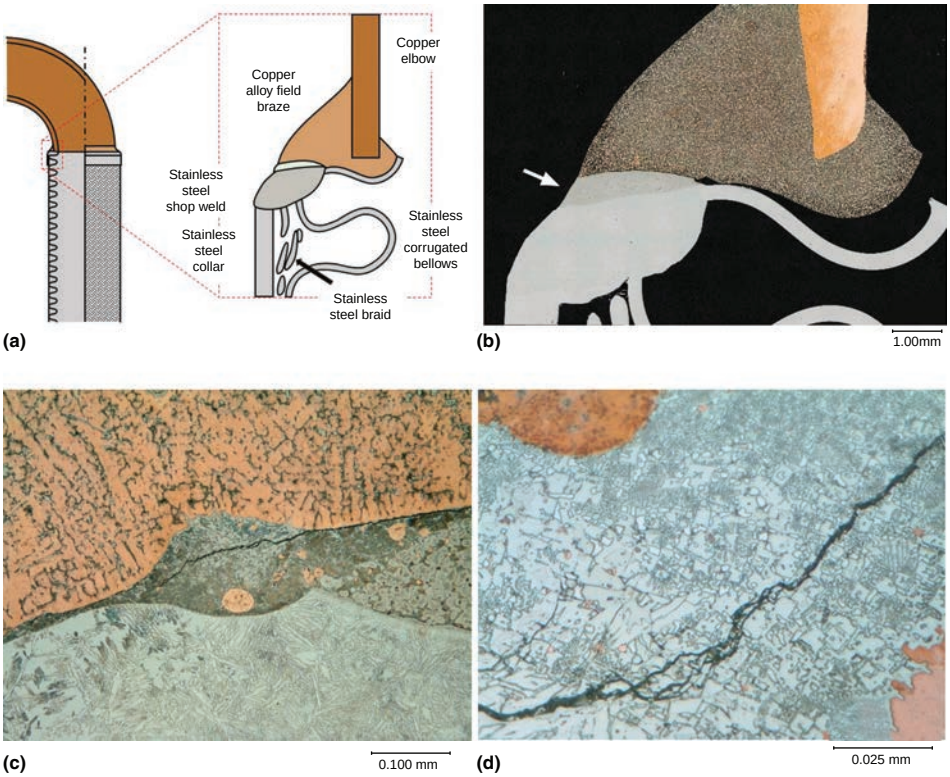

Fig. 30 Braze joint failure (Example 17). (a) Schematic of failed end of expansion joint braze where an intermetallic phase formed. (b) Cross section showing the intermetallic layer (arrow). Original magnification: 15×. (c) Cracked intermetallic phase between the copper braze (top) and the stainless steel weld (bottom). Original magnification: 200×. (d) Cracking through the intermetallic phase. Original magnification: 1000×. Source: Ref 13

Energy-dispersive x-ray spectrometry analysis on cross sections confirmed that the copper elbow was nearly pure copper, possibly a phosphorus-deoxidized alloy. The braze alloy was consistent with the typical requirements for AWS BCuP-5 in accordance with AWS A-5.8 (ISO 17672 type CuP 284), with 14.5 to 15.5% Ag and 4.8 to 5.2% P. The stainless steel weld was likely a type 308 or 309 filler metal with dilution. Energy-dispersive x-ray spectrometry analysis suggested that the intermetallic phase was composed of mixed-metal phosphides, likely M_3P-M_2P, iron, nickel, chromium, and copper phosphides, but this could not be confirmed. Microindentation hardness testing revealed typical measurements for the stainless steel components, weld, braze, and copper elbow. The intermetallic layer hardness was very high at 661 HV.

Conclusions and Recommendations

Brittle fracture of the expansion joint occurred due to the use of an incompatible phosphorus-containing, copper-base braze alloy, which resulted in the formation of an intermetallic phase. The braze welding operation created a hard, brittle intermetallic phosphide phase at the stainless steel component interface. Applicable brazing filler-metal guidelines highlight this incompatibility, and the probable root cause was inadvertent substitution of a brazing filler that was successfully used for nonfluxed copper-copper joints elsewhere in the riser system.

This type of embrittlement could have been avoided by using a proper brazing filler alloy.

Overaging and Precipitation Embrittlement

Many nonferrous and ferrous alloys are precipitation or age hardened, because they do not exhibit a polymorphic character for transformation hardening by quenching and tempering. Room-temperature (natural aging) and elevated-temperature (artificial aging) precipitation hardening provide strength and, in some cases, ductility. The maximum yield strength occurs at a combination of aging temperature and time. Excessive thermal exposure can lead to overaging, which typically reduces both strength and ductility. The drop in strength on overaging can be substantial. This effect is evident in high-manganese steels where carbides precipitate. Aluminum and titanium alloys

can also be degraded by overaging. However, in some cases, intentional overaging has been found to be beneficial when maximum strength is not required. For example, some 7*xxx*-series aluminum alloys are overaged to the T7 condition for better stress-corrosion cracking resistance, although a decrease in strength of 10 to 15% occurs. Additionally, optimal fracture toughness is also obtained for this temper.

Avoidance/Remediation

Precipitation from solid solution occurs during intentional precipitation treatment or during moderate-temperature service exposure. The rate of embrittlement is a function of both the exposure time and temperature, and service at embrittling temperatures should be avoided. Alloying and heat treatment in some cases can suppress precipitation. Example 18 illustrates some changes in monotonic overload fracture behavior from this mechanism.

Example 18: Bicycle Head Tube Cracking.

The head tube of an aluminum alloy bicycle frame cracked in service. No information was provided concerning the circumstances of the crack. The tube was reported to be aluminum alloy 6061 in the T6 tempered condition.

Investigation

An image of the head tube crack is provided in Fig. 31(a). The cracking appeared relatively brittle, with no permanent plastic deformation. Cracking occurred at the end of the head tube, where bending forces on the handlebars would be concentrated. The chemical composition and mechanical properties of the formed and welded tube were consistent with the specified aluminum alloy and the specified T6 temper condition. Scanning electron microscope examination of the fracture surface from the tensile specimen revealed primarily ductile dimple morphology, as shown in Fig. 31(b). Scanning electron microscope examination of the head tube fracture surface revealed primarily intergranular fracture evidence, as shown in Fig. 31(c). This "woody" intergranular morphology was substantially different than the tensile failure morphology.

Conclusions and Recommendations

Insufficient background information about the cracking circumstances prevented full root-cause analysis in this case. However, the head tube exhibited typical brittle fracture characteristics, which diverge from the ductile monotonic loading behavior confirmed for this aluminum alloy. Although the tube satisfied the strength requirements of T6, it is probable that an insufficiently fast quench permitted some grain-boundary precipitation during heat treatment.

This is not an unusual condition for bicycle frame tubes, but it also has been seen in aluminum ladders and other consumer items. Precipitation embrittlement in aluminum alloys can be avoided by rapid quenching after solution annealing (T6) or hot forming (T5). Embrittlement is more likely in T5 tempers, quenched from hot forging, extrusion, and so on, because temperature and quench rate can be harder to control than in normal solution annealing.

Quench Cracking

Although quench cracking is not an alteration of a material occurring in service, it is unpredictable. These cracks can be instantaneous upon quenching, or they can be delayed. It is not unusual for some components to be crack-free, whereas seemingly identical components, processed identically, have cracked. Quench cracking occurs in steels due to thermal contraction stresses coupled with the volumetric expansion accompanying the martensite transformation. The contraction from austenite to martensite or pearlite on cooling is more than 1%. The volumetric expansion of martensite is directly proportional to carbon content and microstructural factors. Quench cracking can also occur in other alloys such as superalloys during heat treatment. Thick materials and components with sharp corners and thickness transitions are most susceptible to quench cracking, because temperature gradients form severe stress gradients. Quench cracking of water- and brine-quenched alloy steels also can be promoted by soft spots on the surface of the part. These soft (unhardened) regions can be due to the fixture used to hold the part during quenching, or from tongs, or can be caused by vapor pockets during quenching due to inadequate agitation or contamination of the quench.

Quench cracking typically initiates at the surface, particularly at geometrical changes, corners, defects, and inclusions. Quench cracks have characteristics that are easily recognized. First, the fracture generally runs from the surface toward the center of mass in a relatively straight line with either a longitudinal or radial orientation unless located by a change in section size. The crack is also likely to open or spread and can exhibit a shear lip at the extreme surface. The fracture surfaces of quench cracks are always intergranular.

When cracked parts are tempered, the intergranular morphology can form a thick oxide scale from tempering. A quench crack exhibiting tempering scale is shown in Fig. 32. The microstructure adjacent to the crack will not be decarburized unless a specimen with an undetected quench crack is rehardened. In quenched-and-tempered steels, proof of quench cracking is often obtained by opening the crack and looking (visually) for temper color typical for the temperature used.

Delayed quench cracks are the result of additional transformation of retained austenite in steel. Delayed quench cracking occurs when heavily stressed retained austenite continues to transform to martensite prior to tempering heat treatment. In highly alloyed steels, delayed

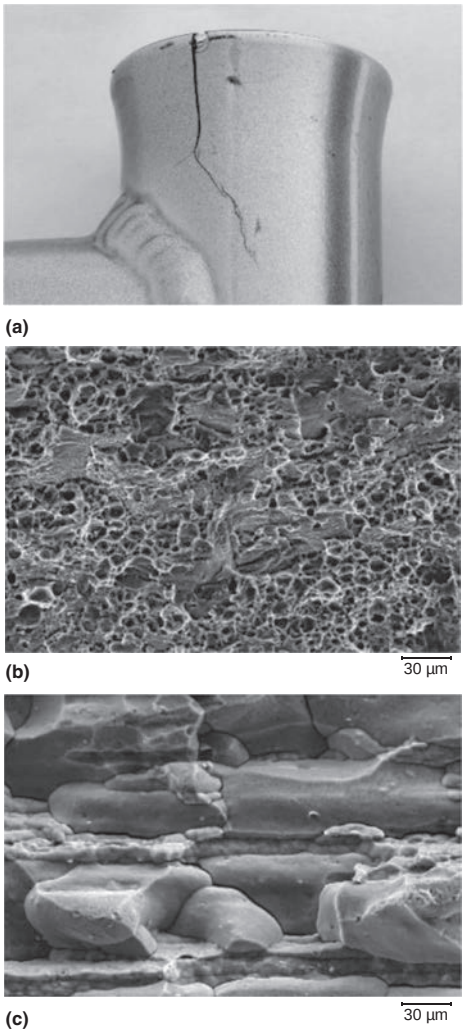

Fig. 31 Bicycle head tube cracking (Example 18). (a) Crack on head tube. (b) Scanning electron microscope image showing mixed ductile fracture of a tensile specimen from the head tube. Original magnification: 500×. (c) Head tube fracture surface reveals intergranular brittle fracture. Original magnification: 500×

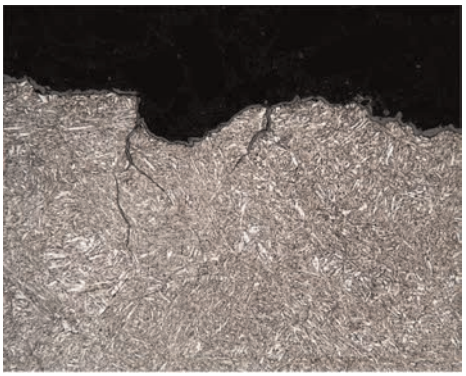

Fig. 32 Quench cracking in a hypoeutectoid steel. The intergranular cracks are filled with tempering scale. 2% nital etch. Original magnification: 297×

cracking can be avoided by tempering immediately after quenching. Many highly hardenable steels receive multiple tempering heat treatments or cryogenic treatment to minimize retained austenite. In many cases, this austenite is not considered desirable.

Avoidance/Remediation

Many factors can contribute to quench-cracking susceptibility: carbon content, hardenability, M_s temperature, part design, surface quality, furnace atmosphere, and heat treatment practice. As the carbon content increases, the M_s and martensite finish (M_f) temperatures decrease, and the volumetric expansion and transformation stresses accompanying martensite formation increase. Steels with less than 0.35% C are generally free from quench-cracking problems. The higher M_s and M_f temperatures permit some stress relief to occur during the quench, and transformation stresses are less severe. Alloy steels with ideal critical diameters of 4 or higher are more susceptible to quench cracking than lower-hardenability alloy steels.

In general, quench-crack sensitivity increases with the severity of the quench medium. Quench-cracking propensity can be reduced by avoiding excessive austenitizing temperatures, unnecessarily rapid quenchants, and quenching to an unnecessarily low temperature. Additionally, sometimes the problem can be solved by selecting a material with higher hardenability, so that quench rates can be less severe. Heated quench baths and immediate tempering are very beneficial. Salt-bath heat treating methods such as austempering and martempering can be advisable in complex components manufactured from steels with high hardenability. This often has the added benefit of reducing distortion. Components can be designed to be more quench-crack resistant. Providing generous fillets and rounded edges is beneficial.

Creep Embrittlement

Under creep conditions, embrittlement can occur and result in abnormally low rupture ductility. While creep strength and rupture strength are given considerable attention as design and failure parameters, rupture ductility is an important mechanical property when stress concentrations and localized defects such as notches are a factor in design. Rupture ductility, which varies inversely with creep and rupture strength, influences the growth of cracks or defects and thus affects notch sensitivity and toughness, as discussed in more detail in the article "Creep and Stress-Rupture Failures" in this Volume.

As voids and microcracks nucleate and grow during creep deformation, the development of creep embrittlement is invariably associated with a transition from transgranular to intergranular fracture. At high stresses (low time to stress rupture), ductility is fairly high and constant, with fracture characterized as transgranular. Below a threshold value of stress, ductility drops, with fracture becoming increasingly intergranular. This decrease in ductility with decreasing stress for elevated-temperature (creep) regimes is generally attributed to increasing localization of creep strain in narrow zones adjacent to the grain boundaries (Ref 14). This process is assisted by impurity effects and precipitate-free zones near the grain boundaries. For example, impurities such as phosphorus, sulfur, copper, arsenic, antimony, and tin have been shown to reduce rupture ductility, although rupture life increases. This behavior appears to be due to the grain-boundary segregants blocking grain-boundary diffusion, which reduces the cavity growth rate. High impurity contents increase the density of the cavities. Substantial intergranular cracking is observed in high-impurity material and is absent in low-impurity steel heats (Ref 15).

Creep embrittlement of heat-resistant steels after long-term exposure at elevated temperature has been noted for many years, and one of the first indications was observed in the unexpected failure of boiler flange bolts (Ref 16). In low-alloy heat-resistant steels, embrittlement occurs as a result of small amounts of creep strain along with the precipitation of fine, intergranular precipitates during the creep process (Ref 16). Failure of creep-embrittled ferritic steel material occurs through the prior-austenite grain boundaries in a manner similar to temper embrittlement, and temper-embrittling impurities (phosphorus, tin, antimony, arsenic) can assist the creep embrittlement. However, creep embrittlement is irreversible, while temper embrittlement is reversible. Thus, the term *reverse temper embrittlement* has been used (for example, Ref 17). In ferritic steels, creep embrittlement appears to occur in the temperature range of 425 to 595 °C (800 to 1100 °F).

In steels, creep damage often occurs together with oxidation and other changes, as illustrated by the case study in Example 19. Overheating also appears to have been a factor.

Example 19: Failure of a Steel Superheater Tube.

Failure occurred in a steel superheater tube in a power plant. The tube was specified as ASME SA-213 grade T22, and the reported operating conditions were 13 MPa (1900 psi) at 480 °C (900 °F). The tube carried superheated steam and was coal fired.

Investigation

The tube failed at a bend and deformed significantly. The tube had ruptured and buckled, with some secondary internal cracks apparent (Fig. 33a). The fracture surface was "thick-lipped," and the inside diameter exhibited a tenacious, black magnetite coating.

Chemical analysis confirmed that the tube satisfied the specified chemical compositional requirements, that is, a 2.25Cr-1Mo alloy steel. The strength determined on a sample remote from the fracture was higher than required, but the elongation at fracture was very low. Fractographic examination by scanning electron microscope (SEM) revealed generally intergranular features, but the level of oxidation damage to the features was severe. The cross section (Fig. 33b) exhibited creep voids and spheroidization of the pearlite within the ferrite matrix. Some features suggested hydrogen may have also contributed to the failure.

Conclusions

The superheater tube failed as a result of long-term overheating. Substantial creep damage reduced the strength of the tube to the point that overload failure occurred. The rupture was "thick-lipped," which is also consistent with long-term overheating. Technical literature indicates the scaling temperature of this alloy is approximately 595 °C (1100 °F), also suggesting service in excess of the stated 480 °C (900 °F) operating temperature. There

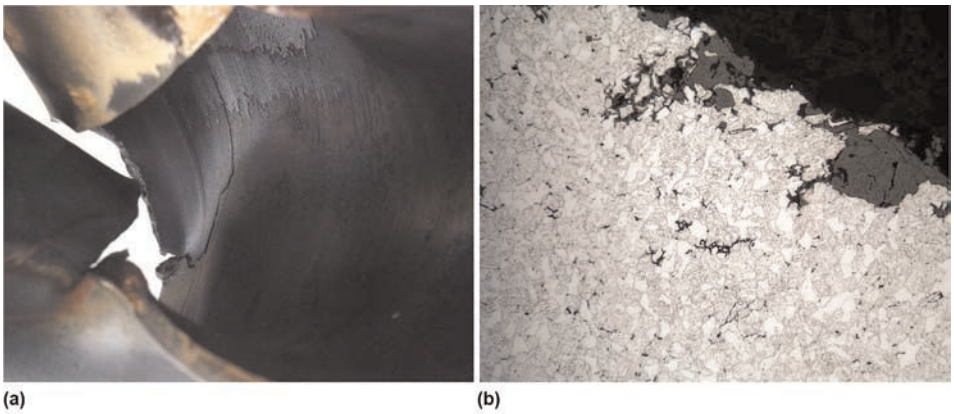

Fig. 33 Fracture of a steel superheater tube (Example 19). (a) Interior of the tube that fractured showing secondary cracks and a black contamination layer. (b) Microstructure of the tube showing triple-point cracks and intrusive oxidation damage. The creep damage was throughout the entire wall thickness. 2% nital etch. Original magnification: 297×

was no apparent graphitization, because this alloy has been shown to resist graphitization.

Overheating, Burning, and Incipient Grain-Boundary Melting

The mechanical properties of metals and alloys can be altered or degraded by overheating during hot working, heat treatment, and service. This is sometimes called burning and initiates as incipient melting, usually at the grain boundaries. Intergranular oxidation can also accompany this melting. Excessive grain growth without incipient melting can also occur, thus increasing the grain separation and assisting in the growth of cracks. Furthermore, excessive hot working temperatures can also result in solution of inclusions that may reprecipitate, often in grain boundaries, upon subsequent cooling, with a loss in fracture toughness.

In many materials, burning occurs during improperly controlled thermal processing, where heating for hot working or annealing is excessive. It is especially prevalent in hot working such as forging and swaging, where temperature control is more difficult than in simply heating the material in a furnace. Incipient melting can also occur due to poor temperature control in age-hardening alloys. A similar phenomenon is HAZ cracking in welding, because regions of the HAZ adjacent to the fusion line are nearly melted. The term *burning* is also sometimes used for surface damage from abusive grinding practice.

Avoidance/Remediation

Prudent manufacturing process development should obviate any overheating concerns. Material that has been overheated in this manner is not typically salvageable.

Environmentally Induced Embrittlement

Hydrogen Damage and Embrittlement

Hydrogen damage in metals occurs in many forms, including embrittlement, cracking, blistering, and grain-boundary methane formation (also called high-temperature hydrogen attack) during high-temperature service. Some materials also form internal flake and fisheye defects during solidification and welding. In addition, hydride formation can occur in a number of nonferrous alloy families, such as titanium alloys, but not steels. These types of hydrogen damage are discussed in more detail in the article "Hydrogen Damage and Embrittlement" in this Volume.

Hydrogen appears to facilitate other types of embrittlement, and it can be complex to diagnose and separate from other contributing factors, such as intergranular impurities and, in some cases, stress-corrosion cracking. As a single proton, hydrogen atoms are sufficiently mobile with significant diffusivity in all metals, even at low temperatures. Individual hydrogen atoms will combine into diatomic gaseous molecules, often at grain boundaries, inclusions, and lattice imperfections. Embrittling hydrogen, which can be as low as several parts per million, is supplied by an extensive list of possible sources. Hydrogen charging, or infusion of a damaging amount of hydrogen, also can occur during primary processing (for example, the steelmaking process) or a variety of fabrication and secondary operations, such as acidic cleaning (pickling), electroplating, and welding. Hydrogen can also be introduced from chemical reactions in service due to gas exposure, lubricant degradation, and corrosion. In many instances, the presence of cathodic poisons can increase the quantity of hydrogen atoms absorbed. Increasing the exposure temperature also increases the level of hydrogen absorption. However, both low- and high-temperature service appear to reduce the level of hydrogen damage over room-temperature service.

Hydrogen embrittlement results in cracking or catastrophic failure during service, generally in a delayed manner under static loading. It reduces the ductility of the materials (with or without a decrease in strength, depending on the material and the location and extent of hydrogen in the material) and accelerates subcritical crack growth rates. Cracks from hydrogen embrittlement typically exhibit little branching and are often intergranular, but caution is required when characterizing hydrogen embrittlement based on fracture appearance. Other contributory factors may be involved, and, in some cases (such as highly stressed conditions), transgranular fracture can be observed. These complexities are discussed in a little more detail in the article "Hydrogen Damage and Embrittlement" in this Volume.

Many ferrous and nonferrous metals are prone to hydrogen damage. Steels and precipitation-hardenable steels are particularly susceptible to hydrogen embrittlement. Increasing the hardness and/or the level of cold work increases the embrittlement susceptibility. Basically, hydrogen embrittlement requires three factors: tensile stresses (residual, applied, or both), a susceptible metal, and hydrogen above a threshold level. Many failures in steels occur at loads below the yield strength, and no plastic deformation is evident. Steels at a tensile strength level below 690 MPa (100 ksi) are often considered resistant to hydrogen cracking. However, these steels can still be susceptible to hydrogen damage in the form of blistering. Austenitic ferrous alloys are much less susceptible to hydrogen embrittlement than the martensitic or cold-worked ferritic grades, but fcc metals are not immune to hydrogen embrittlement. Hydrogen embrittlement can also be difficult to distinguish from stress-corrosion cracking in some cases.

Avoidance/Remediation

Hydrogen embrittlement in steels and other metals can be avoided by removing production- and service-related sources of potential embrittlement. Close control of fabrication processes that produce hydrogen is a necessity. In welding, underbead cracking and other hydrogen-assisted weld-cracking types can be reduced by better material control. Using better-quality shielding gases, special low-hydrogen electrodes, and moisture-free electrodes and fluxes is beneficial. Reduction of cooling-rate-induced hardening and joint restraint can result in a final stress state below the threshold necessary for embrittlement and cracking.

The practice of baking soon after electroplating has been shown to reduce the possibility of hydrogen embrittlement. Stress relief prior to plating to remove residual stresses is also beneficial. However, baking cannot remove all the hydrogen and is by no means a panacea. Plated high-strength steel fasteners that have been properly baked, most notoriously the grade 8 bolts and higher-strength socket head cap screws, can still fail via hydrogen embrittlement. Example 20 discusses one such failure incident. This example also illustrates the difficulty of hydrogen embrittlement, because it is not always possible to *prove* hydrogen embrittlement in an exacting fashion, even though indications point to hydrogen. In many cases, the main issue may not be proof but rather education toward eliminating hydrogen embrittlement as a potential problem (see the article "Hydrogen Damage and Embrittlement" in this Volume).

Example 20: Hydrogen Embrittlement Failure of Cap Screws.

Socket head cap screws used in a naval application evinced delayed fracture in service. Standard 8 mm (0.031 in.) diameter ISO 898 class 12.9 (formerly ASTM A574) screws were zinc plated and dichromate coated. Two unused, exemplar fasteners from the same lot were submitted for comparison.

Investigation

Several cap screws exhibiting representative cracking and fracturing are shown in Fig. 34(a). All cracking was at the head-to-shank fillet, and no plastic deformation was apparent. One screw that cracked 360° around the circumference is shown in Fig. 34(b).

The fracture and opened crack surfaces were dull but had the crystalline appearance of an intergranular fracture. Examination by SEM revealed that the peripheries of the surfaces exhibited primarily intergranular brittle and transgranular dimple-rupture features, whereas the core morphology consisted primarily of dimple-rupture features. Figure 34(c) shows some of the intergranular features, which also contained secondary grain-boundary separation, ductile hairlines, and micropores on the grain facets.

The chemical composition of a failed screw was consistent with grade 4037 alloy steel and satisfied the fastener specification. Tension testing of two exemplar screws revealed failure strengths that exceeded the minimum

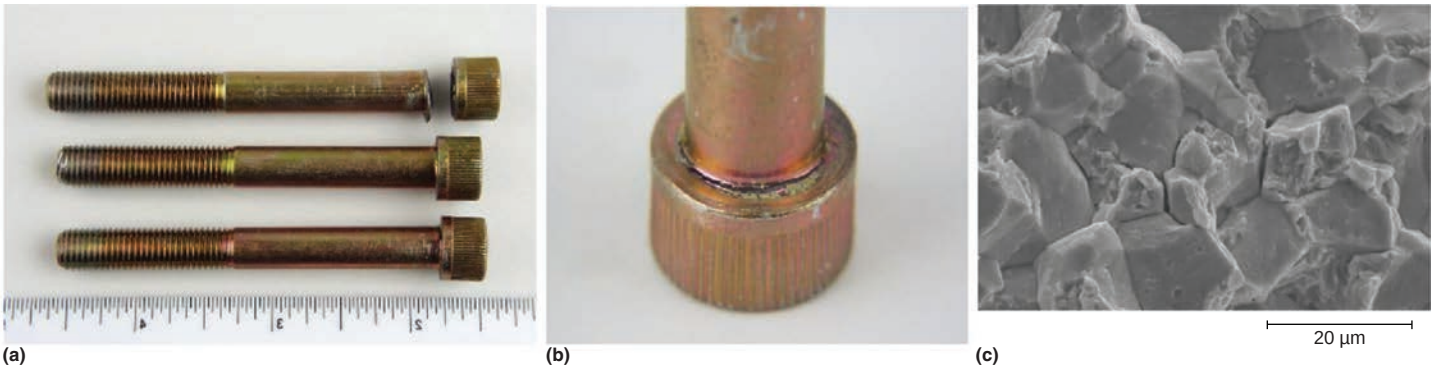

Fig. 34 Delayed fracture of cap screws (Example 20). (a) Cap screws that either cracked or fractured in a delayed manner at the underside of the heads. (b) One screw that cracked 360° around the head without separating. (c) Representative electron image of the primarily intergranular fracture features. Secondary grain-boundary cracks, ductile hairlines, and micropores are apparent. Scanning electron micrograph. Original magnification: 1187×

requirement, and the fractures consisted of ductile-rupture features.

Metallographic cross sections were prepared through both fractured and cracked screws. Cracking had an intergranular aspect in many regions, with some secondary grain-boundary cracks adjacent to the primary cracks. The microstructure was uniform and consisted of fine, tempered martensite, indicative of the required quenched-and-tempered condition.

Conclusions

The cap screws appeared to have failed due to hydrogen embrittlement, as revealed by the delayed cracking and intergranular fracture morphology. Static brittle overload fracture occurred due to the tension preload, and prior hydrogen charging did occur in manufacturing. The probable source of hydrogen charging is the electroplating, although postplating baking was reportedly performed.

This example illustrates the difficulty of analyzing the hydrogen embrittlement problem. The samples satisfied the composition and property requirements for the identified cap screw grade. However, antimony, phosphorus, tin, sulfur, lead, and other low-melting-point impurities, which are generally very expensive to analyze, also can be factors contributing to the embrittlement situation. These elements, like hydrogen, are more damaging when they are present in the grain boundaries, and thermal exposure can concentrate these elements in the grain boundaries. In fact, some of the extended baking times that have been recommended for hydrogen embrittlement prevention in electroplated parts can actually increase the concentration of these other low-strength elements in the grain boundaries.

Therefore, it is necessary to be cognizant of other potential contributory factors and to be aware of how the potential problems of hydrogen can be reduced. In this case, one important factor is that the cap screws were at the highest strength (1220 MPa, or 177 ksi, minimum tensile strength) for steel fasteners in wide commercial use. This increases the risk of embrittlement, and it may be necessary to examine the manufacturing processes in more detail, depending on the criticality of service and the frequency of occurrence.

Neutron Embrittlement

Irradiation by neutrons of nuclear reactor pressure vessel steels is a serious form of materials degradation that can result in an increase in the DBTT. The DBTT, or nil ductility transition temperature, increase can be as much as 200 °C (360 °F). In some cases, the upper-shelf energy is decreased, with an increased propensity for intergranular fracture. Most ferrous metals can be susceptible, including carbon steels, alloy steels, and precipitation-hardening stainless steels. Some austenitic stainless steels, although containing no DBTT, have been found to exhibit reductions in ductility when irradiated.

On the crystalline structure level, neutron bombardment of susceptible materials results in atomic displacement, thereby creating self-interstitials and vacancy defects, along with phase and precipitate formation. These discontinuities, singly and in clusters, also prevent plastic deformation via dislocation pinning. The extent of embrittlement is based on a large number of service variables, including exposure time, service temperature, and neutron fluence.

Research has shown that heat treatment and composition greatly affect the sensitivity of steel to neutron embrittlement. Tempered martensitic microstructures are less sensitive than ferritic and tempered bainitic microstructures, and finer grain sizes are also beneficial. Steels containing nickel as an alloying addition and/or copper and phosphorus as impurities are known to be particularly susceptible.

Avoidance/Remediation

Avoidance of neutron embrittlement is typically achieved by the selection of materials in appropriate heat treated conditions found to be less sensitive in nuclear service. Normal annealing heat treatments have been shown to partially or fully restore embrittled materials due to the effects of recovery and, possibly, recrystallization. Some of the effects, such as precipitation of deleterious phases, may not be entirely eliminated, and affected steels can incur embrittlement at a different rate upon reintroduction to service.

Stress-Corrosion Cracking

Stress-corrosion cracking (SCC) is manifested as transgranular or intergranular brittle cracking, which can lead to final overload failure. Although it is a corrosion failure mechanism, it is included in this discussion of overload fracture due to its embrittling nature. A similar mechanism exclusive to steels is sulfide stress cracking. The SCC mechanism does not always include gross general corrosive attack, and differentiation from the other possible embrittling phenomena may be necessary during failure analysis.

The synergistic combination of a corrodent, a susceptible material, and the presence of a tensile stress can result in progressive cracking and reduction in ductility. Nearly all metallic materials have been shown to be susceptible to SCC under certain circumstances. Steels, even those of the corrosion-resistant varieties, are susceptible in many types of service. Hydrogen has been shown to accelerate stress corrosion, as in the case of hydrogen sulfide cracking. In high-strength steels, SCC has been attributed to the hydrogen generated by the corrosion process. When examined metallographically, SCC cracks typically exhibit branched cracking as opposed to a single crack.

Avoidance/Remediation

Removal of one of the three requisite factors is typically sufficient to prevent SCC. Materials in conditions that evince little susceptibility in the intended service environment can often be selected. Alternatively, it may be possible to remove the corroding substance from the local service environment. A threshold stress is typically required for SCC, with both applied and residual stresses below this level not initiating cracking. More specific information is provided

in the article "Stress-Corrosion Cracking" in this Volume.

Example 21: Centrifugal Pump Shaft.

A pump shaft fracture occurred shortly after the impeller nut was tightened and the pump was placed into service. The shaft was reportedly fabricated from nickel-copper precipitation-hardened alloy Monel K-500 (UNS N05500). No information was available concerning the pump size or configuration, but the service was identified as part of a hydrofluoric acid (HF) alkylation unit in a petroleum refinery.

Investigation

Figure 35(a) shows the shaft failure location, which was at a relatively severe change in diameter from 67 mm (2.64 in.) to the threaded 31 mm (1.22 in.) impeller nut diameter. This transition exhibited a small fillet radius, approximately 1.9 mm (0.075 in.). The surface of the failed pump shaft contained white and dark-colored deposits but no significant wastage. Liquid penetrant inspection showed no other cracklike indications.

The chemical composition of the failed pump shaft was consistent with the requirements specified for Monel K-500. Tensile properties were also consistent with the precipitation-hardened condition for this alloy, with an ultimate tensile strength of 1055 MPa (153 ksi). Guided bend testing confirmed that the pump shaft was not inherently brittle.

Deposits on the pump shaft fracture consisted mainly of sodium, oxygen, and fluorine, with lesser concentrations of silicon, aluminum, sulfur, chlorine, potassium, calcium, iron, nickel, and copper also detected. Fracture-surface regions without substantial debris were intergranular, as shown in Fig. 35(b).

A deionized water extract of the fracture-surface debris was slightly acidic, with a pH of 5.7. Ion chromatography analysis detected a fluoride ion concentration of >6000 ppm, with low levels of chloride, nitrate, and sulfate ions.

Branching intergranular cracking was apparent throughout the shaft cross section during metallographic evaluation. Typical crack profiles are shown in Fig. 35(c). The microstructure was consistent with an annealed and age-hardened nickel-copper Monel K-500 material, with no observed grain-boundary phases or other anomalies.

Conclusions and Recommendations

The pump shaft failed due to intergranular SCC. Cracking was localized to the highly stressed transition from the larger shaft to the smaller-diameter impeller nut threads. The rapid crack propagation was likely the result of a highly stressed region together with a high concentration of fluoride ions. The cracking suggested that the shaft was likely exposed to wet hydrogen fluoride vapors. Hydrofluoric acid is known to cause SCC in this alloy in the presence of oxygen. The pump shaft was fabricated from the specified material in the required heat treatment condition.

Monel K-500 has been shown to exhibit good SCC resistance in HF service as long as oxygen is excluded from the process. In addition, dealloying in the form of denickelification also has been reported in oxygenated HF. If oxygen cannot be excluded from this process, it would be necessary to use a different alloy.

Liquid-Metal-Induced Embrittlement

Liquid-metal-induced embrittlement (LMIE, formerly liquid-metal embrittlement) occurs when contact with molten material of a lower-melting-point alloy results in a severe reduction in ductility and, very often, strength. This occurs primarily by intergranular entry of the molten metal into a stressed material, effecting progressive separation cracking or grain-boundary decohesion. Cycles of solidification and liquation of the low-melting-point alloy can also affect the extent and speed of this embrittlement, if volumetric expansion occurs during cycles of solidification or liquation.

Liquid-metal-induced embrittlement occurs for most loading conditions except for compressive loading. Both residual and applied stresses, together with a temperature dependency, contribute to this complicated embrittlement mechanism. A stress threshold value for this mechanism has been suggested by research. Parameters that have been shown to increase susceptibility to LMIE include grain size, strain rate, time under static loading, and the strength and hardness of the component. High stresses can result in instantaneous fracture, whereas low stresses can have a more delayed effect. Fracture from LMIE can occur below the elastic limit in high-strength materials, but some plastic deformation may be evident in softer materials.

Most engineering metals and alloys have been shown to be susceptible to LMIE. The presence of a molten metal is necessary, but not by itself a sufficient condition for LMIE. Metal couples that exhibit low intersolubilities and that do not form intermetallic compounds can be susceptible. Zinc embrittlement in steel is a notable exception to this generalization, because it can participate in both LMIE and intermetallic compound embrittlement.

Metals that form surface oxides can prevent ingress of liquid metal due to the adverse effect on the necessary wettability. Initiation of LMIE attack does not apparently depend on the amount of molten metal available, and the required threshold for damage is very small. However, continued degradation requires a steady supply of molten metal. As would be expected, brazing and soldering can cause LMIE, as shown in Fig. 36. In this case, the cold-worked steel fractured due to excessive heat input during manual torch brazing. Many plating and coating metals can serve as embrittling agents.

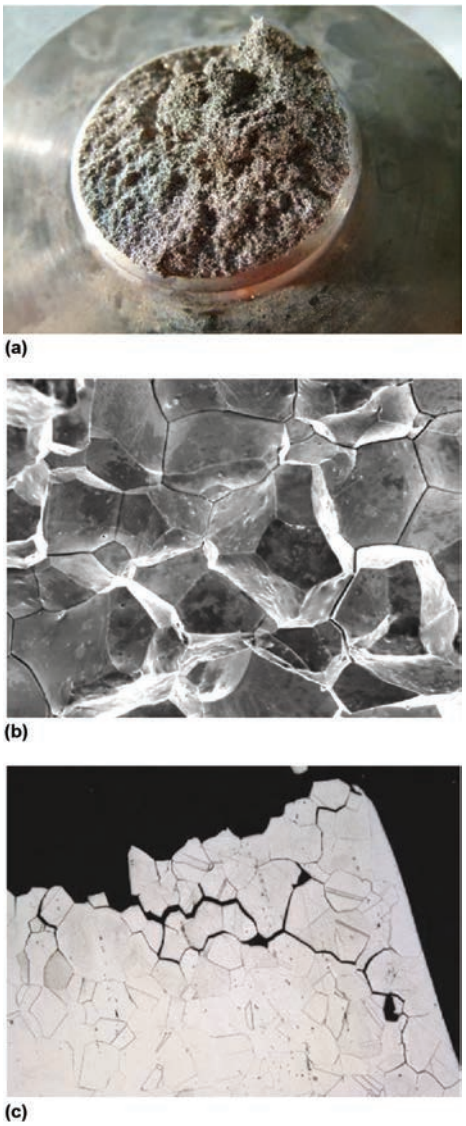

Fig. 35 Centrifugal pump shaft (Example 21). (a) Image of the rough pump shaft fracture surface. (b) Electron image showing intergranular fracture surface. Original magnification: 274×. (c) Shaft cross section showing branching intergranular cracking of brittle fracture. Original magnification: 100×

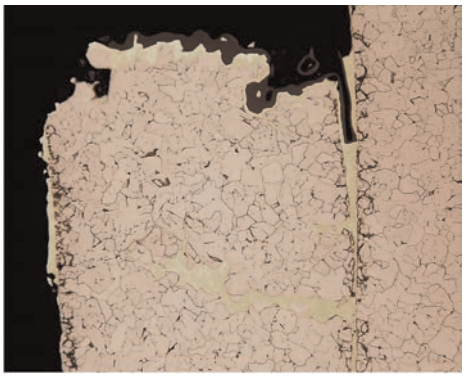

Fig. 36 Liquid-metal-induced embrittlement and cracking evidence that occurred during torch brazing. 2% nital etch. Original magnification: 119×

Alloys that contain a discrete low-melting-point phase rather than an external molten material have evinced LMIE failures. Rapid heating of these materials in the deformation-processed condition may not permit recovery and relaxation of the surrounding matrix prior to liquefaction of the low-melting-point inclusions. The expansion pressure of the liquefying phase forces this liquid metal into the adjacent grain boundaries, resulting in embrittlement or fracture. This has been observed in many alloy systems, such as leaded steels and leaded copper alloys, where it is sometimes referred to as fire cracking.

Avoidance/Remediation

The use of susceptible material pairs should be avoided if the constant or transient service temperature is above the melting point of the low-melting-point material. Once it has manifested, LMIE is not reversible and the damage is permanent.

Solid-Metal-Induced Embrittlement

Solid-metal-induced embrittlement (SMIE) occurs in steels as well as many nonferrous materials. This phenomenon appears to be related to LMIE, because the materials and couples susceptible to SMIE are those for which LMIE is known to occur. In some instances, contact of a metal with a low-melting-pointalloy at a temperature below the melting point of the low-melting-point material has been shown to cause delayed brittle fracture and cracking in addition to decreasing strength and ductility. The relative level of damage increases with temperature up to the melting point of the low-temperature species.

Research suggests SMIE is probably caused by a number of complicated interrelated processes. By whatever mechanisms, empirical evidence shows that the embrittling species can diffuse into the grain boundaries of the base metal, causing embrittlement and cracking. Applied and/or residual stresses above a threshold level are necessary for cracking to occur. In some cases, the embrittling species can be an immiscible, discrete solid phase, such as lead in leaded steel grades. Intimate contact between the two materials is necessary, and other factors such as microstructural discontinuities affect SMIE behavior. Solid-metal-induced embrittlement is substantially slower than LMIE, but multiple cracks occur in SMIE.

Avoidance/Remediation

Elevated-temperature service of steels in the presence of solid low-melting-point alloys known to embrittle should be avoided. An intermediate plating with a higher melting point that has been shown to not embrittle can be used to prevent SMIE.

Role of Welding in Embrittlement and Overload Behavior

Fusion welding of metallic materials deserves special mention with respect to embrittlement and overload behavior. The combinations of thermal gradients, welding consumables, alloying effects, cooling effects, and residual stresses can result in nearly every manner of embrittlement. Every phase and constituent that can exist in a metal or alloy up to its melting point can be present in a weld or surrounding HAZ. Welding-related features contributing to overload failure include incipient melting/burning, grain coarsening, grain refinement, precipitation effects, hardening, and tempering. In addition, there can be problems associated with lack of fusion and residual stresses created by the thermal exposure. Thermal stresses can cause both hot cracking and cold cracking, and cracks can be present in the weld, at the fusion line, in the HAZ, and in the base metal. An example of hot cracking in a tube weldment is shown in Fig. 37. The interdendritic nature of the cracking is evident. Example 22 shows a variety of welding changes that combined to initiate failure in a heat exchanger.

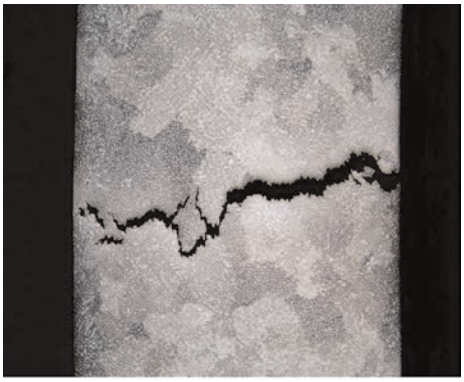

Fig. 37 Hot cracking that developed in a stainless steel tube weld. 10% oxalic acid electrolytic etch. Original magnification: 30×

Example 22: Weld Cracking of a Stainless Steel Heat Exchanger.

A welded ferritic stainless steel heat exchanger cracked prior to service. The sheet steel weld joint design is depicted in Fig. 38(a). The welding filler metal was identified as an austenitic stainless steel, and the joining method was gas tungsten arc welding.

Investigation

Examination of the supplied sample revealed a single crack, transverse to the fillet weld axis. No bulk macroscopic plastic deformation was associated with the cracking.

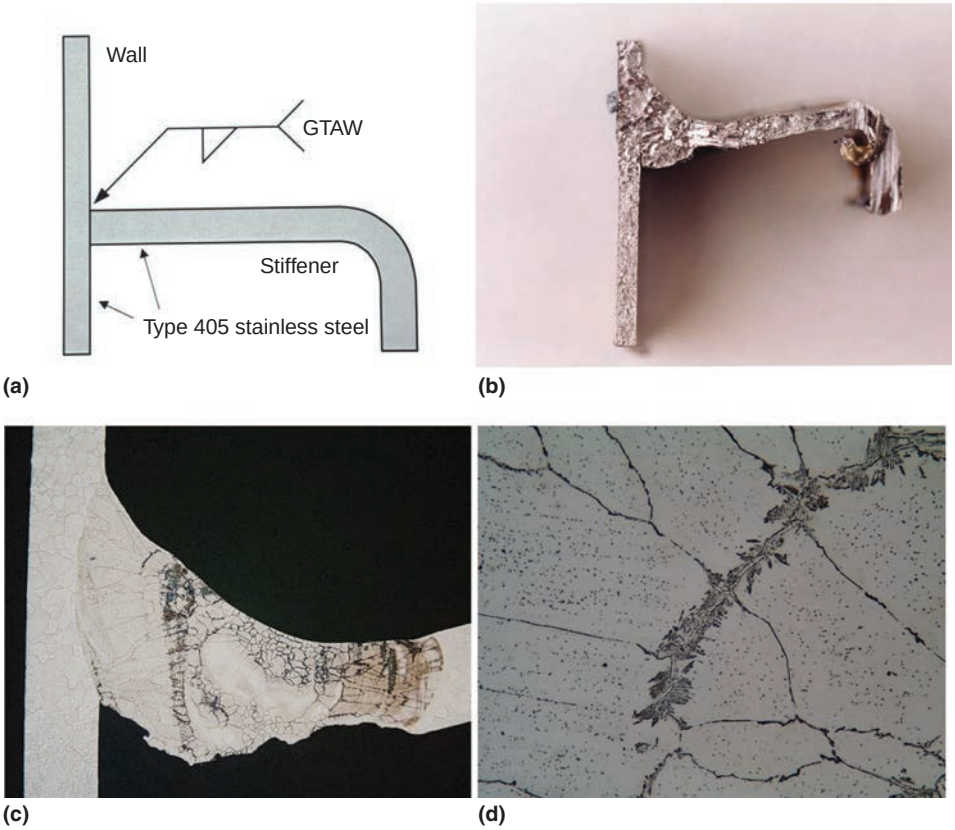

Fig. 38 Cracking of a welded ferritic stainless steel heat exchanger (Example 22). (a) Diagram showing the heat-exchanger weld joint design. GTAW, gas tungsten arc weld. (b) Transverse crack that occurred through the weld. Original magnification: 5.9×. (c) Metallographic profile of the weld near the cracking, showing melt-through, grain growth, and precipitation. Original magnification: 8.9×. (d) Grain-boundary precipitates in the weld zone. Original magnification: 119×. (c) and (d) were etched with Vilella's reagent followed by electrolytic etching in 10% oxalic acid.

Relatively high heat input during welding was suggested by the extent of the oxide or heat tint discoloration. The underside of the weld joint contained melt-through. The crack surface after excision is shown in Fig. 38(b). The fracture surface had a faceted appearance, with significantly larger facets within the weld and HAZs. Grain growth is not uncommon in arc welding of ferritic stainless steels.

Inspection by SEM confirmed the failure mode as both cleavage and intergranular fracture. A metallographic cross section through the weld, parallel and adjacent to the crack, is shown in Fig. 38(c). Dramatic grain coarsening was evident in the weld and HAZ. The microstructure within the resolidified weld was not uniform. Isolated regions of the weld were determined to be austenitic due to the filler metal applied. Grain-boundary phase segregation was apparent, as shown in Fig. 38(d).

Conclusions

It was concluded that the heat exchanger cracked due to weld cold cracking or postweld-ing brittle overload, which occurred via flexure during fabrication. The brittle nature of the weld was likely due to a combination of high residual stresses, a mixed microstructure, inclusions, and gross grain coarsening. These synergistic factors resulted from extreme heat input during fillet welding. It was recommended that the welding variables such as voltage, amperage, and travel speed be altered to substantially reduce the heat input.

Laboratory Fracture Examination

Among the most important, yet insufficiently used, procedures of the failure analyst is the examination of laboratory fractures at a range of magnifications from visual to more than 1000×. Tensile, impact, and bend testing can provide excellent fractographic comparison samples. This can often be done on specimens used to quantify the mechanical properties. Service conditions, such as elevated or low temperature, can be used in lab evaluation to help explain the actual failure conditions. In some cases, it is possible via laboratory testing to duplicate the fracture appearances to support a proposed set of circumstances causing failure. A laboratory testing program that results in duplication of the appearance of the failed component can be especially helpful when initial evaluation of the failed component does not lead to strong indication of a root cause.

Laboratory fracture study is particularly efficient in cases of suspected embrittlement. Based on the nature of the embrittlement, it may not always be detectable by electron microscopy, chemical analysis, or metallography. Fractures created in a known manner can also be used to test the null hypothesis, namely that they did not fail in a certain manner. These methods have been used to estimate service temperature after the fact, and other loading conditions can often be deduced. One application in particular is in the evaluation of hydrogen embrittlement. Slow-strain-rate tensile fracture features are typically not affected by this static cracking phenomenon.

ACKNOWLEDGMENT

This article was revised from B.A. Miller, Overload Failures, *Failure Analysis and Prevention*, Volume 11, *ASM Handbook*, ASM International, 2002, p 671–699.

REFERENCES

1. P.F. Thomason, *Ductile Fracture of Metals*, Pergamon Press, Oxford, England, 1990, p 19–24
2. R. Reed and A. Clark, *Materials at Low Temperature*, American Society for Metals, 1983
3. N.J. Petch, The Ductile-Cleavage Transition in Alpha-Iron, *Fracture*, B.L. Averbach, Ed., Technology Press, 1959, p 54–67
4. G.F. Vander Voort, Embrittlement of Steels, *Properties and Selection: Irons, Steels, and High-Performance Alloys*, Vol 1, *ASM Handbook*, ASM International, 1990, p 689–736
5. G.F. Vander Voort, Visual Examination and Light Microscopy, *Fractography*, Vol 12, *ASM Handbook*, ASM International, 1987, p 91–165
6. J.R. Davis, Ed., Thermally Induced Embrittlement of Steels, *ASM Specialty Handbook: Carbon and Alloy Steels*, ASM International, 1996, p 309, 312
7. R. Bruscato, Temper Embrittlement and Creep Embrittlement of 2¼Cr-1Mo Shielded Metal Arc Weld Deposits, *Weld. J.*, Vol 9 (No. 4), 1970, p 148s–156s
8. Y. Murakami, T. Namura, and J. Watanabe, *Heavy Section 2¼Cr-1Mo Steel for Hydrogenation Reactors*, STP 755, American Society for Testing and Materials, 1982, p 383–417
9. J.A. Peters et al., On the Mechanisms of Tempered Martensite Embrittlement, *Acta Metall.*, Vol 37, Feb 1989, p 675–686
10. C.L. Briant and S.K. Banerji, Tempered Martensite Embrittlement and Intergranular Fracture in an Ultra-High Strength Sulfur Doped Steel, *Metall. Trans. A*, Vol 12, Feb 1981, p 310
11. D. Peckner and I.M. Bernstein, *Handbook of Stainless Steels*, McGraw-Hill, 1977, p 44–6, 44–7
12. T. Fushimi, "Life Evaluation of Long Term Used Boiler Tubes," paper presented at the Conference on Boiler Tube Failures in Fossil Plants (Atlanta, GA), Electrical Power Research Institute, Nov 1987
13. B.A. Miller, P.D. Swartzentruber, and J.T. Barnes, Failure of a Dissimilar Metal Braze in an Expansion Joint, *J. Fail. Anal. Prevent.*, Vol 19 (No. 2), April 2019, p 314–319
14. R. *Viswanathan*, *Damage Mechanisms and Life Assessment of High-Temperature Components*, ASM International, 1989, p 77
15. L.K.L. Tu and B.B. Seth, Effect of Composition, Strength, and Residual Elements on Toughness and Creep Properties of Cr-Mo-V Turbine Rotors, *Met. Technol.*, Vol 5, March 1978, p 79–91
16. G. Sachs and W. Brown, *A Survey of Embrittlement and Notch Sensitivity of Heat Resisting Steels*, American Society for Testing and Materials, 1952, p 6–21
17. J.J. Hickey and J.H. Bulloch, The Role of Reverse Temper Embrittlement on Some Low and High Temperature Crack Extension Processes in Low Carbon, Low Alloy Steels: A Review, *Int. J. Pressure Vessels Piping*, Vol 49, 1992, p 339–386

SELECTED REFERENCES

- D.G. Altenpohl, *Aluminum: Technology, Applications, and Environment*, 6th ed., The Aluminum Association and The Minerals, Metals & Materials Society, 1998
- G.M. Boyd, *Brittle Fracture in Steel Structures*, Butterworths, London, 1970
- D.N. French, *Metallurgical Failures in Fossil Fired Boilers*, 2nd ed., John Wiley & Sons, 1993
- R. Gibala and R.F. Hehemann, Ed., *Hydrogen Embrittlement and Stress Corrosion Cracking*, American Society for Metals, 1984
- G.E. Linnert, *Metallurgy*, Vol 1, 4th ed., American Welding Society, 1994
- D.P. Miannay, *Fracture Mechanics*, Springer-Verlag, 1998
- R.D. Port and H.M. Herro, *The Nalco Guide to Boiler Failure Analysis*, McGraw-Hill, 1991
- G.W. Powell and G.F. Vander Voort, Ductile and Brittle Fractures, *Metals Handbook Desk Edition*, American Society for Metals, 1985, p 32–9 to 32–13
- *Temper Embrittlement of Alloy Steels*, STP 499, American Society for Testing and Materials, 1972
- P.F. Wieser, *The Morphology of Brittle Intergranular Fracture of Steel Castings and the Effects of Processing Variables on Its Occurrence*, Steel Founders' Society of America, 1975